A CONTACTLESS NON-INTRUSIVE APPROACH FOR MACHINE LEARNING-BASED
PERSONALIZED THERMAL COMFORT PREDICTION

by

Roshanak Ashrafi

A dissertation submitted to the faculty of
The University of North Carolina at Charlotte
in partial fulfillment of the requirements
for the degree of Doctor of Philosophy in
Sustainability

Charlotte

2022

Approved by:

_____

Dr. Mona Azarbayjani, Dr. Hamed
Tabkhi

_____

Dr. Ahmed Arif

_____

Dr. Mark DeHaven

_____

Dr. Yaorong Ge

_____

Dr. Min Shin

_____

Dr. Stefano Schiavon

ABSTRACT

ROSHANAK ASHRAFI. A Contactless Non-Intrusive Approach for Machine Learning-Based Personalized Thermal Comfort Prediction. (Under the direction of DR. MONA AZARBAYJANI, DR. HAMED TABKHI)

Indoor thermal environmental conditions play a significant role in protecting occupants' well-being. In this regard, schedule-based and predefined environmental control is one of the main reasons for the current discomfort and dissatisfaction with the thermal environment. These general standards make it impossible to consider people's differences in thermal sensation and personal preference. Recent research is attempting to leverage occupants' demand in the control loop of the buildings to consider the well-being of each individual based on their own physiological properties. These thermal comfort models are called "personalized comfort models". In this regard, studies are trying to utilize skin temperature recorded by infrared thermal cameras for developing personal comfort models through machine learning prediction algorithms. However, there are some critical gaps in the current methods that have limited the application of this platform in real buildings. Some of the main shortcomings of the current approaches are the limited distance from the camera, the absence of automated and accurate detection of facial areas, and the limitation on the detectable facial positions. To capitalize on the potential and address the existing constraints, new solutions are required that take a more holistic approach to non-intrusive thermal scanning by integrating the benefits of sensor fusion, image processing, and machine learning. The contribution of this dissertation is in the three main aspects of literature review, data collection, and model development. This study presents a comprehensive and systematic review of the current machine learning-based personalized thermal comfort studies. In addition, we introduce "Charlotte-ThermalFace", our recently developed dataset, and how it addresses some of the existing gaps in the subject. Charlotte-ThermalFace contains more than 10,000 infrared thermal images in varying thermal conditions, several distances from

the camera, and at different head positions. The data is fully annotated with the facial landmarks, ambient temperature, relative humidity, air velocity, distance to the camera, and subject thermal sensation at the time of capturing each image. By using this dataset, we have developed a personalized comfort model for subjects at a farther distance in a completely non-intrusive method. We have accomplished this by incorporating both visual and thermal images to create a multi-modal sensing platform. Through this interconnected system, we use visual images and the deep learning based HR-net algorithm for localizing facial landmarks, and thermal images to measure the temperature values of the detected areas. This research implements an automated approach to register simultaneous thermal and visual frames and read the facial temperature accurately for subjects at a distance from the camera. Through this method, we could extract facial skin temperature at a distance and in several head positions. For creating machine learning-based personalized thermal comfort models, we have implemented two powerful classification algorithms: Random Forest and K-Nearest Neighbor. The prediction results indicate an average accuracy of 86% for the Random Forest and 74% for the K-Nearest Neighbor algorithm. This study presents promising findings for the creation of automated thermal comfort prediction platforms from a distance through the utilization of thermal cameras.

DEDICATION

This work is dedicated to my father, Parviz, who had been a constant source of support and encouragement. He loved to learn and never stopped exploring throughout his life. The motivation and inspiration to continue the education journey was one of the gifts that he had brought to my life.

ACKNOWLEDGEMENTS

TABLE OF CONTENTS

LIST OF TABLES

LIST OF FIGURES

LIST OF ABBREVIATIONS

AI   Artificial Intelligence

ANN   Artificial Neural Networks

API   Application Programming Interface

AT   Air Temperature

AV   Air Velocity

CLO   Clothing level

EDA   Electrodermal Activity

EEG   Electroencephalogram

GT   Globe Temperature

HVAC Heating Ventilation Air Conditioning

IEQ   Indoor Environmental Qualities

IR   Infrared

ML   Machine Learning

MR   Metabolic Rate

OH   Outdoor Humidity

OT   Outdoor Temperature

PMV   Predicted Mean Vote

RH   Relative Humidity

RL   Reinforcement Learning

SBS   Sick Building Syndrome

SSI   skin sensitivity index

ST   Skin Temperature

TIR   Thermal Infrared Reading

CHAPTER 1: INTRODUCTION

1.1   Introduction

In our current society, people spend more than 90% of their time indoors, which causes indoor environmental qualities to have a significant influence on their health conditions. Although the building sector consumes approximately 40% of the globally produced energy, the majority of which is used in heating, ventilation, and air conditioning (HVAC) systems, people are generally dissatisfied with their environmental comfort conditions. In this regard, a recent large-scale survey reports that approximately 40% of building occupants are dissatisfied with the thermal conditions in their indoor environment. This global survey, which is the result of a 20-year study, focuses mostly on office environments, which account for 77% of the research investigated buildings [1]. Another study on 52,980 occupants in 351 predominately North American office buildings has indicated that only 2% of the studied buildings are providing thermal comfort for 80% of their occupants [2]. This wide range of dissatisfaction with thermal conditions urges the need to improve the indoor environment to prevent the health problems resulting from discomfort caused by poor indoor thermal conditions. Sick Building Syndrome (SBS) is a recent concept about the influence of the built environment on human health conditions and has attracted the attention of researchers in this area. It has been proven that temperature and humidity conditions are significant contributors to the SBS symptoms, which include fatigue, headache, susceptibility to cold and flu, and disruption of sleep patterns [3]. The thermal state is one of the primary factors of Indoor Environmental Qualities (IEQ) that can impact occupants' well-being. One of the main causes of these poor environmental conditions is relying on explicit, predefined models of thermal comfort, which do not correspond to the actual preferences of dif-

ferent occupants in the environment [4]. Depending on general standards, it is nearly impossible to accommodate varying degrees of people's thermal preferences. [5]. Recent research in human-centered design is attempting to leverage occupants' demand in the control loop of the buildings to consider the well-being of each individual based on their own physiological properties. This approach to thermal comfort modeling is also referred to as personalized comfort. Personalized comfort is a recent approach in the area of human-centered building that focuses on providing comfortable conditions for each occupant based on their own preferences. To create a comfort model for each user, we need a real-time feedback system to provide data about occupants' physiological or psychological conditions. The developed model can then be used for controlling the associated HVAC system. The innovations in environmental data gathering have provided a unique opportunity to collect large amounts of information from the buildings' occupants, which can be studied to develop a personalized environmental control system. In this regard, the emergence of thermal imaging technology has made contactless skin temperature data collection possible without interfering with occupants' activities. The collected physiological data can then be utilized for predicting and controlling each occupant's thermal conditions in the built environment through personalized comfort models. In addition to environmental monitoring, facial thermography is one of the most widely studied areas of infrared thermography due to its proven practical applications. Facial thermal imagery has been successfully studied as an indicator of human presence [6, 7, 8], identity[9, 10], and emotions[11, 12, 13] in several research. The current pandemic has also highlighted the facial thermography potential in the non-intrusive evaluation of human conditions more than before [14, 15]. The promising results of non-contact thermal comfort modeling make it an excellent component for smart buildings. Smart buildings are known for their capabilities in using Artificial Intelligence (AI) and data processing to provide energy savings, enhanced occupant comfort, improved safety, and better maintenance. The "learning ability" was

added to this definition after the increasing use of AI to design smart buildings that can learn their performance from the occupants and environment [16]. Therefore, the *learning* approach is another key factor that influences the reliability and efficiency of the proposed personal comfort models. Machine Learning (ML) methods, as a subset of AI, have great potential for creating thermal comfort models [17]. Several machine learning algorithms have been used lately to compare the prediction accuracy of different models in both lab and field environments. The promising results of the initial studies in the area of facial thermography have attracted researchers' attention to utilizing facial skin temperature as an input for machine learning algorithms to create thermal comfort models [18]. While there is currently an increasing interest in utilizing infrared thermal cameras in public buildings because of their non-invasive quality, state-of-the-art methods need additional modifications to become more reliable and holistic. There are some critical gaps in the current methods that have limited the application of this platform in real buildings. Firstly, although the machine learning-based thermal comfort models and personalized comfort models seem promising, the methods used for data collection, model construction, and control strategy vary greatly, which has resulted in different outcomes. A comprehensive review of pertinent technology and methods to better understand state of the art is missing in the sector. Secondly, there are several constraints in current personalized comfort models that limit the application of these approaches in the actual world setting. The restricted distance between the subjects and the thermal camera, the limited head positions, and the lack of automation in some aspects of model development are some of the addressable issues. Thirdly, while facial thermography has gained lots of recent attention, this is still a new research area that needs to be evaluated and studied in different domains. The lack of facial thermography public datasets is a significant obstacle to research improvement in this area. The limitations in current facial thermography datasets include low resolution[19], limited head position, restricted distance from the camera, and lack of related radiometry data,

which can provide the temperature for each pixel [20]. To capitalize on the potential and address the existing limitations, this dissertation takes a more holistic view of non-intrusive thermal monitoring for personal thermal comfort prediction. In this study, we present a comprehensive and systematic review of the current machine learning-based personalized thermal comfort models. In addition, we will look into collecting facial thermal images from subjects at a farther distance from the camera. We will also create a platform for thermal comfort prediction from facial skin temperature through a completely non-intrusive automated method. The dissertation is unique because it creates an automated approach for utilizing both thermal and visual images to detect facial landmarks in several different head positions.

1.2   Research Background

Thermal comfort models are an approach for quantifying the subjective evaluations of a human's thermal state, which enables a shared understanding of thermal satisfaction. Thermal comfort evaluation is a difficult task due to many influential variables such as air temperature, air velocity, relative humidity, solar radiation, and the subjects' age, gender, clothing level, and activity level. For over thirty years, scientists have studied and applied many human thermal comfort models based on physiological and psychological responses[21]. The Predicted Mean Vote (PMV) is a frequently used model for assessing thermal comfort. Although PMV is currently the most widely used thermal comfort model, it has performed poorly in recent research [22]. The second conventional thermal comfort model is the adaptive model, which works based on the concept that an individual's thermal acceptance is under the influence of outdoor conditions during different times of the year [23]. The majority of today's building control systems rely on these two explicit predefined models, which do not accurately reflect the actual comfort of various occupants in the environment [22]. As a space may be used for various purposes or duties over time, the occupants and their thermal comfort preferences may change. Additionally, the thermal comfort level would be influenced by

human attributions such as age, gender, and metabolic rate. Along with physiological qualities, psychological factors such as emotional state (happiness or anger), and level of stress can significantly influence a person's subjective thermal sensations[22]. This makes it impossible to analyze individuals' thermal preferences and the relative value of each contributing component based on general standards [5]. Personalized comfort is a recent concept in the building design area that focuses on providing a comfortable condition for the occupants based on their preferences. This results from zonal conditioning, instead of the central air conditioning system, and the ability of occupants to change their thermal environment [24, 25]. Personalized models are based on the Human-in-the-Loop (HITL) concept, which has redefined the relationship between humans and their surroundings. Based on this concept, to achieve a high-performance building throughout the operation phase, it is necessary to embrace subjective human aspects in the control loop. Personal thermal comfort models are created based on behavioral or physiological variables associated with an individual's thermal comfort. This research deploys the three basic methodologies of voting, behavior, and physiological sensing as direct feedback from the occupants to regulate their thermal condition[26].

1.2.1   Non-Contact Personalized Thermal Comfort

In an attempt to reduce or eliminate the need for occupants to interact with the environment through voting or other processes, some studies have aimed to discover personalized feedback from human bio-signals. Physiological data is a group of bio-signals that have been proven to have acceptable prediction accuracy for creating data-driven thermal comfort models. Thermal comfort is a cognitive inference that relies on physical, physiological, and other human-related contextual elements and is attained when physiological efforts for thermoregulation are minimal, and the core body temperature is maintained within a narrow range. As a part of this process, the blood flow to the skin's surface is regulated by vasodilation in higher temperature conditions and vasoconstriction in lower ones. Through the operations of vasoconstriction and vasodila-

tion using subcutaneous heat receptors, skin temperature plays an important role in the thermoregulation process. The emergence of thermal imaging techniques provides a great opportunity for contactless skin temperature data gathering with no interruption in occupant conditions and activities. Infrared cameras have the ability to assess the temperature of targeted areas, making them an excellent tool for measuring skin temperature from a distance. Thermal cameras have been proven to be a reliable, non-invasive way to predict the need to change thermal conditions with a 94–95% level of accuracy, while Fanger's PMV method had a prediction accuracy of less than 65% [27]. Researchers have also developed a real-time feedback system using the FlirA35 thermal camera and a depth sensor to analyze both the face temperature and the body pose of the occupants [28]. Further research has revealed the possibility of replacing the previous cameras with a less expensive and smaller infrared camera capable of predicting skin temperature with an acceptable accuracy of 85% [29]. This study has further investigated the possibility of developing a smart thermostat based on the developed prediction algorithms [30]. Thermal cameras have also been integrated with visual RGB cameras for landmark detection and higher accuracy, [31]. Moreover, studies have assessed the effectiveness of several facial feature detection algorithms in identifying areas of interest (ROIs) [32]. In this regard, research has compared the accuracy of three distinct sensor types, including air temperature sensors, wristband-based skin temperature monitoring, and thermal imaging-based facial temperature monitoring. This development proves the marginal improvement in accuracy when physiological sensors are combined with environmental sensors and casts doubt on the efficacy of physiological sensors as a consequence of this marginal improvement in accuracy (3% to 4%)[33] . Li et al. proved successful in monitoring and recording the skin temperature of two subjects concurrently utilizing two thermal camera nodes, each camera catching sections of the subjects' faces [34]. Although facial skin temperature is used as the primary physiological factor for thermal comfort prediction, other studies have considered several

other body parts, including hands, shoulders, and torso [35, 36, 37]. Thermal cameras have also been shown to be a promising tool for the non-invasive prediction of elderly thermal comfort in nursing homes [37].

1.3   Problem Statement

The presented review shows that although the initial results are promising, the platform's application in actual buildings has been limited by a number of major shortcomings. Firstly, the greatest subject-to-camera distance in the present investigations is two meters, making the platform appropriate for relatively small spaces. In addition, it has been proven that one of the major factors that influence Thermal Infrared Reading (TIR) is the shooting distance, which is defined as the distance between the object and the thermal camera. This measure becomes more important in remote thermal readings, where the shooting distance is well over one meter. Although there is awareness of this factor's influence on thermal readings, there has been very little research conducted on this area until recently. Most of the previous researchers had performed their studies at equal distances from the camera to avoid this inconsistency. One main study on the influence of distance on TIR of living organisms was performed in 2016, which studied the shooting distance range from 0.3 to 80 meters. The study showed the powerful influence of the measuring distance on the first 20 meters of the subject [38]. This non-linear decrease can result in an underestimation of the surface temperature. Other studies on the influence of distance on human facial (inner-canthi of the eye) TIR have shown a measurement error in distances larger than 80 cm from the camera [39]. This field application of thermography has shown the strong influence of spot size and shooting distance on the surface temperature of both calibrated temperature sources and wild birds. The decrease in temperature can be as high as 6°C at a 10 meters distance from the subject [40]. Secondly, required Regions of Interest (ROIs) for thermal measurements are often selected manually or with insufficient detection precision. Therefore, in the majority of the current studies, participants are instructed to keep a frontal face posture or have

minimal head position movements due to the limitations of their landmark identification approach. Any change in the human head position will result in a change in the degree between the camera and the facial area. Research has shown that the influence of object position on the camera alters the TIR by affecting the apparent emissivity[40]. This effect may result in errors as high as 8 °C, depending on the target area's emissivity. Additional research has also studied the influence of the angle of the camera on the inner-canthi of the eye temperature, which also aligns with the previous findings. The mean temperature of the inner canthi of the eye has decreased by 0.5 °C at 75 degrees to the camera [39]. Thirdly, the current publicly available facial thermography datasets have several limitations, which make them ineffective for environmental monitoring applications. Due to the lower quality of older thermal cameras, several current thermal datasets are of low resolution[19]. Most of the existing public datasets are not in the original raw format and are converted frames, which results in the loss of important information [20]. In addition, the current public datasets lack diversity in several aspects, such as face resolution and environmental properties. The available datasets are appropriate for facial recognition purposes with no variation in environmental properties such as air temperature and relative humidity. None of the current public datasets include data on controlled thermal variations, which is one of our top objectives in collecting this dataset. While some of the current datasets were recorded in uncontrolled thermal circumstances, resulting in temperature fluctuation, yet there is no information about the ambient temperature at the time of thermography recordings. There are currently no publicly available datasets with varying distances from the camera[41], while several studies have indicated the importance of distance in the infrared thermography readings [40, 38, 39].

1.4   Research Contribution and Objectives

The ultimate goal of this dissertation study is to create a personalized thermal comfort model based on each individual's physiological data that can be further used in the

building's controlling system. To that end, we are focusing on physiological data that can provide information on the individual's thermal comfort. We are examining the possibility of utilizing infrared cameras to gather occupants' skin temperature data from a distance. The project is significant because it creates an automated approach for utilizing both thermal and visual images to detect facial landmarks in several different head positions. The contributions of this dissertation are as follows:

- Firstly, we have developed and published a facial thermography dataset with more than 10,000 infrared thermal images at several distances from the camera and changing head positions. We have also controlled the air temperature to change from 20.5 °C (69°F) to 26.5 °C(80°F). Images are available in at least four different temperatures, ten different relative distances from the camera ranging from 1m (3.3 ft) to 6.6m (21.6 ft), and 25 different head positions.The dataset is annotated with the environmental properties, including air temperature, relative humidity, air speed, distance from the camera, facial landmarks, and subjective thermal sensation of each person at the time.

- Secondly, to address the limitation of a subject's distance from the camera and their position, we implement deep learning-based algorithms for image segmentation and facial landmark detection. By utilizing the powerful HRnet algorithm [42, 43], we have successfully investigated the subjects at a maximum distance of 6.6 meters from the camera and at 25 different head positions. In addition, to resolve the lack of accuracy, we have utilized an automated mapping approach for registering thermal and visual images that can detect the specific ROIs in images of any resolution and head position.

- Thirdly, to increase the accuracy of thermal comfort prediction, we have included the distance from the camera and head position as inputs to the prediction algorithms. Our results have indicated that including the distance and head position

in the prediction process can increase prediction accuracy in general.

- Finally, we conducted a comprehensive search of the most current personalized thermal comfort research that has utilized machine learning approaches to create their comfort models. The purpose of this contribution is to emphasize the use of machine learning to personalize thermal comfort studies. In addition, we highlight and compare their associated methodologies and performances in several aspects.

Our research deliverable will address the following hypotheses: *By using integrated thermal and visual cameras and including physical conditions as input variables, we can create an accurate personal thermal comfort model for subjects at different distances from the camera* In this research, we will answer two fundamental questions:

1. Can we perform automated facial skin temperature readings at farther distances from the camera by adding visual cameras to the platform?

2. Can we develop a non-contact personalized thermal comfort model for subjects in the distance?

The objectives of this project are in three key areas:

1. Integrating visual and thermal cameras for a higher resolution reading of facial temperature.

2. Developing a comprehensive facial thermography dataset that includes images in different thermal conditions, in addition to several distances from the camera and different head positions.

3. Creating a personalized thermal comfort model for controlling the building's indoor temperature and comparing the prediction accuracy of different supervised learning algorithms.

1.5   Dissertation Outline

The rest of this dissertation has four main sections. Chapter 2 presents a comprehensive and systematic review of the current machine learning-based personalized thermal comfort studies. Chapter 3 presents our recently developed dataset, which we call the Charlotte-ThermalFace dataset. In this chapter, we look into the applications of facial thermography in different domains. Then we study and compare the existing publicly available thermal datasets with a brief description of each. Moreover, we introduce our developed dataset and how we address some of the existing gaps by publishing our dataset. Finally, we provide a preliminary analysis of the dataset to show its applicability for future projects. Chapter 4 presents a detailed explanation of the model development and evaluation. In this chapter, we explain the data collection process, followed by data extraction and analysis. In addition, we present the influence of room temperature, distance from the camera, and head positions on the skin temperature and infrared thermal readings. The results of the two selected prediction algorithms are discussed in detail. Include a final review of the highlights of this dissertation and the achievements of our study in Chapter 5. We also present a future outlook in the continuation of this work.

CHAPTER 2: A Review of Machine Learning Applications in Smart Buildings to Provide Personalized Thermal Comfort

2.1   Introduction

Thermal comfort models are an approach for quantification of human subjective evaluation and their thermal state to provide a common understanding of thermal satisfaction. Thermal comfort evaluation is a difficult task due to many influential variables such as air temperature, air velocity, relative humidity, solar radiation, and the subjects' age, gender, clothing level, and activity level. Scientists have been studying and using several human thermal comfort models for over 30 years based on both physiological and psychological responses [44]. Although the building sector consumes approximately 40% of the globally produced energy, the majority of which is used in heating, ventilation, and air conditioning (HVAC) systems, people are generally dissatisfied with their environmental comfort conditions [1]. Schedule-based and predefined environmental control is one of the main reasons for the current discomfort and dissatisfaction with the indoor thermal environment. These general standards make it impossible to consider people's differences in thermal comfort levels. Recent research is attempting to leverage occupants' demand in the control loop of the buildings to consider the thermal satisfaction of each individual based on their own physiological properties, which is called personalized comfort models. Personalized comfort is a recent concept in the building design area that focuses on providing a comfortable environment for the occupants based on their preferences. Personal comfort models are developed based on each individual's physiological or behavioral data that are linked to their thermal preferences. The promising results of personalized thermal comfort modeling make it an excellent component for smart buildings. The Internet of Things is one of the recent

technologies that have made this approach easier by providing a connection network among several devices and occupants in a building. A real-time monitoring system is used in buildings equipped with IoT to provide the needed infrastructure and make this a feasible task. IoT-based systems, in combination with HITL approaches, warrant intercommunication between various devices and also facilitate the communication of information that is used for sensing, actuation, and control. The information collected by IoT sensors from the users regarding their behaviors and preferences has been used to modify and regulate building systems such as heating, ventilation, and air conditioning. Smart buildings are known for their capabilities in using Artificial Intelligence (AI) and data processing to provide energy savings, enhanced occupant comfort, improved safety, and better maintenance. The term "learning ability" was added to this definition after the increasing use of AI to design smart buildings that can learn their performance from the occupants and environment [16]. Therefore, the *learning* approach is another key factor that influences the reliability and efficiency of the proposed personal comfort model. Machine Learning (ML) methods as a subset of AI have great potential for creating thermal comfort models [17]. Several machine learning algorithms have been used lately to compare the prediction accuracy of different models in both lab and field environments. The purpose of this work is to emphasize the use of machine learning to personalize thermal comfort studies. In this review, we conducted a comprehensive search of the most current personalized thermal comfort research that has utilized machine learning approaches to create their comfort models. In addition, we highlight and compare their associated methodologies and performances in several aspects.

2.1.1   The necessity of a literature review

While machine learning and personalized thermal comfort are relatively new subjects in the area, there has been increasing attention to both of these topics in recent years. Nevertheless, despite the considerable advancements in the field, a detailed and critical review of the subject is still missing. There are currently several review studies on the

related research areas, especially since 2020. Qolomany et al. have surveyed the area of smart building with a special focus on the role of techniques from machine learning and big data analytics [45]. Researchers have also provided a comprehensive overview of different data-driven approaches and processes for predicting personal thermal comfort in a building environment [46]. In their study, through a classification procedure and a comparison of their prediction accuracy, a particular focus was made on modeling methodologies throughout the chosen research. Intelligent buildings in general, were also the subject of review articles with regard to both thermal comfort and energy saving. Qavidel et al. have reviewed the application of machine learning in thermal comfort studies and highlighted the latest methods, findings, performance, and challenges [17]. Moreover, Ref.[47] offers a complete and in-depth systematic analysis of AI-based approaches utilized for building control systems by evaluating the findings of these approaches, their applications in the studied works, and their ability to increase energy-efficiency while retaining thermal comfort. Another survey in the area has investigated the experimental approaches in the design and implementation of thermal comfort monitoring technologies [48]. The work provides insights into the inputs that influence personal thermal comfort, smart technologies and methods used for sensing and detection, and approaches for processing collected data. Another recent study also performed a review to summarize recent occupant-centric thermal comfort practices in three main areas of sensing, predicting, and controlling [49]. In regards to personal thermal comfort modes, Martins et al. have presented a comprehensive review by examining several aspects, including data collection approach, dataset size, participants involved, climate, seasons, building type, model variables, modeling algorithm, performance indicators, and final application [50]. These recent and thorough studies show how important smart buildings, personalized comfort, and data-driven research methods are in this field. However, none of the previous reviews have investigated the current research with a particular focus on the implementation of machine learning algorithms

for developing personalized thermal comfort models. We believe that this review would be helpful in identifying the similarities and differences between the specifics of the study data collection process and the predictive modeling involved. Future fieldwork studies will be facilitated and guided in several research aspects through this methodical review.

2.2   Structured literature review methodology

To conduct a comprehensive search of the publications in this area, we have identified three sets of keywords to create a logic grid for the paper selection process. As Table 2.1 shows, the keywords were selected from our three main focus areas, which are "machine learning", "personal", and "thermal comfort". There are several literature databases and search engines available. Scopus and Google Scholar were chosen because they are believed to be among the most complete databases of abstracts and citations of peer-reviewed literature, and their search engines are easy to use and easy to access. Machine learning-based personal thermal comfort modeling research has only grown in recent years. Since there were few systematic modeling studies before 2015, publications published since 2015 were chosen for investigation. After reading their abstracts, unrelated articles were eliminated. In addition, references and citing articles of the first-stage papers were thoroughly searched to add more related publications. Through this process, 50 peer-reviewed publications, including journal articles and conference manuscripts, were selected to be reviewed. Figure 2.1 presents the reviewed aspects of the collected studies in this survey.

Table 2.1: Logic grid for the keywords

Machine Learning"	AND	"Personal"	AND	"Thermal Comfort
machine learning" OR		"personal" OR		"thermal comfort" OR
supervised learning" OR		"personalized" OR		"thermal " OR
unsupervised learning" OR		"user-centered" OR		"temperature" OR
reinforcement learning" OR		"individual" OR		"HVAC" OR
"Smart" OR		"occupant-centered"		"air condition" OR
"IOT" OR				"comfort" OR
"Artificial Intelligence"				" satisfaction"
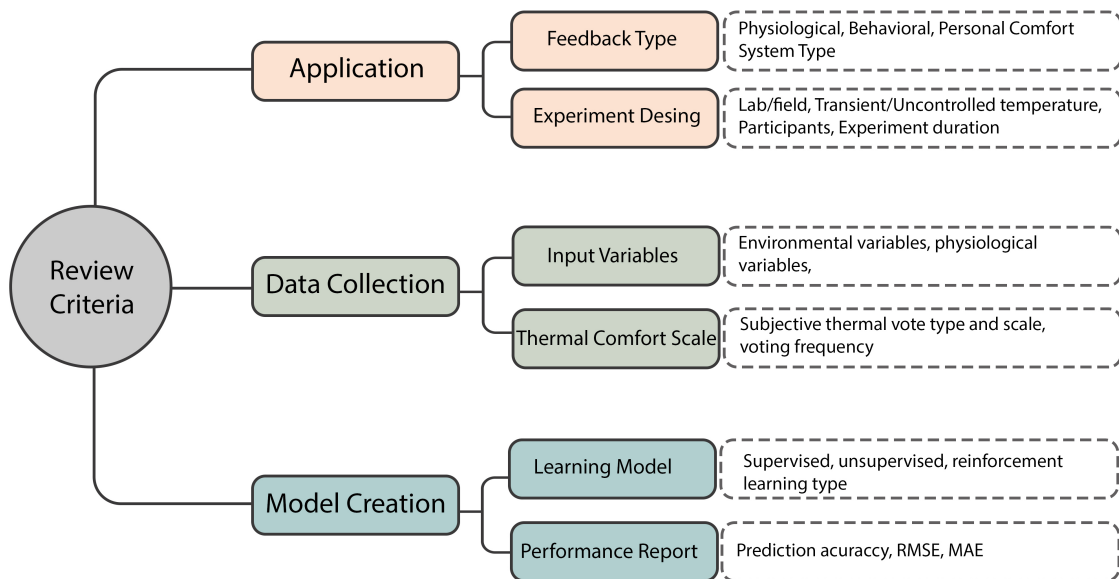
Figure 2.1: Feedback Collection Systems

2.3   review results

We have investigated the selected publications based on three main aspects: their application; data collection method; and model creation strategy. As Figure 2.1 displays, each of the mentioned aspects includes additional review categories, which are explained in the following sections.

2.3.1   Feedback Collection System

For accounting human comfort and preferences in the building system, it is crucial to find the acceptability of the control settings based on the current occupants' feedback. The gap between the conditions that are delivered and those that are desired by the occupants may be narrowed by incorporating the thermal preferences of users into the decision-making processes that are carried out by control systems. In order to achieve this goal, the Human-in-the-loop (HITL) approach has reconsidered the link that exists between people and the indoor environment. In order to maintain a high level of performance throughout the operating phase of a building, it is necessary to take into account a variety of human factors within the control loop. Building management performance may be improved using HITL strategies to make the most of the input provided by users and to obtain an adaptive model after each cycle of the process, Jung et al. [26]. As our investigations indicate, the feedback system structure is one of the main characteristics of a personalized HITL system. The feedback type and collection method can categorize the reviewed research into two main groups: behavioral data collection and physiological data collection. As Figure 2.2 displays, the reviewed personalized comfort devices can be further categorized into four main groups, which are explained in this section.
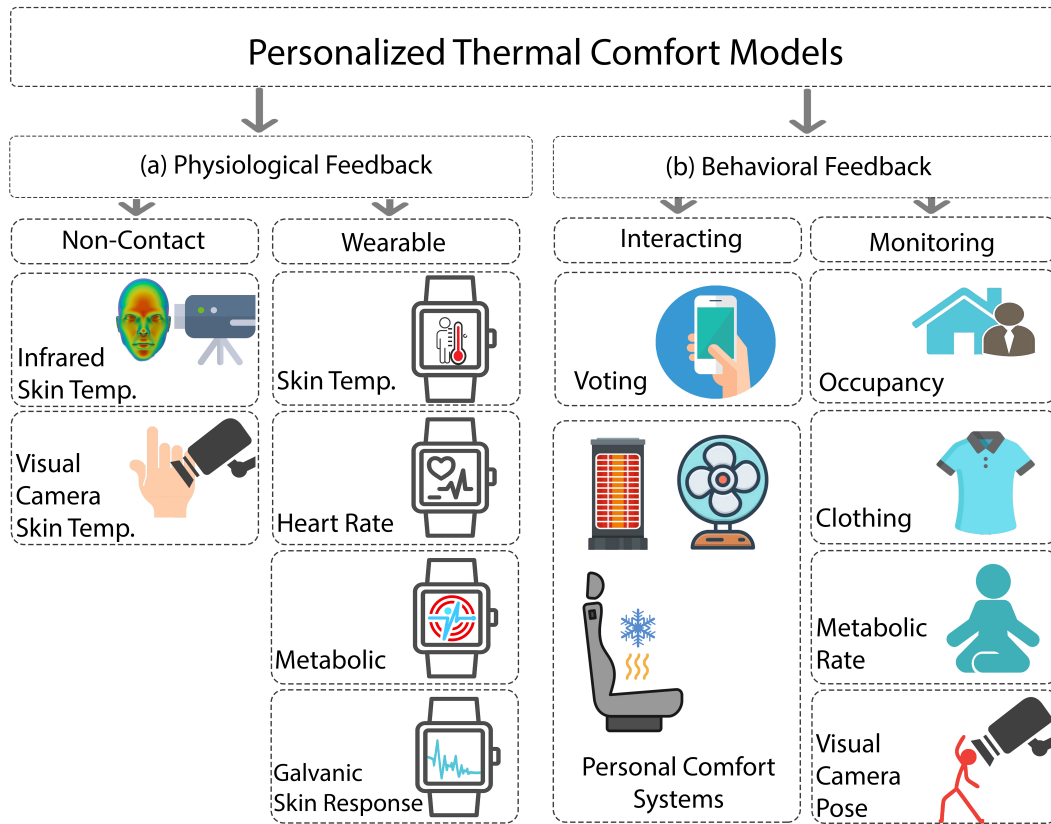
Figure 2.2: Feedback Collection Systems

2.3.1.1   Behavioral

Some of the current personalized thermal comfort research uses behavioral feedback to provide information about the occupants' conditions or preferences to the control loop. A group of these platforms monitors the influencing variables in subjects' thermal state, such as the occupancy status, clothing level, metabolic rate and activity, and discomfort or comfort-related postures. This research utilizes a visual camera or occupancy and motion-related sensors to gather the information without the need for occupants' interaction with the system. Another type of behavioral feedback is the interaction that users have with the environmental control platform, which can be through voting applications or interaction with personal comfort systems.

Monitoring: Based on the reviewed studies, we have categorized behavioral-based mon-

itoring thermal comfort models into four main groups: occupancy, metabolic rate, clothing level, and posture estimation. Peng et al. [51] have proposed thermal comfort prediction models using occupancy data in addition to environmental temperature information in personal office spaces. Using digital data from motion sensors, room occupancy information was extracted. To do this, a time delay is calculated to evaluate the movement data in terms of occupancy, which is the minimum time between two sequential movements. If no movement is detected within the set time frame, it is presumed that no individuals are present. In another research, user personal desk fan usage preferences were recorded, together with user presence data and indoor and outdoor environmental factors. Tree-based approaches were examined to predict the switching on and off of desk fans and to estimate the fan speed that the user desires. In Ref [52], a visual camera is used to recognize indoor human activity, which is then utilized to determine the metabolic rate. Visual cameras were also used for the identification of clothing insulation. Zang et al. proposed a machine learning classification technique that could translate an individual's visual image to various metabolic rates and clothing level [53]. Yang et al. have successfully used machine learning algorithms to identify human thermal conditions based on their poses [54]A digital camera captured images of occupant positions linked to thermoregulation systems, and the appropriate two-dimensional coordinates were acquired. These positions have been transformed into skeleton shapes. An algorithm was created to identify thermal discomfort-related postures, such as self-hugging and wiping sweat from the forehead. The platform could distinguish twelve thermal discomforts associated with human postures.

Interacting: Voting platforms are one of the main types of subject interaction methods with the control system to provide feedback. In the voting system, thermal scale preferences are used for quantifying the comfort to be utilized in participatory sensing systems [55, 56, 57]. Earlier research studies had utilized surveys at office buildings to collect feedback data from the employees, which was successfully implemented in cre-

ating thermal comfort models[58]. Guenther et al. have tried the voting system as the only feedback form from users about their thermal condition in a relatively large office building [55]. User input was gathered as part of everyday work tasks and utilized for the creation of a customized comfort prediction model, which enabled the creation of personalized thermal conditions. In some other studies, voting systems are used as an addition to another type of feedback data, such as physiological conditions, which will be further discussed in the next section. The voting systems require continuous feedback input from the occupants. Another approach is to investigate the user's interaction with the provided thermal regulation devices for the purpose of learning their thermal preference. Monitoring occupant behavior while using thermal control devices may be considered non-intrusive and provide feedback for determining people's thermal comfort. Personal Comfort Systems (PCS) are small portable heating and/or cooling devices that are capable of modifying the thermal condition on a personal level. The thermal conditions are controlled by devices that can be located on desktops, ceilings, or floors based on the building's mechanical system design and architectural planning. "Task Ambient Conditioning" (TAC) was first used to define localized and small space conditioning systems, which were then replaced by the term "Personal Environmental Control" (PEC). This term includes both Personal Ventilation Systems (PVS), and Personal Comfort Systems (PCS)[59]. As it can be inferred from their names, the difference between these two systems is due to ventilation through outdoor air in the former. However, the regulation in the PCS is only related to the thermal conditions of the microzone[59]. As an example, for a PCS, a heated and cooled chair provides local heating and/or cooling through integrated heating strips and fans [60]. Through the use of personal thermal control devices, we can directly connect individual comfort to the corresponding behavior. Recently, monitoring occupant engagement with thermal control systems has become more cost-efficient due to decreasing sensor costs and pervasive wireless connectivity in buildings. In addition, it is promising to include

this feedback into the environmental control loop since IoT advancements have signifi-icantly decreased the difficulty of the required devices' communication. Continuous data collection may be automated when the basic infrastructure is set up, demanding only routine activity from the users. As a result, thermal comfort devices provide a great way to study user thermal preferences. Personal comfort models are developed based on each individual's behavioral data and are linked to their thermal preferences. In addition to using and configuring predictive models correctly, selecting the right equipment for each setting is essential for environmental control to work at its optimum. Some of these devices that have been used and studied until now are heating and cooling chairs [24, 61] , desk fans [62, 63], air jets [64], and foot warmers [18]. One of the early studies on the subject of PCS automation is by Kim et al., which works on the prediction of thermal comfort when utilizing a cooling/heating chair [60]. In this study, the researchers tried to learn the occupant's heating and cooling behavior and predict the thermal comfort based on this data. Their best-performing algorithm for personal comfort models had a median accuracy of 0.73, which was higher than the predictions made by traditional comfort models (PMV and adaptive), which had a median accuracy of 0.51 at the time. Other related research has studied the prediction performance of neural network-based models for the prediction of personalized heating settings, using environmental features as the input factors [65]. According to the results of their online testing, the test participants were satisfied with the heating settings that were automatically regulated using models built based on the acquired data. Researchers of the same study have also combined PCSs with monitoring physiological parameters of skin temperature for the thermal comfort prediction [66]. This research has also compared the prediction performance of the model when utilizing different input parameters, including behavioral factors (PCS control intensity), physiological factors (skin temperature), or environmental factors. The results prove that the prediction accuracy is higher when inputting personal parameters in addition to just environmental factors. Also, the performance of

the model was approximately the same when selecting behavioral or physiological parameters as the input features. Another study in this area has worked with the personal thermostat levels in an office building with individual rooms [51]. The study presents an online-learning-based control method to build an occupant-centric indoor thermal environment. The findings of the experiment indicate that occupant preferences in the different rooms vary with respect to thermal settings. In addition, during the learning period, the number of weekdays per month on which occupants needed to alter room temperatures based on their satisfaction decreased from four to nine to a maximum of one [51]. PCSs can provide thermal comfort for the occupants and energy savings for the building. However, this highly depends on the type of device and the microclimate control strategy. The HVAC systems in commercial buildings regulate the indoor temperature by maintaining a narrow range of set points, which are mostly pre-defined. Not only does this approach fail to provide comfort for all inhabitants of a building, but it is also responsible for around 20% of total energy consumption in buildings [67]. Personal comfort devices provide the possibility of relaxing the central indoor set point in both heating and cooling mode. This will result in 10% of energy savings per degree C and will also prevent energy waste caused by actions such as simultaneous heating and cooling in HVAC systems to maintain the setpoint [68]. Another research has reported energy savings ranging from 4 to 25 percent [51] after providing personal thermostats for occupants of an office building. Ngarambe et al. have also created thermal comfort predictive models using ML and their implementation in building control systems for energy saving [69].

2.3.1.2 Physiological

In an attempt to reduce or eliminate the need for occupants to interact with PCSs during voting or adjusting the devices, studies have aimed to discover personalized attributes from human bio-signals. Physiological data is a group of bio-signals that have been proven to have acceptable prediction accuracy for creating data-driven comfort

models. For personalized comfort model development, a variety of personal characteristics, such as skin temperature, heart rate and pulse, and other occupant information, were investigated [70]. Recent commercially available wearable devices enable the affordable and accurate collection of real-time heart rate, pulse, and activity data. Due to the simplicity with which these wearable devices and computers or smartphone applications may be linked, biometrics can be simply integrated into a predictive thermal comfort model. Thermal comfort is a cognitive inference that relies on physical, physiological, and other human-related contextual elements and is attained when physiological efforts for thermoregulation are minimal, and the core body temperature is maintained within a narrow range. As part of these processes, the blood flow to the skin's surface is regulated by vasodilation at higher temperatures and constriction at lower ranges. Through the operations of vasoconstriction and vasodilation using subcutaneous heat receptors, skin temperature and skin conductance play important roles in the thermoregulation process. Given the strong association between thermal sensation and skin temperature, the most common technique has been to use skin temperature [71]. Skin temperature at different body parts is one of the most successfully used variables for developing a personalized comfort model [72, 31, 73]. Non-contact thermal cameras have also been used to measure the skin temperature for creating a personal comfort model [74, 18, 75]. The heart rate and pulse rate were the second and third most preferred physical factors due to their superior ability to represent variations in metabolic rate when individuals alter their activity level [76]. According to these investigations, there is a moderate correlation between changes in heart rate and thermal sensations or environmental factors. In particular, compared to more complex levels of thermal comfort perception, heart rate seems to correlate with a three-class thermal comfort rating [77]. In the physiological feedback system, these two previously proven indicators of thermal comfort are used individually as skin temperature [78, 79] or together [76]. Some other researchers have utilized the skin galvanic response as

the best prediction variable with a high prediction accuracy among other physiological variables[80, 81]. Skin conductance or skin galvanic response refers to the convective heat transmission by blood circulation and conductive heat transfer through the skin layer [82]. Electroencephalography (EEG) and electrocardiogram (ECG) signals are also used to measure human thermal comfort. We can monitor EEG and ECG signals using biomedical equipment as well as with inexpensive wearable devices that are currently on the market. In the first approach, the user's head is covered with a helmet with electrodes to capture these signals. It is possible to create models that distinguish between various sentiments related to thermal comfort using the spectral power of EEG [83]. It was also shown that correlations between the user's temperature perception and EEG indices are possible. However, wearing an EEG helmet throughout the day is impossible. Table has displayed the research that has used skin temperature, heart rate, metabolic rate, and clothing level as the four mostly user-related variables. In this study, we have categorized the physiological-based data gathering platforms based on their application methods, which can be (a) wearable or (b) non-contact:

Wearable: The wearable data collection devices are either lab-grade sensors or commercially available personal wristbands. Thermocouples and thermistors with connecting wires are often utilized in lab-grade sensors and were frequently used in early thermal comfort studies. Although this sort of sensor often has the benefit of high precision, the connections and wires do significantly reduce the application's convenience. A lot of thermal comfort research requires high precision and continues to employ intrusive sensors with great accuracy [82, 64, 76]. Researchers have also measured the variations in the heat exchange rate (heat flux) and skin temperature during gradual transient temperature shifts by placing heat flux sensors on participant skin at the wrist and facial area. Investigations were conducted into the relationships between occupant thermal preferences, the ambient environment, human-environment heat exchange, and thermophysiological responses. They have found strong positive correlations between

heat exchange rate and thermal preferences, whereas strong negative correlations were found between air temperature and skin temperature. Other user-centered models utilize wristbands to gather physiological data such as skin temperature, heart rate, and skin conductance to predict the comfort condition of each occupant. Due to the personalized character of wearable technology, the data produced by streaming is distinctive. By utilizing Microsoft Band 2, researchers have successfully had the ability to comprehend user behavior and anticipate demands in the[84]. Another study has utilized the Empatica E4 wristbands, which were used to measure Analysing Electrodermal Activity (EDA), heart rate, and skin temperature [85]. In order to be integrated with the IoT data gathering platform, both of these wearable devices provide source data through an API. The Polar H7 strap was outperformed by the use of wearable devices to measure heart rate [76, 86]. Researchers also employed heart rate variability analysis software, which focused exclusively on heartbeat-related factors for thermal comfort study [60]. Wearable devices were also used in another article to investigate the impact of activity-based metabolic rate on predicting personal thermal comfort [87]. In this study, wearable sensors and machine learning techniques were utilized to continually monitor and analyze individual physiological data, activity-based metabolic rates, and environmental indicators. Results indicated that predictive models that took metabolic rate into account produced an improved performance of up to 8.5 percent, suggesting that activity-based metabolic rates provide a better knowledge of individual thermal comfort. These data-gathering approaches are intrusive as the sensor devices need to be in contact with the human skin throughout the day, which may be distracting in a work environment. The need for a contactless data gathering approach is also important in healthcare facilities, where using a wristband sensor may not be preferable for patients. In addition, it requires sensors for each occupant of the workplace, which is not always possible. This data-gathering shows the extent to which considering contactless, non-intrusive approaches can be beneficial for obtaining personal physiological data for each occu-

pant.

Non-contact Devices: The emergence of visual and thermal imaging techniques provides a great opportunity for contactless data gathering with no interruption in occupant conditions and activities. In this research, we are looking into the possibility of a non-contact vision-based method from a distance for gathering occupants' thermal condition data.

Infrared Images: The internal energy of any physical system can be quantified by temperature continuously. Thermal radiation is the electromagnetic wavelength between (0.75-1000m) that is emitted from any object or subject with a temperature above absolute zero [88]. IR cameras produce thermal images by measuring this radiation from a surface, which is a function of its temperature. As body temperature increases, the human body emits more infrared radiation, which is detectable through infrared thermal cameras. There are several studies investigating the feasibility of using a thermal scanner instead of traditional oral or other invasive thermometers. [89]. There has been increasing evidence in the literature that Transmitted Infrared Photography (IRTs) can provide greater accuracy in estimating body temperature than Non-Contact Infrared Thermometers (NCITs). A study that directly compared an NCIT to three IRTs indicated the NCIT was less accurate [90]. The infrared cameras can be installed at a distance from the occupant and capture the skin temperature by reading the pixel values of the desired regions. By proving the feasibility of this technique with an accuracy of 94% -95 % when using FLIR A655sc

Table 2.2: General Study Information

Study		Location		Control Mode			DataCollection			Prediction			Personal Comfort system
Ref.	Year	Lab	Field	Transient	Uncontrolled		Behavior	Voting	Physiological	S	U	R	
[83]	2020	X		16-30°C				X	X	X			Personal comfort prediction using electroencephalo-gram (EEG)

Table 2.2: General Study Information (Continued)

Study		Location		Control Mode			DataCollection			Prediction			Personal Comfort system
Ref.	Year	Lab	Field	Transient	Uncontrolled	Behavior	Voting	Physiological	S	U	R	
[84]	2020		X		NM		X	X	X			Utilizing wearable devices as a component of an IoT setup
[60]	2018		X		22.2-26.9°C	X	X		X			Heating/cooling chair
[66]	2020	X			Avrg. : 20.1°C	X	X	X	X			Heated Chair
[91]	2020		X		20-27°C	X					X	Window opening behavior
[87]	2020		X		Avrg. : 23.3°C		X	X	X			Importance of metabolic rate
[92]	2018		X		NM		X	X	X			Connecting sensors through IoT
[51]	2019		X		20.5-24°C	X			X			Saving energy by learning occupant thermostat preference
[76]	2019		X		17.1-34.8°C		X	X	X			Attached sensors to the body for at least 14 days/ 20 hours per day
[31]	2019	X		21.11-27.78°C			X	X	X			Combination of visual, thermal and depth camera, skin temperatures and mean clothing temperatures for clothing covered body parts
[55]	2019		X		NM		X		X			Considering fan level for comfort prediction
[93]	2019		X	24-27°C		X			X			Predicting desk fan usage and its speed
[64]	2019	X		26-32°C			X	X	X			Thermal Sensation in different body parts and localized airflow

Table 2.2: General Study Information (Continued)

Study		Location		Control Mode		DataCollection			Prediction			Personal Comfort system
Ref.	Year	Lab	Field	Transient	Uncontrolled	Behavior	Voting	Physiological	S	U	R	
[94]	2019	X		20-30°C			X	X	X			Measuring heat flux (heat exchange rate) in face and wrist
[95]	2020	X		Constant: 20°C			X	X	X			Influence of red and blue colors on thermal comfort in real and VR setting
[85]	2018		X		18.8-25.06°C		X	X	X			IoT for utilizing both wearable and environmental sensors in a field investigation
[70]	2021	X		15-26°C			X	X	X			Exposing subjects to cold discomfort, warm discomfort and transient condition
[96]	2021	X		20-21°C		X	X		X			Using a small robot to detect the occupants' metabolic rat and environmental data
[97]	2015		X		NM		X	X	X			Long term monitoring of subjects preference (as long as 90 days)
[98]	2015		X		NM		X	X	X			Study of users' thermal comfort at their home environment-galvanic skin response, heart rate, step count,calorie consumption,approximate sweat level

Table 2.2: General Study Information (Continued)

Study		Location		Control Mode			DataCollection			Prediction			Personal Comfort system
Ref.	Year	Lab	Field	Transient	Uncontrolled	Behavior	Voting	Physiological	S	U	R		
[99]	2016	X		25.6-32°C			X	X	X				Prediction of personal thermal sensation with environmental factors, metabolic rate , and clothing level
[73]	2017	X		14-26°C			X	X	X				Thermocouples attached to 28 body locations
[100]	2017				NM		X	X	X				Predicting thermal sensation through 3 environmental sensors and Microsoft band2
[56]	2017	X			$\approx 19-29C$		X		X				Learning occupants' thermal sensation through long term voting using SVM
[57]	2017		X		NM		X		X				Gathering online votes in a library and office through QR code in a poster by the sensors
[101]	2018	X		18-27°C			X	X	X				In addition to thermal sensation four subjective responses of thermal comfort,thermal preference,humidity sensation,airflow sensation were recorded
[102]	2018	X		18-29°C	25°C		X	X			X		Skin temperature reading through an infrared sensing system installed on an eyeglass frame

Table 2.2: General Study Information (Continued)

Study		Location		Control Mode		DataCollection			Prediction			Personal Comfort system
Ref.	Year	Lab	Field	Transient	Uncontrolled	Behavior	Voting	Physiological	S	U	R	
[103]	2018	X		18-30℃			X	X	X			Predicting thermal comfort through heart rate
[104]	2019	X		18-30℃			X	X	X			Using deep transfer learning techniques to train the thermal comfort model, the model training use the transferred knowledge from the existing datasets
[81]	2018		X		NM			X	X			Creating personal comfort model with physiological factors including Galvanic Skin Response
[65]	2020	X			Avrg. : 20.1℃	X	X		X			The environmental parameters and user behavior to predict thermal comfort using a heated chair
[105]	2019	X		20/24/28℃ 20-28℃			X	X	X			Prediction of thermal comfort through contrast in thermal images
[53]	2019	X			NM			X	X			Machine learning is used for defining subject's metabolic rate and clothing level through RGB videos
[106]	2019						X		X		X	Using ASHRAE database to create a personalized thermal comfort model through reinforcement learning

Table 2.2: General Study Information (Continued)

Study		Location		Control Mode			DataCollection			Prediction			Personal Comfort system
Ref.	Year	Lab	Field	Transient	Uncontrolled	Behavior	Voting	Physiological	S	U	R	
[107]	2019						X		X		X	Deep reinforcement learning-based model in TRNSYS simulated environment
[36]	2019	X		14.4-29.9°C			X	X	X			Personalized thermal comfort using skin temperature extracted from thermal camera
[108]	2019	X		19-29°C			X	X	X			Personalized thermal comfort using skin temperature extracted from different facial parts
[109]	2019		X		Avrg. : 20.1°C		X	X	X			A transfer active learning framework to minimizes the number of labeled examples via active learning
[110]	2020		X	20/24/26°C			X	X	X			Prediction of thermal comfort in and office with natural ventilation and personalized ventilation through simulation
[111]	2020	X		26/33°C			X	X	X			Personal comfort prediction using electroencephalogram (EEG)
[80]	2020		X		NM	X	X	X	X			Thermal comfort learning through user's interaction with an infrared radiant heating panel for 6 weeks

Table 2.2: General Study Information (Continued)

Study		Location		Control Mode		DataCollection			Prediction			Personal Comfort system
Ref.	Year	Lab	Field	Transient	Uncontrolled	Behavior	Voting	Physiological	S	U	R	
[18]	2020	X		19-31°C		X	X	X	X			Personalized comfort systems using personal fan and radiant foot heaters
[112]	2022	X		21-30 °C			X	X	X			Thermal comfort temperature through skin temperature from sensors attached to several body parts in addition to environmental temperature
[113]	2021		X		NM		X		X			Using the existing ASHRAE dataset for personal thermal comfort prediction
[82]	2021	X		18-30°C			X	X	X			Detailed study of thermal sensation
[114]	2021	X		19-30°C			X	X	X			Hybrid physics-based/data-driven model for personalized thermal comfort prediction
[29]	2018	X		22-28°C			X	X	X			Thermal comfort prediction through skin temperature in different facial parts through low-cost thermal camera
[27]	2016	X		23-26°C			X	X	X			Recording thermal images in the field for thermal comfort prediction

2.3.2   Experimental Condition

The experiment design varied in the reviewed research based on the goals and objectives of each study, the available equipment, and the limitations. One of the main aspects that we have reviewed in this article is the experiment location. The experiments were generally conducted at two main locations: the lab environment and the field, based on the research objectives. Field research is research undertaken in the natural environment, such as an existing office building. This type of experiment seeks to observe, analyze, and explain what already exists, as opposed to influencing a studied aspect. Preserving the regularity of the environment, the study settings mimic scenarios seen in everyday life [115]. In contrast, controlled lab research is done in an environment intended exclusively for the thermal condition of the study. Laboratory research is characterized as a controlled examination in which the researcher manipulates a specific component, such as thermal conditions, to evaluate whether or not such manipulation produces a change in the participants. As shown in Table 2.3.1.2, most of the lab-conducted experiments are intended to create a transient thermal condition for the subjects to provide as many data points as possible. The transient or constant thermal condition is an important feature of the data collection experiment. , Cosma [31] , and Aryal [108] have designed their experiment in a transient thermal condition. The model used by Youssef et al. [86] was trained under step-changing circumstances. Because most people spend their time in environments close to thermal neutrality, it is more difficult but more beneficial to anticipate occupants' thermal comfort perceptions in near thermal neutral circumstances than the cold or hot sensation in extreme situations. Another important factor that we have reviewed in our survey is the number, gender, and age range of the participants, which are displayed in Figure 2.3. As the objective of all the studies is the creation of a personalized comfort model, instead of working with many subjects, more data points need to be gathered from a smaller number of subjects. Since gender difference has proved to be an influencing factor in predicting the thermal com-

fort state, it is desirable to have participants from different gender types in relevant experiments.
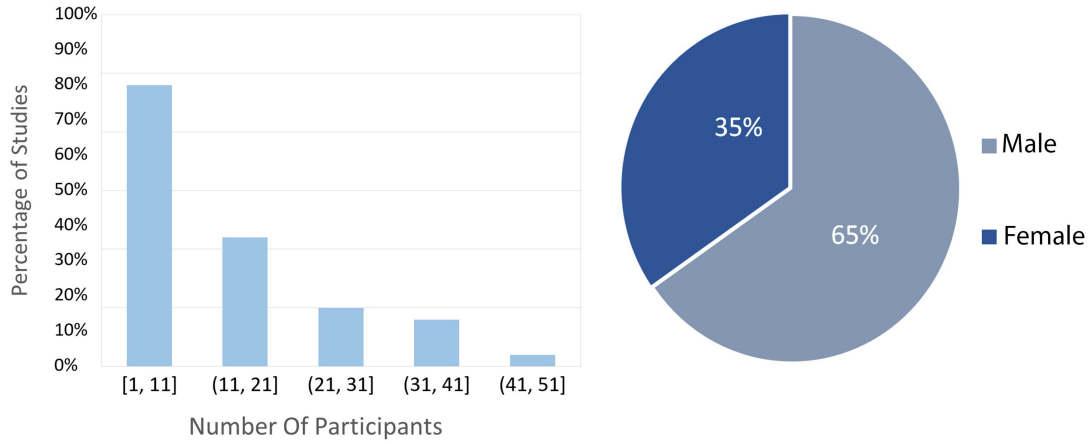
Figure 2.3: Feedback Collection Systems

2.3.3   Thermal Scales

Thermal comfort models are a method for quantifying human subjective evaluations and thermal states in order to provide a common understanding of thermal satisfaction. To evaluate this thermal state, we need a subjective voting scale to report the thermal comfort state as accurately as possible. Generally, a categorical value is used to describe the response variable assessed by either thermal sensation, thermal preference, or thermal acceptance. The majority of the research under consideration utilizes the users' thermal sensation (TS) input to determine thermal comfort along with the seven-point scale Fanger used to define the PMV. Due to its capacity to give enough answer options, the subjective rating system with a seven-point rating scale is the most common rating system for assessing the thermal sensation. The seven-point ASHRAE thermal feeling scale is as follows: hot (+3), warm (+2), slightly warm (+1), neutral (0), slightly cool (1), chilly (2), and cold (3). Since, in some research, the aim is to predict simply thermal comfort or discomfort, they have applied the reduction of scales to two levels after data collection for model training to simplify the models and use a thermal acceptance scale

[82]. The scales might also be reduced to three values for maximum simplicity. It would also allow for reporting the adjustment's direction, such as whether the set point should be decreased or increased. The 3-value thermal preference scale of ASHRAE 55 is recommended for simplifying the model and improving the model's accuracy [61]. Aryal et al. have utilized thermal satisfaction in addition to thermal sensation in their study [18]. Thermal preference is also another scale mostly in research that attempts to control the thermal condition based on the user's preference. To suit their particular modeling needs, several modelers have chosen to adapt existing scales or develop new ones, such as 5-point [105] or 11-point [94] thermal preference. Table

Table 2.3: Subjects' Information and subjective thermal votes

Study	Participants				Timing	Data Points					Total
Ref.	Total	Male	Female	Age	Clothing	TSV	TPV	Scaled	Duration	Voting Frequency	Votes
[83]	3	3	0	23-25	Summer Cloth	7points			15 sessions 30 min.	Every 1 min. for the last 10 mins.	150
[84]	3	2	1	20-24	Variable	12points		3points	Not mentioned	Not mentioned	54-143
[60]	34	NM	NM	NM	Variable		3points		Apr. & Oct. 2016	3 times a day	33-218
[66]	2	0	2	29	0.72-0.92 clo	7points		3points	14 sessions 4 hr.	15 min.	238
[87]	10	6	4	27-36	Summer Cloth 0.5-0.6	7points	3points		8 hr.	5 min.	63-115
[92]	8	5	3	29-61	NM	7point			4-5 Days	NM	NM
[76]	14	8	6	20-38	Variable	7points	3points		14 days 20 hr.	12/day	164-393
[31]	24	11	13	NM	0.44 clo	7points		5points	27 mins.	1 min.	27
[55]	14-20	NM	NM	NM	Variable	7point			NM	1-2 hrs.	NM
[93]	8	5	3	26-35	Variable	12points			Not mentioned	Not mentioned	54-143
[64]	50	34	16	20-25	Summer Cloth 0.4-0.6	7points			2-3 sessions 20 min.	5 min.	NM

Table 2.3: Subjects' Information and subjective thermal votes (Continued)

Study	Participants				Subjective Vote Timing	Data Points					Total
Ref.	Total	Male	Female	Age	Clothing	TSV	TPV	Scaled	Duration	Voting Frequency	Votes
[94]	18	12	6	NM	Variable		11points	3points	100–120 min	When feeling a change in thermal preference	NM
[95]	25	13	12	avrg.: 45.21	Variable avrg. : 0.94 clo	7points			2 sessions, 17 min.	3 times	6
[85]	8	5	3	avrg.: 45.21	Variable avrg. : 0.94 clo	7points			4-5days, 9am-5pm	NM	NM
[70]	18	9	9	24-47	Variable 0.60-0.91clo	7points			25-30 min.	When feeling a change in thermal sensation	NM
[96]	34	NM	NM	NM	Summer: 0.5clo Winter: 0.91clo	7point			July22-August15 January6-March19	Not mentioned	54-143
[97]	33	NM	NM	NM	0.8clo		10points	3points	5-90 days	10votes/day	19-137
[98]	11	6	5	NM	Variable	7/4points		5points	4 weeks	NM	91-187
[99]	20	NM	NM	20-30	0.26clo	7points			10 sessions, 90 mins.	10 mins.	NM
[73]	1	1	0	NM	0.6/1.15clo	7points		3points	13sessions, 30 mins.	NM	59
[100]	1	1	0	NM	Variable	7point			NM	NM	NM
[56]	8	NM	NM	22-26	Variable	7point			3Months	1 hour	185-273
[57]	23	NM	NM	NM	Variable	7points			2 weeks	NA	159 FA*
[101]	20	10	10	Avrg. 23.2	Summer Cloth 0.35-0.58	7points	3point		40 mins.	TSV: 1min other votes: 10mins	20
[102]	10	7	3	NM	Variable	7points		3points	4sessions, 2hrs	15mins	40
[103]	17	17	0	avrg. 22.35	long sleeve Tshirt pants	10points		3points	3 sessions, 30 mins.	once	3
[104]	3	1	2	17-32	Variable	6points			6 sessions, 3hrs.	5-25 mins.	341-345
[81]	3	2	1	20-24	Variable	7points		3points	NM	NM	54-143
[65]	2	0	2	29	0.72-0.92 clo	7points		3points	14 sessions 4 hr.	15 min.	238
[105]	33	21	12	21-43	Both variable and constant	7points	5points		2.5hrs	15 mins	363 FA*

Table 2.3: Subjects' Information and subjective thermal votes (Continued)

Study	Participants				Subjective Vote	Timing	Data Points					
Ref.	Total	Male	Female	Age	Clothing		TSV	TPV	Scaled	Duration	Voting Frequency	Total Votes
[36]	2	1	1	mid 20s	Variable		7points			14 sessions, $\approx 2hrs.$	NM	362-413
[108]	20	12	8	avrg. 26.2	Summer Cloth		7points			1-1.5 hrs.	5 mins.	NM
[109]	5	3	2	avrg. 30	Variable		7points			14days, 9am-5pm	20 mins	97-400
[111]	22	10	12	NM	Variable		9points			4 sessions, 20 mins	1/session	NM
[80]	3	1	2	$\approx$ 30– 50	Variable		5points	3points		6 weeks	whenever needed change	54-143
[18]	15	11	4	avrg. 21.6	0.57 clo		7points			3sessions, 1.5-2 hrs.	5 mins	28
[112]	12	8	4	avrg. 23.5	1 clo		7points	3points	3points	6 sessions, 150 mins.	2 mins.	450
[113]	6	5	1	13- 57	Variable		7points			7 days	$\approx 15/day$	32-116
[82]	6	6	0	avrg. 25	black short sleeves, trousers, cotton socks		7points	2points	3points	2sessions, 40 mins.	20 Sec.	NM
[114]	8	4	4	22- 24	Variable		7points			15 days, 8:50-12:00am, 2:20-5:30pm	30 mins	25
[29]	12	7	5	22- 27	Sweatshirt, pants		5points	3points		3 session, 60 mins.	3 mins.	60
[27]	30	24	6	NM	Variable		7points			5 weeks	twice/week	8-33
[84]	3	2	1	20- 24	Variable		7points			Not mentioned	Not mentioned	54-143
[84]	3	2	1	20- 24	Variable		7points			Not mentioned	Not mentioned	54-143
[84]	3	2	1	20- 24	Variable		7points			Not mentioned	Not mentioned	54-143

FA* : For All Subjects Together

2.3.4 Input variables

All the thermal comfort experiments require some additional environmental or physiological feedback variables in addition to subjective thermal comfort votes. Table 2.3.4 presents the environmental and physiological data utilized in the selected articles. The

type of these variables depends on the experimental design and the objectives of the study. While the reviewed research has included different types of environmental variables, all of them have recorded Air Temperature (AT), and most of them have included Relative Humidity (RH). As we can observe in Figure 2.4 Globe Temperature (GT) and Air Velocity (AV) are the next two most used environmental variables, followed by Outdoor Temperature (OT), Outdoor Humidity (OH), and CO_2 level. This figure also displays the percentage of research that has recorded the presented physiological variables. We need to mention that the percentage value is calculated among the studies that have been designed to record the physiological factors as their default constraints. It can be observed that Skin Temperature (ST) has the highest share of research in this regard. Heart Rate(HR), Metabolic Rate (MR), and Clothing level (CLO) are the next most utilized variables. Some other research has recorded other physiological variables such as Galvanic Skin Response [81, 80], and EEG signals [111] .
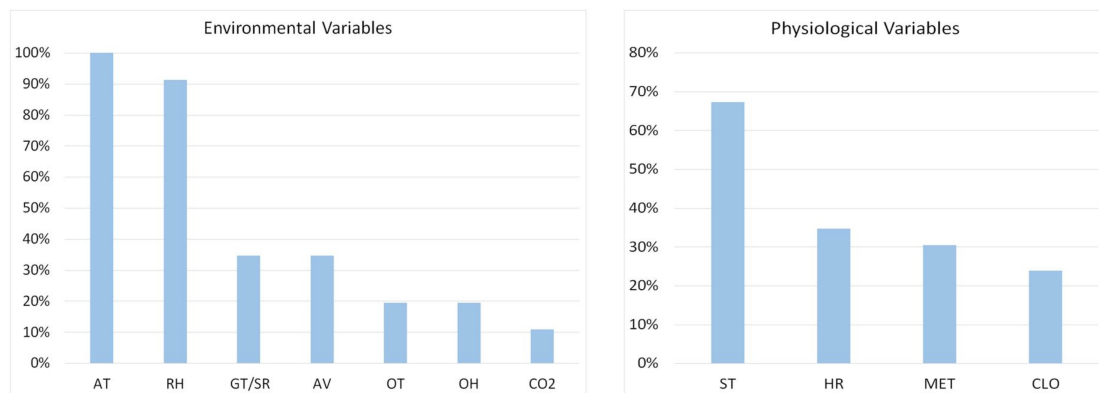
Figure 2.4: The Percentage of Research That Different Environmental and Physiological Variables

Table 2.4: Collected Variables

Study Ref.	Environmental Variables							Physiological Variables				BodyParts
	AT	RH	GT/SR	AV	OT	OH	CO2	ST	HR	MET	CLO	
[83]	X	X						X			X	Wrist,neck,chest, upper arm, thigh, calf
[84]	X	X						X	X	X	X	Wrist
[60]	X	X	X	X		X					X	
[66]	X	X	X	X				X			X	Chest,Back,Arm,Hand,Thigh,Lower leg,Foot
[91]	X	X	X	X	X	X	X					
[87]	X	X						X	X	X		Wrist temperature and 3-axis accelerometer to capture motion-based activity
[92]	X	X					X	X	X	X		Wrist
[51]	X		X		X	X	X					
[76]	X	X	X	X	X	X		X	X	X		Wrist, ankle, body proximity
[31]	X	X						X	X			Hand, elbow, shoulder, torso, head
[55]	X	X	X	X	X	X						
[93]	X	X		X			X					
[64]	X	X		X				X				Forehead, left chest, left back, left upper arm, left lower arm, left hand, right anterior thigh, and anterior calf
[94]	X	X						X				Wrist
[95]	X	X	X	X				X	X	X		Wrist
[85]	X	X	X	X	X	X		X	X	X	X	Wrist
[70]	X	X	X	X	X	X			X			
[96]	X	X						X				Wrist
[97]	X	X										
[98]	X	X						X	X	X	X	Wrist
[99]	X	X	X	X						X	X	
[73]	X	X						X				Forehead, cheek, chest, back, abdomen, upper arm,forearm, hand,finger, thigh, shin, calf,foot*
[100]	X	X		X				X	X	X		Wrist
[56]	X	X										
[101]	X	X	X	X	X	X		X	X	X		Wrist
[102]	X							X				Nose, front face, back of ear, cheek-bone
[103]	X								X			
[104]	X	X						X	X	X	X	Wrist
[81]	X	X						X	X	X	X	Wrist

Table 2.4: Collected Variables (Continued)

Study	Environmental Variables							Physiological Variables				Body Parts
Ref.	AT	RH	GT/SR	AV	OT	OH	CO2	ST	HR	MET	CLO	
[65]	X	X	X									
[105]	X	X										Face
[53]	X	X		X								
[36]	X	X						X			X	Face
[108]	X							X				Wrist, forehead, nose, cheek
[109]	X	X						X	X	X		Wrist
[80]	X	X			X	X	X	X	X			Wrist
[18]	X	X	X	X				X				Wrist, face
[112]	X	X	X					X				Forehead, abdomen, elbow, hand, thigh, calf, foot
[113]	X	X	X	X	X					X	X	
[82]	X	X						X				Forehead, upper chest, lateral arm, dorsum of hand, abdomen, scapular blade, anterior thigh, fibular shin, dorsum of foot
[114]	X	X	X	X								
[29]	X	X						X				Forehead, cheek,ear, nose, mouth, neck
[27]	X	X						X				Forehead, cheeks, lips, jaw,lips, upper neck, lower neck, palm core, palm, back-of-hand
[97]	X	X						X				Wrist
[97]	X	X						X				Wrist
[97]	X	X						X				Wrist

*Only shin,back and hand were used for the prediction

2.3.5   Machine Learning Approaches

While having manual control over the indoor environment provides more comfort for the occupants, it may have an adverse effect on the productivity of the employees by impacting their ability to focus on a given task [116, 117]. This indeterminacy in the better performance of manual or autonomous systems brings the need for a hybrid control system that functions automatically, but that has the potential to be manually overwritten whenever needed. The learning feature of smart buildings can be a solution to the comfort problem that is caused by using fully automated building systems.

In this section, we are looking into the learning methods utilized in the reviewed studies. As Table 2.3.1.2 presents, the learning approaches are divided into three categories: supervised, unsupervised, and reinforcement learning. Figure 2.5 displays the number of researchers that have used the selected machine learning algorithms for the 40 research with the supervised method. As the figure shows, Random Forest, K-Nearest Neighbor, Support Vector Machine, and Decision Tree are the most used algorithms in the reviewed studies. As it is shown in Table 2.3.5.1 researchers have utilized a wide range of machine learning algorithms for creating personalized thermal comfort models. In this table, we have presented the supervised algorithms that were utilized in each study through the maximum reported accuracy of the algorithm in the paper. Although there is still no mathematical justification for this claim, algorithms with the ability to regulate large dimensions, such as the RF are thought to be able to predict thermal sensation and thermal preference better than other algorithms [73]. Using many algorithms in a single task to reduce prediction biases by a single algorithm is a common method in current research since there is no clear conclusion on algorithm selection [118]. Various studies used different ways to compare performance and investigated suitable models for their study [72]. On the other hand, several other studies, such as those in Refs. [99], and [119], have calculated the best performance of a particular modeling technique for thermal comfort assessment. Hu et al. [104] have proposed a new approach for creating the prediction model through the use of deep learning algorithms. Deep learning is defined as a machine learning approach that uses Artificial Neural Networks (ANN) at a hierarchical level, which allows nonlinear data processing. Deep learning utilizes neural networks with more than two layers, a large number of parameters, and layers in one of four defined fundamental network architectures: unsupervised, convolutional, recurrent, recursive, or a hybrid of these. One of the great advantages of deep learning over other machine learning approaches is the automatic feature extraction, which is both time-saving and more accurate [120]. As the difference between deep learning

and traditional neural networks is the number of hidden layers, they can be used for large sets of labeled data to learn directly from them and extract the important features. Using a two-stage learning paradigm, the researchers present the Heterogeneous Transfer Learning (HTL)-based Intelligent Thermal Comfort Neural Network (HTL-ITCNN) for thermal comfort modeling in their research. The schematic representation of the two-stage HTL-based learning model is as follows. In the first step, they employed each source-domain dataset to create a Deep Neural Network (DNN)-based pre-trained base classifier. In the second step, they obtained the knowledge-transferred features of the target-domain dataset using the previously constructed base classifiers and then fed them into a new DNN to train the HTL-based classifier. All the reviewed studies have utilized a type of generalization method for their developed model, which is commonly a k-fold cross validation or a train/test split technique. Cross-validation is a variable selection technique to assess machine learning models with a relatively limited data sample. It is a common technique because it is easy to comprehend and because it often yields a less biased assessment of the model's performance than other techniques, such as a simple train/test split. A single parameter named K specifies the number of groups into which a given sample data would be divided. Consequently, the process is often known as K-fold cross-validation. This approach is intended to decrease prediction issues such as biases and overfitting. In supervised learning models, the random train-test split approach may be utilized for large datasets, whereas the cross-validation split is more suited for small datasets. Reinforcement Learning (RL) is recently getting popular in smart building predictive models due to its capabilities for online learning over time, which makes it a great option for real-time control of the buildings. RL, as an agent-based learning algorithm, has a suitable platform for defining the optimal actions, policies, and interactions with the environment. Through its self-adaptability, model-free nature, and learning from historical data, RL can interrelate human comfort with environmental conditions, making it a perfect candidate for controlling indoor environ-

ment [121]. The first application of RL for controlling the built environment is believed to be in 1998 by Mozer M in controlling a residential building comfort system including HVAC and lighting based on observing the lifestyle of the inhabitants [122]. Recent research has reviewed up-to-date RL-based projects in the building control systems and has found promising results of the capabilities of this system in providing comfort and energy saving; however, there are few incorporations of occupancy patterns or occupant feedback in these control loops [123]. Thermal comfort had the most interest compared to other comfort factors in RL controlling research. To create a user-centered control approach, we will use reinforcement learning as an interactive machine learning algorithm. The system will learn human behavior and adapt itself to the environment over time to request the least amount of interaction from the occupant in the future [121]. Recently, skin temperature and heart rate have also been used as inputs to reinforcement learning-based personal comfort models [124]. Although the online learning quality of the RL is a strength of this model, it can also be an obstacle for the offline training applications where the batch historical data is already gathered and ready for training. Offline reinforcement learning is recently been used in such applications to learn from previously gathered data [107].
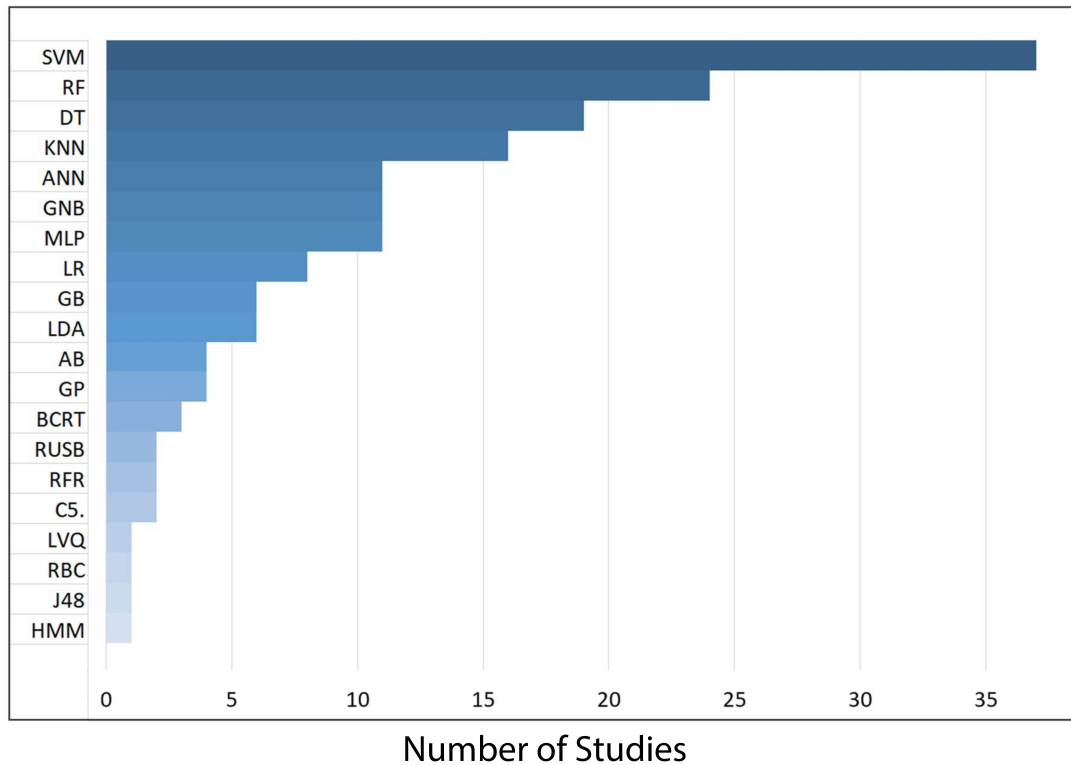
Figure 2.5: Feedback Collection Systems

2.3.5.1 Prediction Performance Report

The prediction performance approach in the reviewed studies is based on the type of selected algorithms. Accuracy, precision, and recall are the three primary measures used to evaluate the effectiveness of a classification algorithm. Accuracy is defined as the proportion of accurate predictions, which may be determined by dividing the true predictions by the total number of predictions. Precision is defined as the percentage of instances that are meaningful (also known as true positives) out of all the examples that were predicted to fall into a certain class. Most of the reviewed papers in this article have reported their model performance through prediction accuracy, as is shown in Table 2.3.5.1 . However, the evaluation measures we outlined for classification models are not the same as those for regression models. The regression-based machine learning algorithms present their model performance through Mean Squared Error (MSE) Mean

Squared Error is one of the most commonly used metrics for regression models, which is the average of the squared differences between the predicted, and actual output [65] [109]. The R2 coefficient indicates the ratio of result variation that our model can predict based on its features. The Mean Absolute Error (MAE) differs from the Mean Standard Error (MSE) in definition just slightly; yet, it exhibits virtually opposite features, and RMSE is the square root of MSE. In addition, the MAE, is the difference between the model's predictions and the ground truth.

Table 2.5: Prediction Algorithms

Ref.	RF	KNN	SVM	DT	ANN	GB	AB	RUSB	GP	LR	LVQ	GNB	MLP	RBC	RFR	J48	C5.	BCRT	LDA	HMM
[83]					94.1%															
[84]	87.5%		86.6%	83.2%		85.9%	83.5%													
[60]	96%		94%	84%		85%			94%	94%										
[66]	97.0%		98.3%				98.3%	87.4%												
[87]	91.76%	86.47%	87.04%			90.02%					87.57%									
[92]		95.9%	97.9%	99.7%								95.3%								
[51]			98%	98%	98%							95%	98%							
[76]	87%	87%	88%		85%	88%				87%		84%		85%	88%	84%	88%	87%	87%	
[31]	80%	80%	76%						80%											
[55]									74%											
[93]	97.73%			NM																
[64]				59.69%	44.91%												83.99%			
[94]	100%		99.3%							98.1%										
[95]	99.8%		72.3%	99.6%						71.6%									71.2%	
[85]		99.19%	98%							82.1%								99.3%	83.7%	
[70]	100%		100%										NM		100%					
[96]		88.31*%																		
[97]		64.8*%	63.5*%	66.29*%						66.67*%			98%							
[98]	NM		NM																	
[99]			100%																	
[73]			94.1%																	
[100]		NM	NM							NM									NM	
[56]			97.04%																	
[101]	94.29%																			
[102]																			82.8%	
[103]	100%	100%	100%	100%			100%			100%		100%	100%						100%	

Table 2.5: Prediction Algorithms (Continued)

Ref.	RF	KNN	SVM	DT	ANN	GB	AB	RUSB	GP	LR	LVQ	GNB	MLP	RBC	RFR	J48	C5.	BCRT	LDA	HMM
[83]					94.1%															
[104]	66.32%*	62.31%*	59.1%	60.01%*								46.61%*	62.19%*							
[81]	87.51%		86.64%	84.59%		85.6%	84.55%													
[65]			NM**		<90%				NM**									NM**		
[105]	76.1%		73.9%																	
[36]	99%		98%																	
[108]	84%	85%	85%																	
[109]			98%	98%	98%							95%	98%							
[111]			100%																	100%
[80]**	≈ 95%	≈ 97%	≈ 97%		≈ 97%							≈ 95%								
[18]	89%	90%	88%	88%	88%															
[112]		92.9%	93%	90.3%				91%												
[113]	73.5%		57.8%		69.6%															
[82]	68%												68%							
[114]	NM**	NM**	NM**	NM**																
[29]	92%																			
[27]	NM	NM	NM																	
[76]			98%	98%	98%							95%	98%							
[76]			98%	98%	98%							95%	98%							
[76]			98%	98%	98%							95%	98%							
[76]			98%	98%	98%							95%	98%							

GB: Gradient Boost, RUSB:RUSBoosted, GP: Gaussian Process, LVQ: Learning Vector Quantization, GNB: Gaussian Naive Bayes, MLP: Multi-Layer Perceptron, RBC: Rule-Based Classifier, BCRT: Bagged Classification and Regression Trees, ET/RFR: Extra Tree/ Random Forest by Randomization, J48: J48 Decision Tree, LDA: Linear Discriminant Analysis, HMM: Hidden Markov Model ** Approxiamte numbers extracted from figures

2.4   Conclusion

This paper offers a comprehensive review of studies on machine learning-based personalized thermal comfort. The purpose of this work is to emphasize the use of machine learning in thermal comfort studies from several aspects. In this review, we have conducted a comprehensive survey of the most current personalized thermal comfort research that has utilized machine learning approaches to create their thermal comfort prediction models. In addition, we have highlighted and compared their associated methodologies and performances in several aspects. We have investigated the selected

publications based on three main aspects: their application, data collection method, and model creation strategy. In the application section, the selected articles were investigated based on their implemented feedback type, which is behavioral or physiological features. In addition, we have compared the experiment design in different studies with regard to the thermal condition, experiment location, and studied subjects. In the data collection comparison report, each study was investigated based on the input variables, including environmental and physiological variables. To study the subjective variables, we have compared the subjective thermal votes based on their type and thermal scale. Finally, the machine learning models were studied based on their learning model type and their performance report method. Based on our review, we highlight a number of observations:

- Personalized thermal comfort modeling is a growing and promising approach due to the potential for decreasing the necessity for long-term feedback collection from occupants. Personal characteristics obtained through physiological sensing technologies might be investigated further following the recent accelerated development of wearable sensor technology.

- The participants of the studies need to be more diverse in terms of including different age groups, gender types, ethnicity, skin color, and health status. In this regard, skin color is particularly important for the non-contact camera-based thermal comfort prediction methods as it results in changing the emissivity of the target area and impacts the thermal readings.

- There are currently several thermal comfort scales utilized for reporting occupants' subjective thermal votes. Most of the researchers are using the thermal sensation scale. However, other thermal scales, such as thermal preferences, maybe a better option for being applied in the building control systems. Different thermal scales of application and performance need more investigation for improved

future research.

- Although supervised learning algorithms, especially RF, KNN, SVM, and DT, have been widely used in the state of the art studies, reinforcement learning RL-based research still needs more research. One main reason for fewer RL papers is the difficulty of application and performance validation of an online system, which has made researchers use offline simulated testbeds for this objective. Future research on online learning approaches for personalized thermal comfort would be helpful for the field.

- The reported accuracy of the thermal comfort model in all the studied papers showed improvement in comparison to the conventional, widely used PMV method. This will highlight the importance of the subject and the necessity of further updated regulations in this area.

Therefore, future studies may benefit from the outlined areas and increase understanding of machine learning-based personalized thermal comfort models from a comprehensive viewpoint.

CHAPTER 3: A Novel Fully Annotated Thermal Infrared Face Dataset: Recorded in Various Environment Conditions and Distances From The Camera

3.1   Introduction

The emergence of thermal imaging techniques has provided an excellent opportunity for contactless data gathering without interruption to occupants' activities. As elevated body temperature is an important indicator of a possible underlying physiological process, thermal imaging is a great non-intrusive tool for presenting that biological state. The non-invasive nature of thermal cameras has resulted in extensive utilization of these devices for detecting and diagnostic purposes in several areas of medicine [125, 126, 127], and none-medical research such as fire safety[128, 129, 130], transportation[131, 132, 133], and building construction[134, 135, 136].

Recent accelerated innovations in thermal imaging devices make it possible to utilize lower-priced thermal cameras to collect high-quality information that can improve several aspects of our lives. Facial thermography, in particular, is one of the most widely studied areas due to its proven practical applications. Facial thermal imagery has been successfully studied as an indicator of human identity[9, 10], emotions[11, 12, 13], and comfort [105, 137, 36] in several research. More than ever before, the current pandemic has also highlighted the facial thermography potential in the non-intrusive evaluation of human conditions [14, 15].

While facial thermography has gained lots of recent attention, this is still a new research area that needs to be evaluated and studied in different domains. The lack of public datasets of facial thermal images is a significant obstacle to research improvement in this area. Currently, there are lots of RGB facial datasets available in diverse conditions [138], but the facial infrared image databases are limited and need improve-

ment for several reasons. First, due to the lower quality of older thermal cameras, several current thermal datasets are of low resolution. They are not appropriate for use in sensitive areas, such as health-related applications [19]. Second, most of the existing public datasets are not in the original raw format and are converted frames, which results in the loss of important information [20]. The original thermal images are created utilizing 14-bit or 16-bit radiometric data that comprises information about the heat flux or temperature of each pixel. However, the majority of these datasets are transformed to lower bit resolutions, such as 8-bit RGB files, to make them smaller and more compatible with common imaging software. As a result of this process, temperature data is lost and cannot be retrieved later. Third, the current public datasets lack diversity in several aspects, such as face resolution and environmental properties. Most of the available datasets are appropriate for facial recognition purposes with no variation in environmental properties such as air temperature, relative humidity, and air speed.None of the current public datasets include data on controlled thermal variations, which is one of our top objectives in collecting this dataset. While some of the current datasets were recorded in uncontrolled thermal circumstances, resulting in temperature fluctuation, yet there is no information about the ambient temperature at the time of thermography recordings. In addition, there are no publicly available datasets with varying distances from the camera[41], while several studies have indicated the importance of distance in the infrared thermography readings [40, 38, 39].In field thermography applications, when precision is required , the temperature variance induced by distance is substantial and needs to be considered.

Fourth, while some recent research has demonstrated the great potential of using thermal cameras in smart buildings to predict occupant thermal sensations, none of them have made their datasets available for use in other projects. The improvements in thermal imaging technology enable the collection of data for use in the control systems of our smart buildings. Temperature data has been shown to be a viable variable

for predicting occupant thermal preferences and controlling indoor environmental systems.While some of the current datasets were recorded in uncontrolled thermal circumstances, resulting in temperature fluctuation, there is no information about the ambient temperature at the time of thermography recordings. However, there are currently no public datasets available that include the thermal sensation of the subjects in different thermal conditions. Finally, the majority of thermal datasets are either missing any landmark annotations or include just a few facial landmarks and the bounding box. Lack of manual facial landmark annotation makes the application of this datasets limited. Facial landmarks provide an extra supervisory signal and assist in the recognition of complex cases, in addition to making it possible to align the face during the face recognition process.
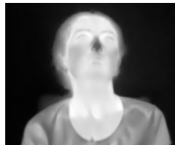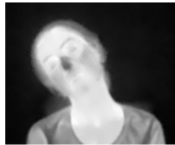

(a) Distance to Camera 1.0 m Face Resolution 130*160					
Environment Temp.	21.19℃	22.53℃	23.10℃	24.05℃	26.19℃
(b) Distance to Camera 3.4m Face Resolution 50*60					
Environment Temp.	21.70℃	22.73℃	24.00℃	24.30℃	26.47℃
(c) Distance to Camera 6.6 m Face Resolution 22*26					
Environment Temp.	21.35℃	22.80℃	23.80℃	24.00℃	26.20℃

Figure 3.1: A Sample of Included Data Frames in Different Thermal Conditions

To address some of the limitations mentioned above, we present the Charlotte-ThermalFace dataset with unique properties. As Figure3.2 shows through some sample images, our dataset includes thermal images of the same subjects in various thermal and physical conditions, including the environmental temperature, distance from the camera, and head position. In contrast to the existing datasets that are recorded mostly at a fixed

distance from the camera, our dataset includes a variation in distance, which has resulted in thermal images with several different resolutions. In addition, each subject is recorded in at least four different thermal conditions at all the specified distances. We have included the environmental temperatures data in the dataset, which we present in this sample figure for each image frame. The first column of the figure shows the lowest temperature range images, which increase as we go to the left side columns. We can also observe in this figure that varying distances from the camera have resulted in a dataset with different thermal resolutions. We recorded the data frames at 10 relative distances from the camera, of which this sample figure includes the three main ones (closest, middle, and farthest).In addition to environmental data annotations, all the images are manually annotated with extensive facial landmark localization, which include 72 points for full or semi-profile positions, and 42 points for profile faces [139].To avoid missing temperature data, our dataset is published in the original high accuracy recording format of Flir cameras, which is 16-bit raw data in the TLinear mode [140]. This capability stores the thermal data for each pixel in the frames, and the users can read the temperature of each pixel independently. Based on the aforementioned information, the Charlotte-ThermalFace dataset is available publicly with the following main characteristics:

- We have captured approximately 10,000 infrared thermal images in varying thermal conditions, several distances from the camera, and changing head positions. We have also controlled the air temperature to change from 20.5°C (69°F) to 26.5 °C(80°F). Images are available in four different temperatures, 10 relative distances from the camera, starting at 1m (3.3 ft) to 6.6m(21.6 ft), and 25 head positions.

- The first public facial thermal dataset annotated with the environmental properties including air temperature, relative humidity, air speed, distance from the camera, and subjective thermal sensation of each person at the time.

- All the images are manually annotated with 72 facial landmarks.

- We are publishing the data in the original 16-bit radiometric TemperatureLinear format, which has the thermal value of each pixel.

This study has two main contributions. First, it presents a comprehensive comparison of the current public datasets in facial thermography. Second, it introduces the Charlotte-ThermalFace public dataset on facial thermography with a brief investigation. The rest of this paper has three main sections. In section 2. literature Review, first, we look into the applications of facial thermography in different domains. Then we study and compare the existing publicly available thermal datasets with a brief description of each. In Section 3, we introduce our developed dataset and how we address some of the existing gaps by publishing our dataset. Section 4. provides a preliminary analysis of the dataset to show its applicability for future projects.

3.2   Literature Review

3.2.0.1   Facial Thermography Applications

A significant decrease in the prices of thermal cameras and their improved quality and resolution are paving the way for the utilization of these sensors in more research and real-world applications. The applications of biometric thermal images are defined in four categories: detection, monitoring, and recognition/identification [141]. In this section, we have looked into the applications of facial thermography in these three major areas in detail.

Face Detection:

While variations in lighting conditions can easily degrade the performance of face detection algorithms, infrared thermography provides accurate results even in complete darkness. This quality has resulted in better performance of thermal images in comparison to visual images in pedestrian detection for autonomous vehicles. Their results show the Missing Rate (MR) when using Histogram of Oriented Gradients (HOG) fea-

tures for visual images is %73, which decreases to %50 by using thermal image [142]. In regards to face detection, it is demonstrated that when employing visual photos for face identification, non-uniform illumination and fake faces may easily make cascade classifiers inoperable. However, the thermal frames do not have this downside. Through utilizing thermal images, machine learning-based face detection algorithms use classifiers such as AdaBoost and Support Vector Machine for considering facial and non-facial patches as positive and negative regions, which have been successful [6]. Additionally, other research teams have conducted field experiments to evaluate and compare the proposed approaches to face detection using RGB photos and have demonstrated the benefits of utilizing thermal images to detect faces [143]. Researchers have shown promising results using Haar-like features combined with a cascade of boosted tree classifiers [7], and Faster R-CNN and YOLO [8] as viable strategies for face detection in the thermal domain. It is important to mention that the accuracy of these face detection algorithms was shown to be significantly reduced when pictures are flipped and rotated. [144].

Face Monitoring:

The two major applications of facial monitoring is in medicine and building science, which are described below:

Medical Facial Thermography: The feasibility of using thermal scanners for reading skin temperature instead of traditional oral or rectal thermometers has been studied in several research [89][90]. The consensus, also supported by recent data, indicates that the temperature of the eye area has the highest temperature on the head, which makes it suitable for detecting fever [145]. It has also been shown that the side temple, inner eye area, and ear have shown the best correlation of internal body temperature [146]. At the same time, because these two areas are most affected by environmental temperature [147], cheeks and nose temperature are promising measured facial areas for calibrating and offsetting the impacts of environmental factors. Thermal imaging

has also been used for respiration rate detection by monitoring the temperature change frequency in the nasal area [148]. This approach can eliminate the adverse effect of the lighting condition; however, the relatively lower resolution of thermal cameras requires lower distances to the camera even in the recent research [149]. The combination of RGB and thermal imaging has led to higher accuracy of respiratory rate monitoring [150][151][14]. Due to the COVID-19 pandemic, the accuracy of infrared thermography in the medical sector has become more critical than ever. Some early studies have shown a few successful cases of using thermal cameras to detect febrile patients worldwide [152, 153, 154]. In this regard, the U.S. Food and Drug Administration (FDA) has enforced policies for Telethermograph systems during the COVID-19 pandemic based on a recent international standard (IEC 80601-2-59)[155].

Environmental Monitoring: Environmental monitoring has recently become of much importance due to the influence of lighting [156, 157, 158] and thermal conditions on both occupants' health [159] and building energy consumption [160, 161, 162]. This has resulted in designing high performance buildings, which is also energy saving [163, 164]. Recent research has also proved thermal imaging to be a successful indicator of the building's occupants' thermal preferences[165]. The infrared cameras can be installed at a distance from the occupant and capture the skin temperature by reading the pixel values of the desired facial regions, proving the feasibility of this technique with 94% -95 % accuracy when using FLIR A655 [27]. A real-time feedback system using FlirA35 thermal cameras was developed in 2018, analyzing both face temperature and occupants' position [28]. A lower-cost could also replace the previously mentioned expensive cameras and smaller infrared camera, Flir Lepton, with an acceptable accuracy of 85% for predicting the skin temperature [29]. The accuracy of thermal comfort prediction was compared between different monitoring devices, including air temperature sensors, wearable skin temperature wristbands, and thermal infrared cameras. The findings highlight a slight improvement in the prediction accuracy by adding physiological sensors to the

environmental sensors. However, it questions the efficiency of using physiological sensors for this slight accuracy increase (%3-%4) [166]. In another recent study in this area, Li et al. had successful experience monitoring and recording the skin temperature of two occupants simultaneously with two thermal camera nodes, while each camera captured some parts of the faces [34].

Facial recognition:

Facial recognition is one of the most studied areas of facial thermography [141]. Face recognition in the thermal spectrum has gained more attention after showing successful results of Long Wave Infrared Imaging (LWIR), which was even superior to the visible spectrum face recognition results[167]. The research in this area has been ongoing ever since through utilizing several image processing methods, which have proved to be promising even in the outdo or environments, where illumination and face alignment vary substantially [168]. Multi-modal face recognition was also introduced in 2005 by utilizing both thermal and RGB images to develop a three-dimensional model of the face, and its thermal texture map [169]. Research has performed experiments involving data fusion of multi-spectral imagery and was able to confirm the improvement in face recognition rate from 0.789 to 0.870 as a result of image fusion[170]. Furthermore, dual camera setups were designed to be used in dynamic illumination conditions to switch between the visible and infrared spectrum and select the most confident result in different lighting situations [171].

Emotion and expression detection as two other application of face recognition, which have also shown promising results [172]. for detecting conditions such as anxiety, fear, and alertness [173]. The main reason for effectiveness of thermal images for this application is variations in the skin temperature while expressing different emotions , which had made thermal data an essential source of additional information to improve in the evaluation of facial expressions and emotions [174]. This quality has helped with creation and robot, capable of communicating with children and recognition of their emo-

tions including disgust, fear, happiness, sadness, and surprise. These emotions could be recognized with an 85% accuracy rate using low-cost hardware and low-cost approaches for visual and thermal image processing [175]. Another research has shown the increased expression prediction accuracy from %89.5 when using visual images to %93.7 by using thermal frames. Multi-modal fusion through utilizing thermal, visual, and depth domains have also been proved to be successful in emotion recognition through utilizing more sophisticated late fusion approaches, such as fuzzy inference systems and Bayesian inference [138]. Intoxication detection is another application of facial thermography in the facial recognition category. Alcohol consumption results in abnormally dilated blood vessels and increased blood pressure. In the facial area, this biological behavior shows itself by increasing the temperature around the nose, forehead, and eye area [176]. Despite several challenges, recent research has shown an average percentage accuracy of %99.63 in identifying drunk individuals through thermal images [177].

In conclusion, we have shown that thermal images can be of great importance in several domains. Although both visual and thermal images are influenced by the change in lighting and thermal conditions, the intensity of the change varies extensively based on the cameras' dynamic range. As a consequence, when using an visual camera, the change in pixel values in the facial regions may be close to 100% of the dynamic range of the sensor. However, the thermal domain changes are much less than the dynamic range that a typical thermal camera can capture, which will result in the higher consistency of thermal images, even in varying thermal conditions [143].
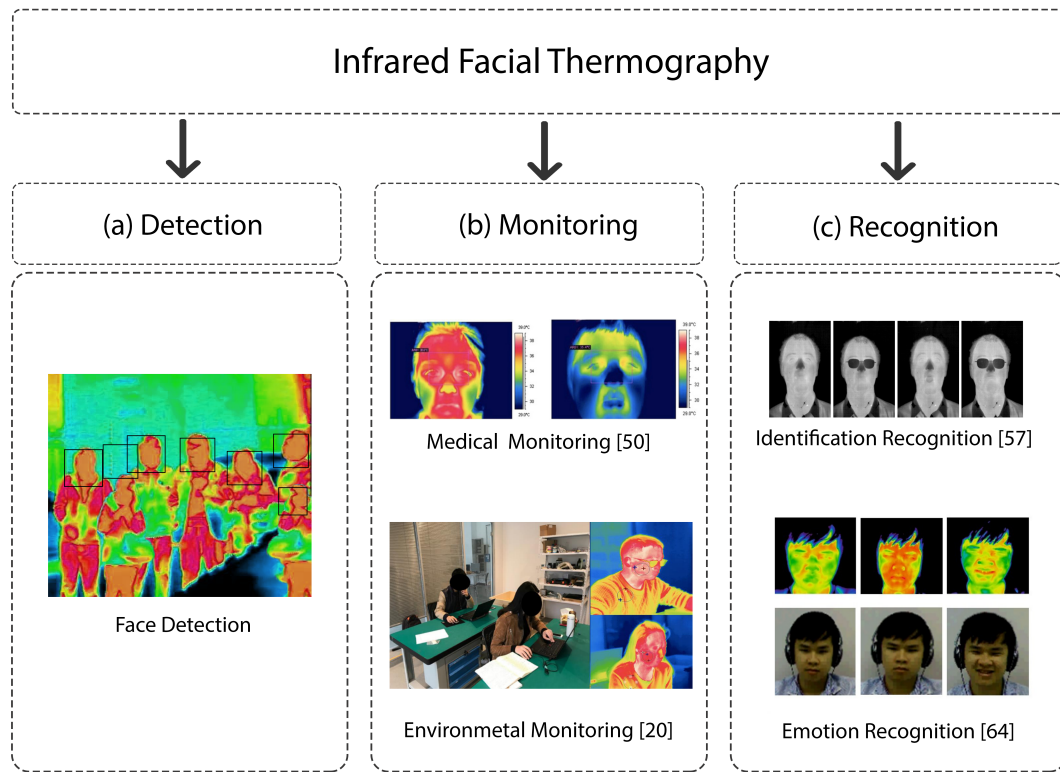
Figure 3.2: A Sample of Included Data Frames in Different Thermal Conditions

3.2.1 Existing Facial Thermal Datasets

Increased application of facial thermography in the mentioned sectors has highlighted the need for a comprehensive database for further studies. This section presents the current publicly available thermal face datasets and compares them to their key characteristics and limitations. This information is also available in Table 3.1 for better comparison.

IRIS: The IRIS (Imaging, Robotics, and Intelligent Systems Lab) database contains 4228 pairs of images in both thermal and visible domains from 32 subjects, captured simultaneously. Similar to the Equinox database, each subject demonstrated three facial expressions: smiling, frowning, and surprised in five different illumination settings. This database also includes a 4-second video in each scenario at 10fps as the subjects

Table 3.1: Public Available Datasets, P: Position, I: Illumination, E/D: Expression/Disguise,S*: Several

Dataset	Thermal	RGB	Subjects	P	I	E	Resolution	Distance (cm)	Landmarks	Size(images)
IRIS [178]	√	√	32	11	5	3	320 × 240	183	-	4228
IRIS-M3 [170]	√	√	82	25	S*	1	640 × 480	120	-	2624
UND [179]	√	√	241	1	3	3	320 × 240	?	-	2624
UH [180]	√		138	5	1	1-5	640 × 512	?	-	7590
FSU [181]	√		10	0-20	1	0-20	320 × 240	?		234
Carl [9]	√	√	41	1	3	1	160 × 120	135	-	7,380
NVIE [182]	√	√	215	1	3	7	320 × 240	75	-	234
KTFE[174]	√	√	26	1	1	7	320 × 240	85	-	126 GB
ARL-MMFDV1[183]	√	√	60	1	1	videoe	640 × 480	250, 500, 750	6	?
ARL-MMFDV2 [41]	√	√	51	1	1	video	640 × 480	250	6	?
ULFMT[184]	√	√	236	1	1	7	640 × 512	100	-	?
Eurocom[185]	√	√	50	4	5	7	160 × 120	150	-	4200
Tuft[186]	√	√	113	9	2	5	336 × 256	150	-	10,000
RWTH[187]	√		90	9	2	8	1024 × 768	90	68	10,000
ARL-VTF[19]	√	√	395	3	1	2	640 × 512	210	6	500,000
Sejong-A[188]	√	√	30	1	1	13	768 × 756	200	-	1,500
Sejong-B[188]	√	√	70	5-15	1	13	768 × 756	200	-	23,000
I2BVSD[189]	√	√	75	1	1	7	720 × 576	?	-	681
Sober-Drunk Database[190]	√		41	1	1	2	128 × 160	30	-	4,100
PUCV-DTF[191]	√	-	46	1	1	4	640 × 480	?	-	11,500
TFW[192]	√	√	147	S*	S*	video	464 × 348	S*	5	9,982
SpeakingFaces[193]	√	√	142	9	1	S*	464 × 348	100	-	4,581,595
TIV[194]	√		20	3	S*	3	320 × 240	?	-	21,676

pronounce the vowels. Each scenario is captured in 11 different positions by rotating the camera 36 degrees for each modality, at a fixed distance of 183 cm from the subject [178].

IRIS-M3: This upgrade of the IRIS lab database contains 2624 pairs of images from 82 subjects in multi-band spectrum information, including one thermal and 25 visual bands per participant, in both outdoor and indoor environments. Another significant contribution of this upgrade is a diverse ethnic collection of Caucasian, Asian, Asian Indian, and African participants, with 24% female and 76% male participants. However, the database includes only one variation in facial expression and one frontal position toward the camera, while the distance from the camera is 1.2 meters for all the images [170].

UND: The University of Notre Dame database had published this database, which includes 2492 image pairs from 241 subjects, which is one of the most significant subject

populations in the thermal/visual datasets. Each subject demonstrates two facial expressions of smiling and a natural face under three different indoor lighting conditions. Another unique feature of this dataset is capturing images in 4 sessions throughout the month. However, there are only four image pairs per subject [179].

UH: The University of Houston database contains 7590 images of 138 subjects, captured in the Mid Wave MW thermal IR domain. There are 55 images of each subject in the database, demonstrating different facial expressions and arbitrary facial positions [180].

FSU: The State University of Florida database contains 234 images from 9 subjects in thermal infrared in 7-14 μm spectral range information, which includes 25 visual bands and one thermal per participant. The images include varying angles and facial expressions for all the subjects. The dataset is at 320×240 resolution and in 8-bit BMP format [181].

Carl: This dataset includes a total of 7,380 images that were recorded simultaneously with visible, near-infrared, and thermal sensors. 41 subjects participated in this study under three different illuminating conditions: natural, infrared, and artificial. The snapshots are all in frontal face position with neutral facial expressions. The Thermographic camera TESTO 880-3, equipped with an uncooled detector, captured both thermal and visible images. The images are captured in four separate sessions in which were two days apart [9].

NVIE: The Natural Visible and Infrared Facial Expression database mainly focuses on capturing different facial expressions among several subjects. The dataset is from 215 subjects and includes two sub-databases: (1) Spontaneous and (2) Pose. The spontaneous dataset contains sequences from starting an expression to the final frame, and the Pose dataset contains only the last expression in both the visual and thermal spectrum. The researchers have captured all the images under three different indoor illumination settings [182] .

KTFE: Kotani Thermal Facial Emotion dataset includes simultaneous thermal and visible images in seven spontaneous emotions, including neutral, anger, happiness, sadness, fear, disgust, and surprise. 26 subjects participated in the study, with an age range of 11-years-old to 32-years-old. An infrared camera, the NEC R300, was used for capturing both thermal and visual videos. The dataset includes 126 gigabytes of visible and thermal facial emotion facial expression data frames. This database is one of the few datasets that mentions the recording room air temperature, kept between 24 °C and 26 °C [174].

ARL-MMFD: Army Research Laboratory Multi-Modal Face Database was recorded simultaneously by a long-wave infrared camera and a visible spectrum camera. The utilized polymetric sensor is capable of recording geometric and textural facial details. The dataset included 60 subjects in the first published version[183] that was then extended to 111 subjects [41]. The researchers have used LWIR polarimetric for capturing images in both datasets, which are named Volume1 and Volume2. The expression change in the subjects' faces was created by counting out loud numerically. The first volume dataset is the only dataset collected at three different distances from the camera, which are 2 m, 5 m, and 7.5 m. However, the second volume is captured only at a single range of 2.5 m from the camera.

ULFMT: Université Laval Face Motion and Time-Lapse Video Database is recorded within four years from 238 subjects. This experiment includes different facial poses and expressions, ethnicities, ages, and sexes. The researchers have recorded the images in 4 different spectrum ranges with different cameras, including a Jenoptik camera for LWIR, a Phoenix Indigo IR camera produced by FLIR for MWIR, a CMOS made by Goodrich for SWIR, and a standard CCD made by Much for the NIR/Visible spectrum. The subjects had changed their facial expression arbitrarily and changed their head position from full-frontal face to complete profile for the video frames captured at 30 fps for 10 seconds [184].

Eurocom: The dataset includes a total of 4200 images from 50 subjects, captured simultaneously in the visible and thermal spectrum. The dataset contains six illumination settings: ambient light, rim light, key light, fill light, all lights on, all lights off; seven expressions: neutral, happy, angry, sad, surprised, blinking, yawning; four head positions: up, down, right at 30°, left at 30°; and occlusion: eyeglasses, sunglasses, cap, mouth occluded by hand, eye occluded by hand. The thermostat temperature was at the average temperature of 25°C for the test room. The thermal camera is a Flir Duo with an uncooled VoX microbolometer and a thermal resolution of 160x120 pixels [185].

Tufts: The Tufts University database focuses on capturing images in various modalities from subjects in 15 different countries, genders, ages (4–70 years old), and ethnicities. A total of 10,000 images from 113 subjects had participated in the dataset. Images are under different scenarios of simultaneous visible and thermal images, near-infrared (NIR) images, a recorded video, a computerized facial sketch using the FACEs software, and 3D images of all the subjects. The researchers have utilized FLIR Vue Pro camera for recording the thermal images. The facial expressions for each subject are neutral, with a smile, eyes closed, an exaggerated shocked expression, and wearing sunglasses [186].

RWTH: The RWTH Aachen University database contains 2935 images in the thermal domain from 90 subjects. The subjects' distance from the camera is 90 centimeters. Each subject demonstrates six facial expressions of contempt, disgust, anger, fear, surprise, sadness, happiness, and a neutral face. The neutral scenario is captured in 9 different positions by rotating the head in vertical and horizontal positions. The database is a manually annotated dataset with 68 facial landmark points, emotions, and positions[187].

ARL-VTF: DEVCOM Army Research Laboratory Visible-Thermal Face Dataset (ARL-VTF) presents 500,000 images from 395 subjects, captured simultaneously with spectrum information. The dataset was recorded with a long wave infrared LWIR camera and three visible spectrum cameras. The FLIR Boson uncooled VOx microbolometer camera captured the thermal images with a spectral band of 7.5 μm to 13.5 μm. The database

includes a variation in facial expressions created by counting out loud the numbers and facial positions created by rotating the head from left to right. The distance from the camera was 2.1 meters for all the images. The database is annotated with face bounding boxes and 6 points of facial landmarks, including left eye center, right eye center, the base of the nose, left mouth corner, right mouth corner, and center of the mouth [19].

Sejong: Sejong is a recent multi-modal disguise face database, which contains images recorded in four modalities including visible, infrared, thermal, and visible-plus-infrared. The database contains two subsets and subset B were captured one year after the first one (subset A). Subset-A has 30 participants (16 men and 14 females) and the total of 1,500 images, whereas Subset-B contains 70 subjects (44 males and 26 females) with the total number of 23,000 images. The highlight of this database is the add-on images that were captured in all four modalities. In the thermal images as they are not a part of the human body, disguise add-ons have a lower temperature than human skin and so seem darker than human skin or hair. In addition, subset B contains five to fifteen different poses for each subject. For the recordings the camera box were placed in the fixed distance of two meters from the subject and the room temperature was kept at 25 ± 5 ∘C. The thermal images were captured by a Therm-App camera with the resolution of 768x756 pixels [188].

I2BVSD: The IIITD In and Beyond Visible Spectrum Disguise (I2BVSD) face database includes disguised/obfuscated face images in both thermal and visual spectrum. The database's disguise modifications are listed as follows. (1) No disguise: unambiguous appearance, (2) Hairstyles: wigs come in a variety of styles and hues. (3) Beard and mustache: many kinds of beards and mustaches (4) Eyeglasses: sunglasses and spectacles (5) Cap and hat several types of caps, turbans, veils, and bandanas (6) Mask-related variation: disposable mask; and (7) Multiple variations: A mix of disguised accessories. The dataset includes 75 subjects, with one neutral and at least five disguised images for each subject. There are 681 images in each spectrum, which includes 6 to 10 images for

each individual. The resolution of thermal images is 720 x 576 pixels.

Sober-Drunk Database: The dataset include images of drunk and sober individuals in thermal modality and was created at Electronics Laboratory, Physics Department, University of Patras, Greece. The images were captured with the FLIR Thermo Vision Micron A10 Model infrared camera with a resolution of 128x160 pixels. The dataset contains thermal images of both drunk and sober states for each individual. 41 individuals were included in this experimental method, 31 males and 10 females. The recording distance was 30 centimeters from the camera. The first 50 frames were acquired for each individual immediately before to initiating alcohol intake, and the second 50 frames were acquired 30 minutes after the fourth glass of wine was consumed. A total of 100 frames were captured for each participant, resulting in a database of 4100 pictures [190].

PUCV-DTF: The Pontificia Universidad Católica de Valparaíso-Drunk Thermal Face database is also a drunk classification dataset. 40 men and 6 women, with an average age of 24 years, have participated in this study. The images were captured with the FLIR TAU 2 thermal camera, which had a resolution of 640x480 pixels, a thermal sensitivity of 50 mK, and a wavelength range of 7.5–13.5 m. The dataset includes 250 images for each subject, which results in 11,500 total images. The room temperature and distance to the camera were not mentioned in the dataset publication [191].

TFW: Thermal Faces in the Wild (TFW) dataset contains thermal images of people both in outdoor and indoor environments with manually labeled bounding boxes and five-point facial landmarks (eye centers, nose tips, and mouth corners). The outdoor images were recorded in a variety of weather conditions, which included thermal photos acquired in both bright and cloudy conditions. The dataset has 9,982 frames and 16,509 labelled faces from 147 subjects. 5,112 images (5,112 faces) are recorded in a controlled setting and 4,870 image frames (11,397 faces) are collected outdoor. Occlusion, head position changes, various scales, face masks, diverse settings, and weather conditions are all part of the set. The FLIR T540 thermal camera, with a resolution of 464 x 348

pixels, a waveband of 7.5–14 m, a field of view of 24, and an iron color palette, was used to capture the datasets [192].

SpeakingFaces: SpeakingFaces dataset combines high-resolution thermal and visual spectral picture streams of fully-framed faces with audio recordings of each participant speaking about 100 sentences. The dataset includes 142 individuals, in nearly 13,000 instances of synced data from 9 different positions (3.8 TB). During a single trial, each individual participated in two different sessions. Subjects were requested to stay quiet and steady throughout the first session, while the operator captured visual and thermal video feeds from a sequence of nine collecting angles. The other session had the subject reading a sequence of words while visual, thermal, and audio data were recorded from the same nine camera angles. The images were recorded with FLIR T540 thermal camera with a resolution of 464x348 pixels. Subjects were seated in a distance of one meter from the camera, and the room temperature was set at 25 degrees Celsius[193].

TIV: Terravic Facial IR Database contains facial images in both thermal and visual spectrum. This database contains twenty individuals, each of whom has a unique set of frames with a variety of modifications, including front, left, and right orientations, indoor/outdoor setting and using glasses or a hat. It contains 21676 thermal facial photos of 20 different individuals. The image frames were recorded with Raytheon L-3 Thermal-Eye 2000AS with a resolution of 320x240 pixels and delivered in the 8-bit gray scale JPEG format [194].

As presented, most of the current datasets include a diverse number of facial expressions, emotions, and head positions, which makes them suitable for facial recognition purposes. However, there is a substantial lack of facial landmark annotation in these datasets. Only RWTH and ARL-VTF have included manual facial annotations, while the ARL-VTF dataset contains only 6 main landmark points. Landmark detection is one of the most important tasks required for extracting biometric data from face thermal images. One main approach to detecting facial landmarks is utilizing visual images,

which requires calibrating an RGB camera and thermal camera together [195]. Other approaches rely on the pixel value differences between the individuals' faces and their backgrounds. However, this approach does not work properly when the subject's head position changes [196]. As presented in RWTH dataset analysis [187] learning-based methods improve the facial landmark detection accuracy. However, there is currently only the RWTH dataset that includes a complete facial landmark annotation for 2935 images, which was inspired by similarly annotated datasets such as HELEN [197]. However, the data is gathered at a fixed distance of 90 centimeters from the camera and is published in 8 bit PNG format, which makes it loose some thermal information in the conversion process [20]. The Charlotte-ThermalFace dataset provides all the images in a 16 bit TIFF format. Furthermore, none of the currently available datasets covers controlled thermal variation, which is one of the main focuses of our data collection. Some of these datasets are recorded in uncontrolled thermal conditions, which results in temperature variation, but there is no information about the ambient temperature while thermography. Another value of our dataset is the ambient temperature and relative humidity variation, which is not been considered previously. We have recorded the thermal images for each subject in at least four different room air temperatures and included that information in the dataset annotations.

In addition, the only dataset that has included distance in the facial thermography variation is the recent ARL-VTF dataset that has been developed by the DEVCOM Army Research Laboratory in 2021 and includes images at 3 different distances from the camera [19]. However, this dataset does not include any controlled ambient temperature variation, and only 6 facial landmarks are tagged.

Finally, as most of the presented datasets were recorded for computational purposes, and the human aspects such as the thermal sensation of the subjects were not considered. With the recent advances in thermography and its application in smart buildings [30, 108, 36] thermal imaging is going to be part of the future infrastructures. Our dataset

would be a great help for researchers in this area.

3.3 Charlotte-ThermalFace: UNC Charlotte Thermal Face Database Overview

As discussed in the previous section, the current facial thermography datasets are still very limited in quality and quantity and need improvement in many aspects. The facial thermal data is provided based on variation in environmental temperature, distance, and head position. We have gathered 10000 infrared thermal images from 10 healthy subjects in varying thermal conditions, several distances from the camera, and different head positions. We have annotated the data with the ambient temperature, relative humidity, and air speed of the room at the exact time of capturing each image. In addition, 72 facial points are manually marked and added to the annotations.

UNCC-ThermalFace is the first publicly available thermal database annotated with the thermal sensation of each subject in different thermal conditions. It also enables radiometric enabled raw data frames. The radiometric option defines retaining the electromagnetic radiation in the data frame files[140]. By enabling this option, our dataset provides information about the captured radiance in each pixel of the recorded images. All the data is in the original 16-bit radiometric raw format, with a thermal value for each pixel. Flir A700 has recorded the frames, which is one of the most recent Flir Systems' cameras [198]. The thermal sensor is an uncooled microbolometer with the temperature range of 0°C to 650°C and accuracy of ±2°C (±3.6°F) or ±2% of reading for ambient temperature 15°C to 35°C. The images are captured at 10 relative distances to the camera for each temperature range, as is shown in Figure 3.3. The original resolution of the thermal sensor is 640x480 pixels, and the resolution of the cropped facial area varies for each distance range.

3.3.1 Data Collection Methodology

The Office of Research Protections and Integrity UNCC-IRB183845 has approved this study. The data collection process took place in Jun 2021. We have collected the data in

Table 3.2: Subjects' Information

ID	Sex	Age	Height(cm)	Weight(kg)	BMI(kg/m²)
1	Female	34	168	69	24.4
2	Male	42	170	87	30.1
3	Female	30	170	54	18.7
4	Male	33	173	70	23.4
5	Female	34	163	57	21.5
6	Female	35	171	89	29.4
7	Male	32	168	70	24.8
8	Male	34	183	78	23.3
9	Female	33	168	72	25.5
10	Male	27	175	72	23.5
AVG	-	33.4	170.9	71.8	23.3

a one-day long session or two shorter sessions over two days based on the subject's preference. Participants are five males and five females, healthy adults. We made certain that the subjects did not have any thermoregulatory illnesses, heat intolerance, colds, flu, or infections. The participants did not use any makeup or facial cream and removed their glasses for the recordings. All participants wore light-colored short-sleeve shirts and pants. Two of the male participants had facial hair. Table 3.2 shows the information for each subject in detail. Each recording session is designed for capturing thermal recordings from one subject at ten relative distances from the camera and 25 different head positions in each interval. In addition, the temperature of each session is different from the previous session, which have resulted in several variations in the thermal condition. All the ten subjects have participated in at least four recording sessions.

After taking the informed consent, the researchers recorded the participant's age, gender, height, and weight. Adaptation is a common part of human-related thermal condition research, which helps subjects' bodies reach a steady metabolic rate and thermal state, as it is influenced by their prior activities and environments. Earlier research has suggested that the mean skin temperature and thermal sensation stabilize after 40 minutes of being exposed to a new thermal environment with a temperature difference of less than 10°C [199, 200, 201]. The adaptation time period is sometimes selected to be

less than this period in similar previous research, such as 20 minutes[35] or 30 minutes [202]. As one purpose of our experiment has been the development of a facial thermography dataset, we have decided to choose a longer acclimatization period so we can be sure of the reliability of our dataset. The participants had entered the test room and stayed in a seated position for 60 minutes before the test, so their metabolic rate had reached a stable state, and any influence from the prior outdoor temperature was eliminated. The experiment for each participant was a combination of five sub-sessions in an approximately one-hour time frame for each sub-session. The recording was initiated at a temperature of 21°C while the thermostat held the ambient temperature constant with a 1°C fluctuation allowance in each steady state session. Each subsequent session started at a 1.5°C higher temperature in the same one-hour time frame.

Figure 3.3 displays the test room layout and the positioning of the following: (1)thermal camera, (2)subject's stations, (3)data loggers, (4)temperature and relative humidity sensors, and (5)air diffuser and airflow sensor. This figure shows that the temperature and humidity sensors are placed at the number(4) and mounted on a pole at three different heights (0.1, 1.1, and 1.7 meters). The recordings are at ten different relational distances from 1 to 6.6 meters, which this figure shows by number(2). Participants were seated in front of the camera during the study and changed their head positions as instructed while recording RGB and thermal frames pairs.
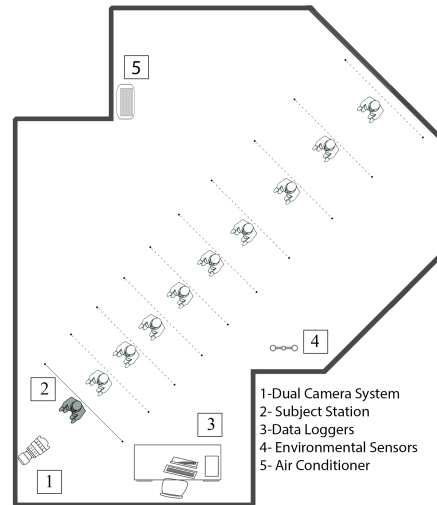
Figure 3.3: Test Room and Recording Stations' Layout

The researchers performed the recordings in each station from the camera and in 25 different head positions instructed to the subjects (Figure 3.4). The user logged the thermal sensation in each station from the camera through a "Google Form" with three standard levels: cool, slightly cool, neutral, slightly warm, and hot. An approximate number of 1,000 frames were captured for each subject, with a total of 10,000 thermal frames for the dataset. Table 4.3 shows the recorded variables and recording sensors' information in more detail. The air temperature and relative humidity are measured with HOBO Pro v2 temperature/relative humidity data logger sensors, which were calibrated with ice water before the experiments. The airspeed is recorded at the air diffuser proximity with an average distance of 3 meters from the subject's station. The dataset is annotated with the face landmarks coordinates, distance to the camera, room air temperature, relative humidity, airflow, and subject thermal sensation.
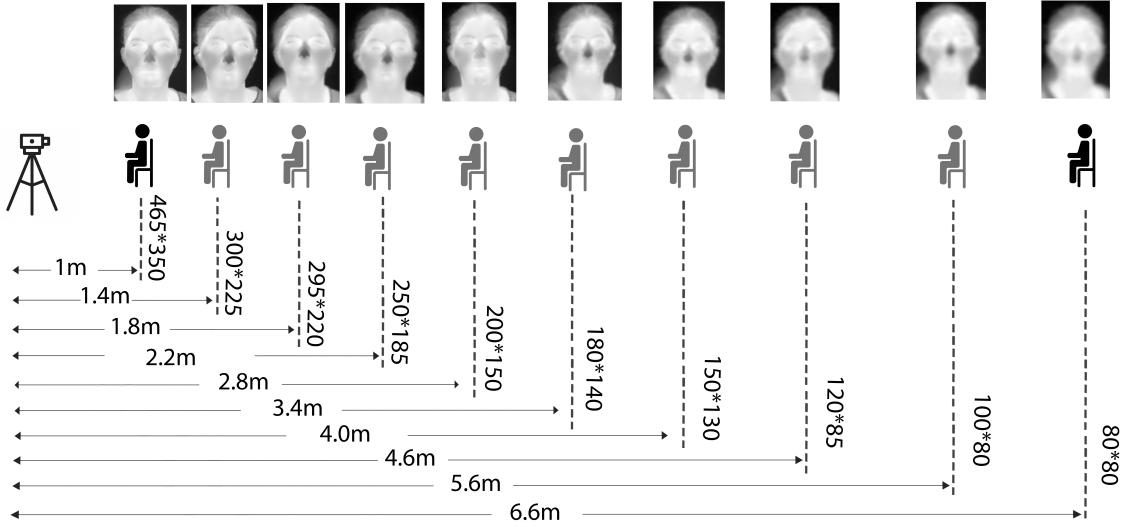
(a). Distances From The Camera and The Coresponding Thermal Resolution
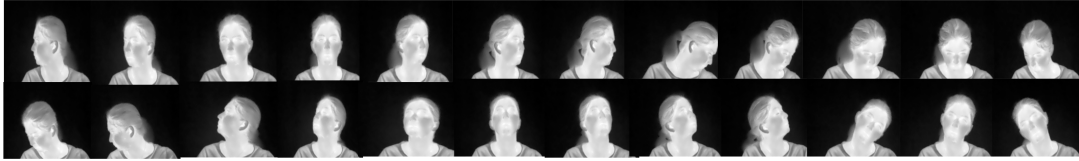
(b). Head Positions in Each Station

Figure 3.4: Distances From The Camera and Head Positions

table[h]

Variable	Device Brand	Model	Accuracy	Resolution
Indoor Air Temperature	Onset	S-THB-M008	+/- 0.21°C from 0° to 50°C	0.02°C at 25°C
Relative Humidity	Onset	S-THB-M008	+/- 2.5% from 10% to 90% RH	0.1% RH
Air Velocity	Fluke	922 Airflow Meter	±2.5% of reading 10.00 m/s)	0.001 m/s

3.3.2 Dataset Analysis

This section presents a preliminary study of the gathered dataset. The goal of this evaluation is to investigate the applicability of the data. The analysis of the subjects' thermal sensation based on their skin temperature is not in the scope of this study and will be covered in our next publication as our objective in this section is to show the key statistical properties of the whole dataset. First, we analyze the main independent vari-

ables, including environmental temperature, relative humidity, and distance from the camera. Then, we look into the correlation of facial skin temperature in different facial areas with the environmental temperature and each other. The authors will also compare sample frames together to study skin temperature differences in diverse thermal conditions and among different subjects. The provided results for facial area correlation are based on our developed method for detecting facial landmarks. The complete explanation of this method is outside the scope of this paper and will be explained in detail in another relevant publication. In addition, we have not included the utilized visual images in the published dataset. Some recent research has succeeded in detecting facial thermal images without using RGB data [8].

(a)   (b)   (c)
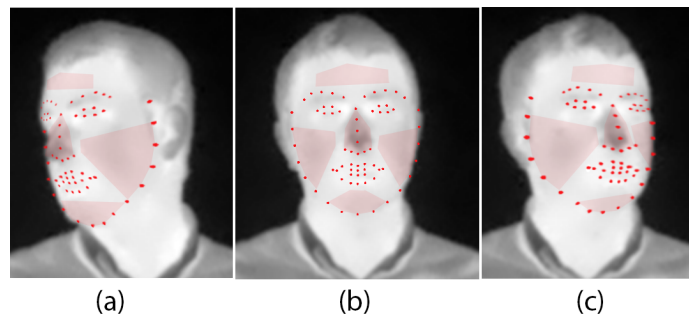
Figure 3.5: Identified Facial Areas Based on Landmarks In Three Different Facial Positions

Since our dataset includes images with various resolutions, it would be a great fit to evaluate the prediction accuracy of such algorithms, which would be one of our future objectives. Here we provide a brief explanation of data preparation and the results' analysis. We have first cropped the images to the facial area with some margins. We have utilized the Dlib-based model for face recognition, which is based on a 29 convolutional layer in Residual Networks ResNet. This model is a version of the ResNet-34 network that works by removing some layers and reducing the number of filters per layer to half [203][204]. For locating the facial areas, the position of the facial landmarks has been transferred from the RGB image to the thermal image by calculating the homography matrix between the two frames, as is presented in detail by Negishi et al. [205]. As the

covered distance is 1-6.6 meters from the camera and the facial area resolution gets as low as 25*30 pixels, the HRNet algorithm has been used to identify facial landmarks in the RGB images [42]. Four facial areas (nose, cheeks, forehead, and chin) have been selected based on the literature to be studied individually in detail [166, 34].

The authors have utilized the estimated facial landmarks to define the selected facial areas, as shown in Figure 4.4. Since the recorded frames are raw radiometric data, the value of each pixel presents the temperature of the pixel's representing area in the actual world. According to the Flir camera's datasheet, when using the TemperatureLinear (TLinear) option, the temperature of each pixel in degrees of Kelvin can be defined with Formula 4.1. This is also very important to set the emissivity of the measuring target to the correct number before the captures, which is 0.98 for the human skin. We have set the TLinear resolution is set to 100 mK(millikelvins) in our recordings [140].

$$SkinTemperature = (PixelValue/Tlinear resolution – 273.15K) \tag{3.1}$$

3.4 Dataset Evaluation

First, the dataset frames' environmental properties are studied to ensure the proper coverage of different thermal conditions in the dataset. Figure 3.6 displays the (a)temperature and (b)relative humidity coverage based on the number of images for each range. The temperature range is between 20.6 °C and 26.6 °C, divided into four groups with a 1.5 °C range for each. This figure shows an approximately uniform distribution in the room (a)air temperature, which means the number of data frames in different temperature ranges is approximately the same. Although we have not controlled the (b)relative humidity in the recording process, controlling the air temperature has resulted in changes in relative humidity, which were recorded and added to the annotations. Additional statistical information about the environmental properties, including air temperature, globe temperature, relative humidity, and airflow, is provided in Table 3.3. Most of the

sessions had zero airflows to ensure image consistency; however, the air conditioner was at 0.5 m/s airspeed at the diffuser proximity in extremely cold conditions.
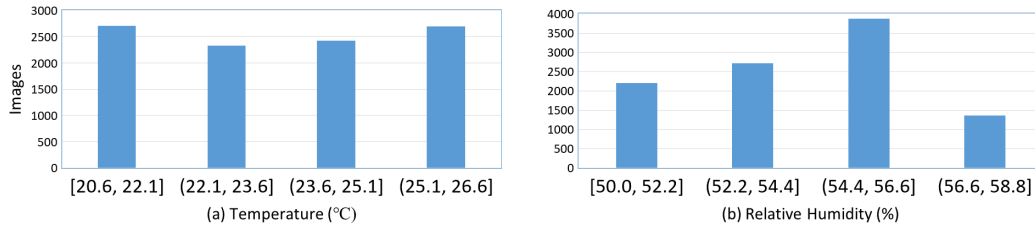
Figure 3.6: Covered Environmental Temperature and Relative Humidity in the Dataset

Table 3.3: Environmental Properties Measurement Results Overview

	Mean	Median	Range	Minimum	Maximum	Standard Deviation
Air Temperature(°C)	23.62	323.65	6.00	20.61	26.59	1.76
Globe Temperature(°C)	23.89	24.05	7.38	20.63	28.01	1.84
Relative Humidity(%)	54.16	54.45	8.63	49.96	58.59	2.07
Air Speed(m/s)	0.08	0.0	0.508	0.0	0.508	0.18

Furthermore, we have studied the changes in the skin temperature in each region for the whole dataset. The temperature of each pixel in the desired Region of Interest (ROI) is calculated by the equation4.1, used to identify the average temperature in each facial area. Table 3.4 shows an overview of the dataset's skin temperature measurement results for all the recorded frames. As the table shows, the temperature in the forehead area has the highest mean value (34.3 °C), while other facial areas' mean values are closer together in the range of 33.17 °C to 33.82 °C. The low standard error numbers (0.02-0.03) in all facial regions demonstrate that a sample data set can be an acceptable representation of the entire dataset. In addition, the close amounts of mean and median numbers show the relatively symmetrical distribution of the data. Additionally, Figure 3.7 presents box plots for the temperature variation of each facial region based on the environmental temperature. As expected by the literature, the nasal area has the highest variation, and the forehead temperature shows the lowest variation.

Table 3.4: Skin Temperature Measurement Results Overview For All Subjects

	Right Cheek	Left Cheek	Cheeks Average	Nose	Forehead	Chin
Mean	32.72	33.17	33.71	33.82	34.30	33.18
Standard Deviation	2.18	2.01	1.28	1.41	1.31	1.897
Standard Error	0.03	0.02	0.02	0.02	0.02	0.03
Median	33.15	33.57	33.86	34.07	34.47	33.55
Sample Variance	4.76	4.03	1.63	1.98	1.71	3.56
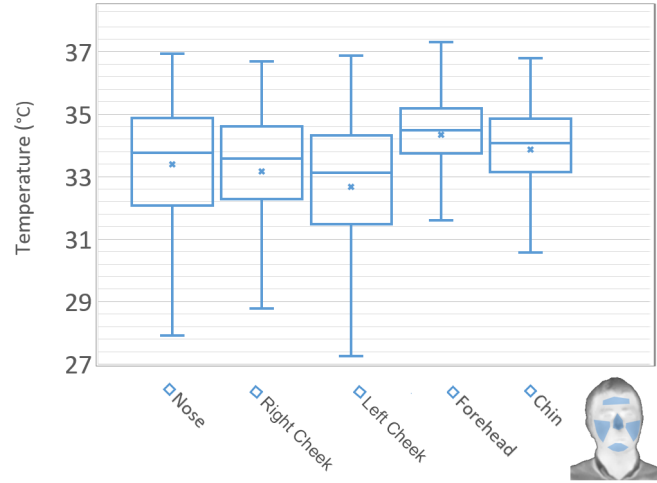
Figure 3.7: Skin Temperature Range For Each Facial Location

To have another holistic view of the changing patterns of different facial parts with room temperature, figure 4.9 shows the relationship between skin temperature and room temperature. The changing pattern of these charts shows that the temperature in all facial areas for the whole dataset has a positive weak linear association with the room ambient temperature. The The R^2 values for these linear patterns are chin 0.13, forehead 0.4, nose 0.4, cheeks' average 0.6, left cheek 0.25, and right cheek 0.25, which backs up this linear relation. The linear correlation values with the Pearson method are also presented in Table 3.5, which will be further discussed. As it is shown the forehead area has the lowest linear slope (0.1918) and the temperature range as the air temperature increases to the highest amount. On the other hand, the nose temperature shows the most significant change as the air temperature increases with a linear slope of 0.5742. These findings are in line with the literature [147] , highlighting that the nose area has the highest correlation with the room temperature. In contrast, the forehead area changes the

least and can be a good indicator of internal body temperature. As shown in this figure, we have looked into both rights and left cheek temperature and their average temperature. The average cheek temperature is the average temperature of the left and right sides when both sides are visible in the thermal frame. If the head position is a full profile, the invisible cheek is excluded from the calculation. Therefore, although the number of data points for the right and left cheek is less than the other facial parts, the cheek average has the same data point as the other face areas.
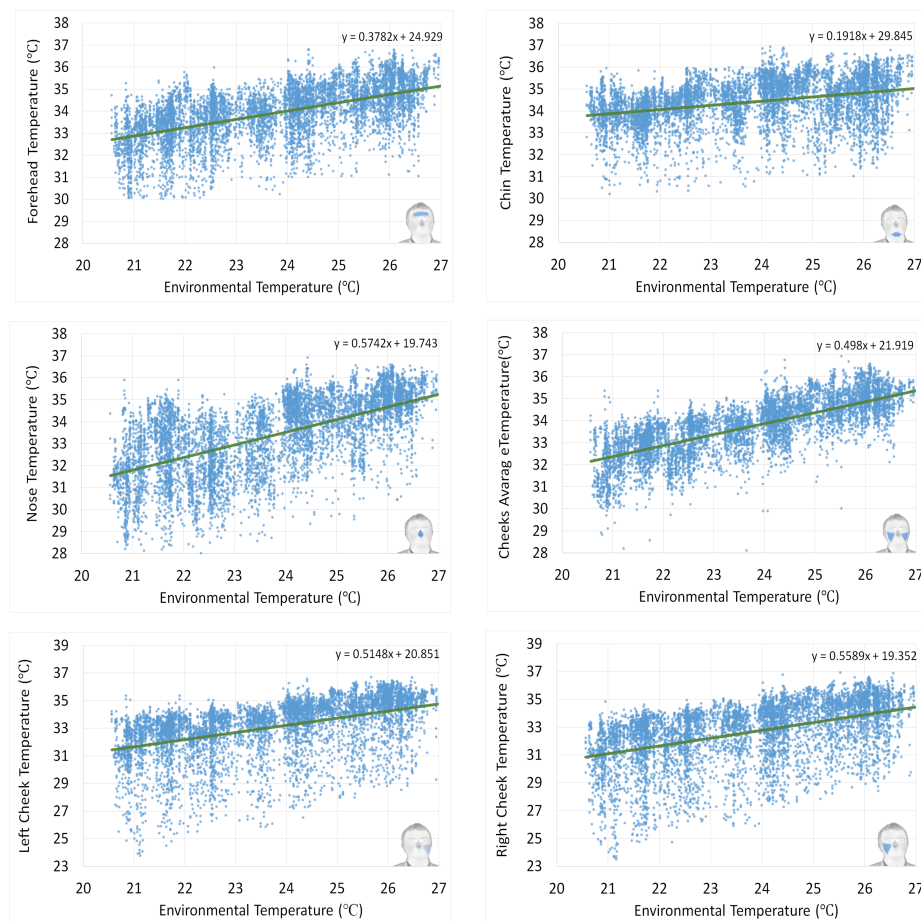

Figure 3.8: Correlation of Facial Locations With Room Temperature for All Subjects

Furthermore, Table 3.5 presents the "Pearson Correlation Values" for different facial regions with the environmental temperature and the subjects' thermal sensations across the whole dataset. The Pearson correlation coefficient indicates the strength and direc-

tion of a linear relationship between different variables, and it would be a relevant factor for our investigation. Table 3.5 shows that the cheek average and nose area have the highest correlation with the environmental temperature, which is 0.76 and 0.67, respectively. On the other hand, the forehead area has the lowest correlation with the environmental temperature, which proves the applicability of this facial area as an indicator of core body temperature, as environmental properties less influence this area. This result is in line with the previous findings from the literature[147] on the correlation of different facial regions with the environmental temperature. In addition, we can see that the cheeks and the nose area are the best indicators of subjective thermal sensation, while the forehead area is not that suitable for that purpose.

Table 3.5: Correlation of Facial Regions With Room Temperature and Thermal Sensation

	Right Cheek	Left Cheek	Cheeks Average	Nose	Forehead	Chin
Correlation with Room Temperature	0.5	0.5	0.76	0.67	0.35	0.55
Correlation with Thermal Sensation	0.42	0.43	0.63	0.55	0.22	0.45

The relationship between different facial regions among all the subjects is also calculated based on the Pearson Correlation Coefficient and visualized in a heat map figure. As Figure 3.9 shows, most of the facial regions have a moderate to relatively strong correlation . The right and left cheeks show no correlation, which results from the change in the head positions that makes the two sides have different angles with the camera in most of the data frames. When the head is in a semi-profile position, one of the cheeks is right in front of the thermal camera, while the other side has an angel with the thermal camera, which makes the reading of that side lower than the actual temperature. As a result, the two facial sides can only have an approximately similar reading condition in the full frontal face position. This correlation heatmap also shows that the cheek area has the highest correlation with other facial regions, especially the nose and chin region (0.62). On the other hand, the forehead has the lowest correlation values with other fa-

cial regions, which was expected based on both literature and the correlation values of the forehead area with the environmental temperature from Table 3.5.
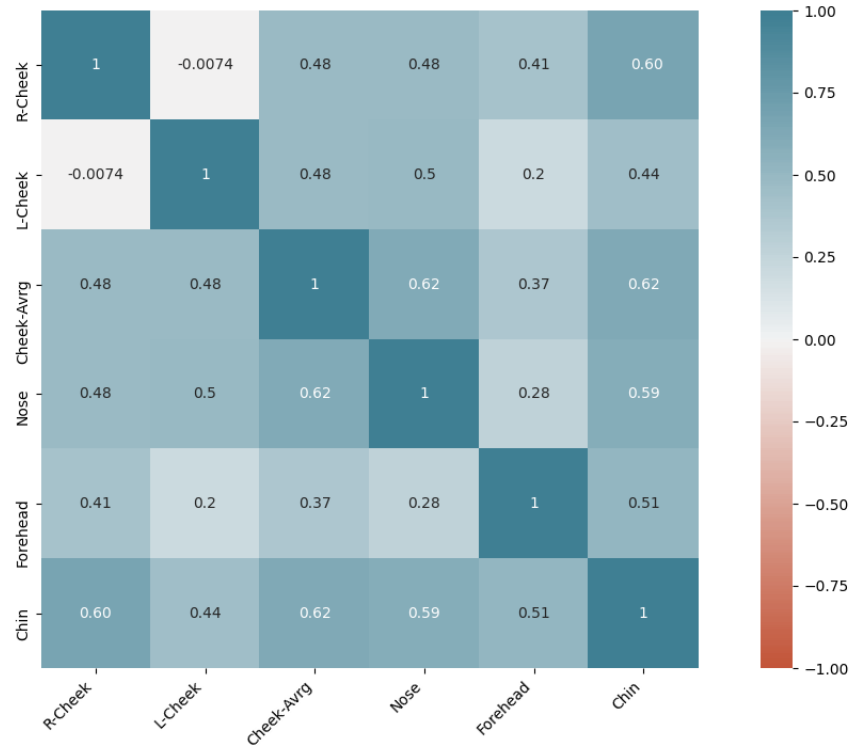
Figure 3.9: Correlation of Different Facial Areas Among All Subjects

Moreover, as one of the main focuses of this study, the importance of environmental temperature in changing the facial thermal images is highlighted by studying some sample images from the dataset of three selected subjects. Figure 3.10 shows how the facial skin temperature changes in three different thermal conditions for these three individuals. The first row has the lowest Room Temperatures (RT), which increases gradually as we reach the last row. The RT for each row is approximately the same for all three subjects. In addition, the reported Thermal Sensation (TS) of each subject is included, which is also the same for images of subjects in the same row. Ironbow A false-color pallet is used for easier identification of changes in different facial areas.

The authors have selected an ellipse-shaped Region of Interest (ROI) in the facial area.
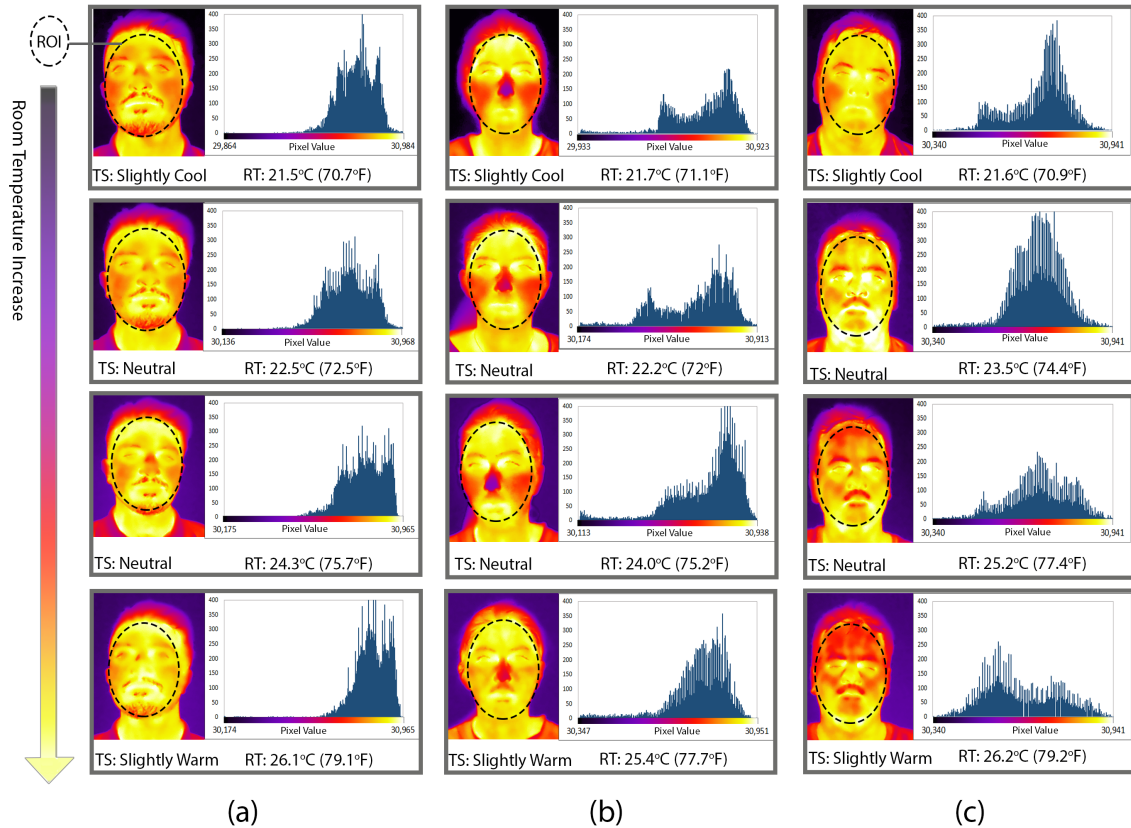
Figure 3.10: False Color and Histogram Representation of Sample Data In Different Temperatures, TS: Thermal Sensation, RT: Room Temperature

The histogram of the pixel value distribution in the defined ROI also shows how skin temperature changes on the whole face for each subject. As mentioned in Equation 4.1 the skin temperature is calculated linearly from the pixel value, so the larger amounts of this value show a higher skin temperature. We can observe that the nose and cheek area show more apparent changes than the forehead and chin for all three subjects. In addition, we can see in both the false-colored images and histograms subjects (a) and (b) have a noticeable increase in their skin temperature as the room temperature increases.

The individual differences in facial regions' temperatures can also be detected easily in images of different subjects in the same row when the Room Temperatures (RT) are relatively close together. For instance, in the first row, the room temperature is in the range of (21.5°C-21.7°C), but the user's skin temperature shows apparent differences in different facial regions. It is also important that all three subjects have re-

ported their thermal sensation as "Slightly Cool," while their facial thermal image and the ROI histogram vary to a great extent. While subjects (a) and (b) show an increase in the facial skin temperature, subject (c) shows a different pattern in skin temperature changes, which is an initial increase followed by an identifiable decrease when the temperature reaches 25.2°C (77°F). The explanation for this behavior change is that the subject was beginning to sweat in the forehead area, which was not noticeable even by himself. The higher ambient temperature was the cause of the sweating. As mentioned by the individual, he typically has a lower tolerance for increased ambient temperatures, which results in him sweating more frequently in a hot room temperature. However, the perspiration was insignificant and therefore not noticeable by the researchers or the subject at the time of the experiment. This behavior highlights the importance of including ambient temperature variation in the facial thermography dataset. We can observe that the forehead area of this subject shows an increase when the room temperature changes from 21.6 °C to 23.5 °C and the subject's thermal sensation changes from "Slightly Cool" to "Neutral". However, as the unnoticeable sweating begins in the next two rows, the forehead temperature decreases, while the subject's thermal sensation changes to "Slightly Warm". These individual differences in the facial thermal images have reoccurred in the three next rows, as well as the whole dataset. The personal differences in facial thermal images are one of the main reasons we need a comprehensive dataset in several different thermal conditions for our investigations into facial thermography.

Although the subjects show personal differences in their facial thermal images, we can observe a linear correlation between the temperature of different facial areas and the environmental temperature in all of them. Figure 3.11 presents this linear correlation in all the facial regions and for all the included subjects. The horizontal axis presents the room temperature, and the primary vertical axis shows the facial skin temperature. In addition, each person's reported subjective thermal sensation as the temperature in-
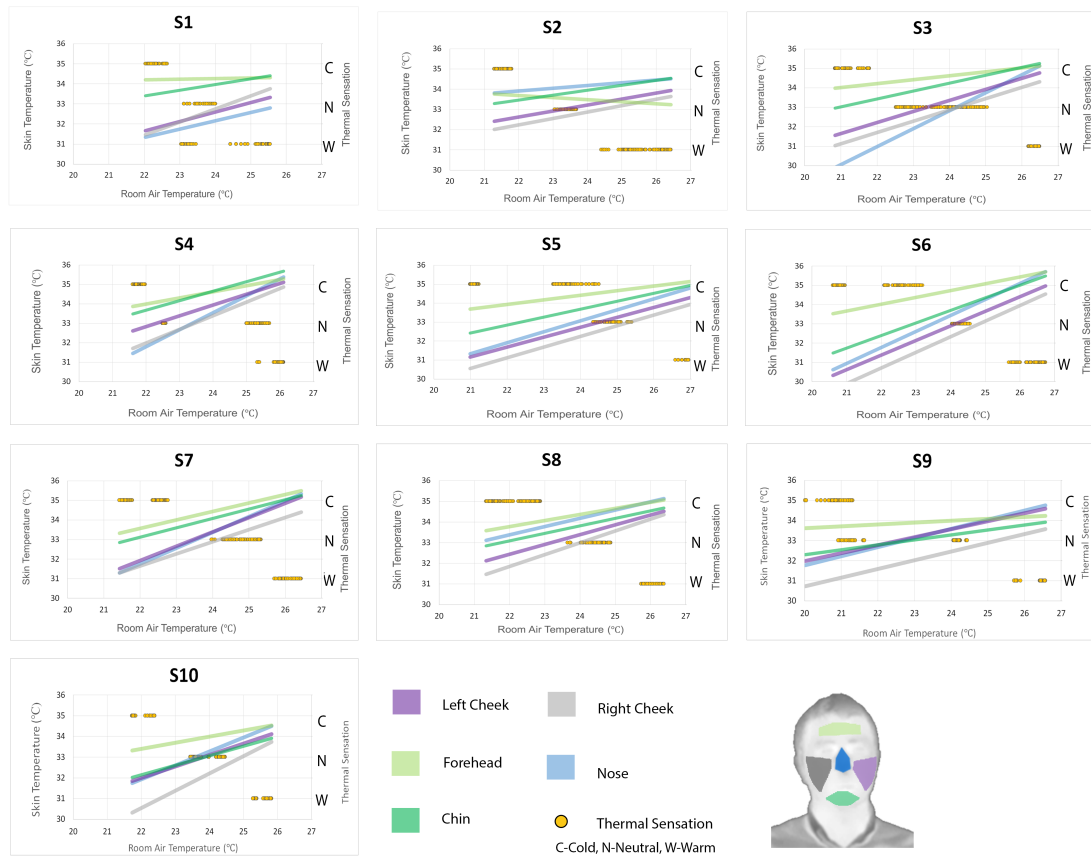
Figure 3.11: Linear Correlation of Facial Skin Temperature in Different Areas With Room Temperature For Each Subject In Addition To Their Thermal Sensation (C-Cold, N-Neutral, W-Warm)

creases is displayed in the secondary vertical axis. As shown in Figure3.11, for all the individual subjects, the highest skin temperature variations as the room temperature increases are in the nose and cheeks area, and the lowest variation is in the forehead and chin area. This is important to note that subject 2's forehead temperature decreases as the room temperature increases, which was previously explained in Figure3.10 for the same subject in column (c). Another important observation from this figure is the higher temperature differences in facial areas when the room temperature is low compared to higher room temperatures. This pattern is repeated in all the subjects, while the differences are much greater in some of them, such as subjects 3 and 10. These figures also show that all the subjects have experienced different thermal sensations; however,

the pattern and frequency of each thermal vote are different and based on individual differences.

3.5   Discussion and Future Work

This paper presents a novel facial infrared thermal dataset with variation in environmental properties, distance from the camera, and head position in raw 16-bit data frames. The data is annotated with each person's environmental conditions, facial landmarks, and at the time of recording each frame. The subjective thermal sensation annotations are a new addition to the face thermal image datasets. The comparative study of the temperature in different facial areas shows the importance of environmental temperature in facial thermography. Variation in environmental temperature, facial resolution, and head position makes our dataset an excellent fit for training facial recognition algorithms. Another important consideration is identifying facial landmarks for a more precise evaluation of facial skin temperature. Although we have used the RGB paired images for facial area identification in this paper, there is other state-of-the-art research for facial landmark detection. Since our dataset includes images with various resolutions, it would be a great fit to evaluate the prediction accuracy of such algorithms, which would be one of our future research objectives. The explanation for this behavior change is that the subject was beginning to sweat in the forehead area, which was not noticeable even by himself.

In the data analysis section for this paper, we have focused on the reliability of the dataset for future research. Therefore, we have looked into the temperature range of the images and the correlation of ambient temperature with the skin temperature of each subject. However, other analyses can be performed on this dataset, including investigation of the performance of different learning algorithms on facial landmark detection. In addition, studies can be performed to investigate the accuracy of detecting subjects' thermal comfort based on their skin temperature. Although previously included research has already proved this possibility [34], it is important to study this feature in a

farther distance from the camera if we want to apply it in real buildings. Another subsequent study would be on the prediction of subjects' thermal sensations based on the infrared thermal images by utilizing the current dataset. We will analyse the influence of distance and head position on the thermal camera readings and the prediction accuracy of thermal comfort based on the subjects' skin temperature. The manual annotation of the facial frames will provide us with the ground truth facial landmarks in the thermal frames, which will be used for the validation of our presented approach.

More projects are in progress for the improvement of this dataset based on its current limitations. Our dataset does not include different facial expressions, which are included in some datasets and will be added to our updated versions. Currently, due to the high variety of recording conditions for each subject, we have included ten subjects in our experiment. We are planning on adding more subjects in the future version of our dataset from different ethnic groups. The current dataset was recorded in a controlled indoor environment. Including images that were taken outdoors could make this dataset more suitable applicable. In addition, our current dataset does not include RGB images, which can be included in our following versions to make the dataset helpful for a broader range of projects. The complete dataset is available for downloading on our Github page [206].

CHAPTER 4: Deep-Comfort: A Deep-learning Based Multi-Camera Approach for Personalized Thermal Comfort Prediction at the Distance

4.1   Introduction

In our current society, people spend more than 90% of their time indoors, which causes indoor environmental qualities to have a significant influence on their health conditions. Although the building sector consumes approximately 40% of the globally produced energy, the majority of which is used in Heating, Ventilation, and Air Conditioning (HVAC) systems, people are generally dissatisfied with their environmental comfort conditions. In this regard, a recent large-scale survey reports that approximately 40% of building occupants are dissatisfied with the thermal conditions in their indoor environment. This global survey, which is the result of a 20-year study, focuses mostly on office buildings, which account for 77% of the investigated buildings [1]. Another research on 52,980 occupants in 351 predominately North American office buildings has indicated that only 2% of the studied buildings are providing thermal comfort for 80% of their occupants [2]. This wide range of dissatisfaction with thermal conditions urges the need to improve the indoor environment to prevent the health problems resulting from discomfort caused by poor indoor thermal conditions. Sick Building Syndrome (SBS) is a recent concept that has attracted the attention of researchers in this area to the influence of built environments on human health conditions. The thermal state is one of the primary factors of Indoor Environmental Qualities (IEQ) that can impact occupants' well-being. It has also been proven that temperature and humidity conditions are significant contributors to the SBS symptoms, which include fatigue, headache, susceptibility to cold and flu, and disruption of sleep patterns [3]. One of the main causes of these poor environmental conditions is relying on explicit, predefined models of ther-

mal comfort, which do not correspond to the actual preferences of different occupants in the environment [4]. Depending on general standards, it is nearly impossible to accommodate varying degrees of people's thermal preferences. [5]. Recent research in human-centered design attempts to leverage occupants' demand in the control loop of the buildings to consider the well-being of each individual based on their own physiological properties. This research is also referred to as personalized comfort. Personalized comfort is a recent concept in the area of human-centered building that focuses on providing comfortable conditions for each occupant based on their own preferences. Therefore, a real-time feedback system is needed to provide data from occupants' physiological conditions that can be used for controlling the building's HVAC system. The innovations in environmental data gathering have provided a unique opportunity to collect large amounts of information from the buildings' occupants, which can be studied to improve building control conditions. In this regard, the emergence of thermal imaging technology has made contactless data collection possible without interfering with occupants' activities. The collected physiological and environmental data can then be utilized for predicting and controlling each occupant's thermal comfort conditions in the built environment through personalized comfort models. The promising results of initial studies in this area have attracted researchers' attention to utilizing thermal cameras as a feedback system in the buildings' control loop. While there is currently an increasing interest in utilizing infrared thermal cameras in public buildings because of their non-invasive quality, these state-of-the-art methods need additional modifications to become more reliable and holistic. There are some critical gaps in the current methods that have limited the application of this platform in real buildings. Firstly, the distance of the subject in the current studies is a maximum of 2 meters from the camera, which makes the platform applicable only to very small rooms. Secondly, desired Regions Of Interest (ROIs) for thermal readings are generally defined manually or with a lack of accuracy in detection. Thirdly, in most of the current research, subjects are asked

to maintain a frontal face position or have minimal changes in head position as their landmark detection methods are limited. In this research, we are studying the collection of facial skin temperature data in a completely non-intrusive approach through thermal cameras for thermal comfort prediction. In addition, we create a platform for more precise readings from larger distances, which makes it a great fit for real-time applications in the current world. This is accomplished by leveraging both visual and thermal cameras to create a multi-modal sensing platform. To capitalize on the potential and address the existing limitations, this study takes a more holistic view of non-intrusive thermal monitoring for thermal comfort prediction. In this research, we are looking into collecting thermal conditions from subjects at a farther distance in a completely non-intrusive method. The project is significant because it creates an automated approach for utilizing both thermal and visual images to detect facial landmarks in several different head positions.

- Firstly, to address the limitation of a subject's distance from the camera and their position, our study takes into account facial thermal images from subjects at several distances and different head positions. By utilizing the powerful HRnet algorithm [42, 43], we have successfully investigated the subjects at a maximum distance of 6.6 meters from the camera and 25 different head positions. In addition, to resolve the lack of accuracy, we have utilized an automated mapping approach for registering thermal and visual images that can detect the specific Region Of Interest in images of any resolution and head position.

- Secondly, to increase the accuracy of thermal comfort prediction, we have included the distance from the camera and head position as an input to the prediction algorithms. Our results have indicated that including the distance and head position in the prediction process can increase prediction accuracy in general.

In this paper, we have combined deep learning-based object detection and facial land-

mark detection through the HRnet algorithm with supervised machine learning algorithms to accurately predict personalized thermal comfort from a distance. We have utilized the two powerful classification algorithms of Random Forest and K-Nearest Neighbor to predict the thermal preferences of the subjects at different distances from the camera and head positions. For both algorithms, we have conducted a comprehensive grid search to select the best combination of input variables and hyperparameters. The results of our study highlight the superior performance of the Random Forest machine learning algorithm in comparison to K-Nearest Neighbor algorithms. In this study, we could achieve an accuracy of 92.3% for personalized thermal comfort prediction, and the average accuracy among all subjects was 86.1%, which proves the successful application of our platform. In addition, we have investigated the influence of distance from the camera and head position on the thermal reading of infrared thermal cameras.

The rest of this paper has three main sections. In Section 2. Literature Review, we study the conventional and personalized thermal comfort models and provide a comparison of the current thermal camera-based personalized comfort prediction. Section 3. Methodology explains the data collection process, followed by data extraction and analysis. In Section 4. Results present the influence of room temperature, distance from the camera, and head positions on the skin temperature and infrared thermal readings. In addition, the results of the two selected prediction algorithms are discussed in detail. Section 5. Conclusion, including a final review of the highlights of our study and future work.

4.2   Literature Review

Thermal comfort models are an approach for quantifying the subjective evaluations of a human's thermal state, which enables a shared understanding of thermal satisfaction. Thermal comfort assessment is a tough process due to the presence of numerous influential variables such as air temperature, air velocity, relative humidity, solar radiation, clothing level, and level of activity. Here, we are reviewing two conventional ther-

mal comfort models, which include one widely used Predicted Mean Vote (PMV)and adaptive model, and more recent personalized models.

4.2.1   Conventional Thermal Comfort Models

For over thirty years, scientists have studied and applied many human thermal comfort models based on physiological and psychological responses[21]. The Predicted Mean Vote (PMV) is a frequently used model for assessing thermal comfort, which was developed by Fanger in 1960 to represent the average thermal sensation vote of a wide group of individuals. The model is based on the differential between generated and released heat from the human body, as well as its correlation with subjective comfort perception. The final contributing factors to this model are environmental factors, including air temperature, mean radiant temperature, air velocity, and relative humidity, and human-related factors, which are activity and clothing level. Subjective comfort is measured on a scale of +3 for very hot, -3 for very cold, and 0 for neutral. Although PMV is currently the most widely used thermal comfort model, it has performed poorly in recent research for three main reasons. Firstly, this model was developed in a chamber setting under the air conditioning of the space, so the result is expected to be different in actual settings and naturally ventilated buildings. Secondly, several physiological and psychological differences in individuals result in different subjective thermal preferences, which were not accounted for in the PMV calculation. The third major reason for PMV model inaccuracy is the adaptable behavior of humans to their environment during different temperatures at different times of the year. This behavior is hypothesized as *adaptive hypothesis* highlighting the different features such as past history, thermal expectations, and thermal controls to have an impact on human thermal preferences. The second conventional thermal comfort model is the adaptive model, which works based on this theory. In other words, the individual's thermal acceptance and preference are under the influence of the outdoor conditions during different times of the year. [23]. The adaptive comfort model was incorporated into the ASHRAE 55-2004 standard and

continued to improve in further versions. The adaptive model has shown better performance in occupant-controlled buildings and naturally ventilated spaces due to the wider tolerance range of temperature when the buildings are ventilated naturally. Adaptive processes are known to be both physiological, such as thermal expectancy, or behavioral, such as changing the clothing level or other controlling options. According to this model, the range of thermal conditions that are acceptable to the occupants is dependent on the outdoor temperature and also on the actions that can be performed to reduce the discomfort or the possibilities for change. The majority of today's building control systems rely on these explicit predefined models, which do not accurately reflect the actual comfort of various occupants in the environment [22]. As space may be used for various purposes or duties over time, the occupants and their thermal comfort preferences may change. Additionally, the thermal comfort level would be influenced by human attributions such as age, gender, and metabolic rate. Along with physiological qualities, psychological factors such as emotional state (happiness or anger), and level of stress can significantly influence a person's subjective thermal sensations[22]. This makes it impossible to analyze individuals' thermal preferences, and the relative value of each contributing component based on general standards [5].

4.2.2 Personalize Thermal Comfort Models

Personalized comfort is a recent concept in the building design area that focuses on providing a comfortable environment for the occupants based on their preferences. This results from zonal conditioning, instead of the central air conditioning system, and the ability of occupants to change their thermal environment [24, 25] . Personalized models are based on the Human-in-the-Loop (HITL) concept, which has redefined the relationship between humans and their surroundings. Based on this concept, to achieve a high-performance building throughout the operation phase, it is necessary to embrace subjective human aspects in the control loop. Personal thermal comfort models are created based on behavioral or physiological variables associated with an individual's thermal

comfort. Research employs the two basic methodologies of the voting system and physiological sensing system to regulate the circumstances through direct feedback from the occupants regarding their comfort [26]. Thermal scale preferences are utilized to evaluate the level of comfort in participative sensor devices in the voting system [199, 207]. These voting methods are obtrusive and may be considered inefficient since they require continual feedback from the occupants. In some other platforms, individuals' preferences are learned over time through their habits, such as adjusting their desktop fan, heater, or other personal or central air conditioning devices. Several of these devices have been used and studied previously, including heating and cooling chairs [24, 208] , desk fans [62, 63] , radiant floors [209] . Physiological data is another type of information that has been demonstrated to have high predictive accuracy when used to create personalized comfort models. The temperature of the skin at various body locations is one of the most effective variables for developing a personalized comfort model [76, 31, 73]. In this regard, non-contact thermal cameras have been utilized to determine the skin temperature in order to develop a personal comfort model [36, 18, 34]. Incorporating IoT-based systems with HITL techniques enables the communication between various devices and also facilitates the exchange of data for sensing, actuation, and control [210]. The information acquired from users via IoT sensors is used to adjust and regulate building systems, including air conditioning [211]. A critical prerequisite for an efficient IoT system is data collection devices that provide real-time feedback on the controlling loop's current state. By utilizing different sensors, we can collect both environmental and physiological data on the building's occupants. In the Physiological feedback system, in addition to psychological data, we utilized established markers of thermal comfort, including skin temperature[73], heart rate [212], or both [76]. Some user-centered models incorporate wristbands to collect physiological data such as skin temperature and heart rate, as well as environmental data, in order to predict each occupant's comfort level [73, 212]. To develop another accurate data collection method,

infrared sensors were embedded in eyeglasses to measure the temperature of the front face, cheeks, nose, and ears. This increased the accuracy of predicting unpleasant situations to 82.8 percent [102]. The data gathering techniques listed above are invasive since the sensor devices must remain close to the human skin throughout the day, which may be distracting in a work environment. Furthermore, some users may be hesitant to utilize wearable sensors or may just forget to do so. Additionally, it requires the installation of sensors for all individual occupants, which is not always practical. These problems demonstrate how helpful it might be to use contactless, non-intrusive methods to collect physiological information from individual occupants.

4.2.3   Infrared Camera Based Thermal Comfort

Infrared cameras have the ability to assess the temperature of targeted areas from the occupants, making them an excellent alternative for measuring skin temperature from a distance. In this section, we review the current studies on thermal comfort prediction through infrared thermal cameras, which are also listed in table 4.1. Researchers started to extract facial skin temperature for detecting thermal stress by using infrared thermal cameras in 2007 [213]. Thermal cameras have been proven to be a reliable, non-invasive way to predict the need to change thermal conditions with a 94–95% level of accuracy [27]. This study has shown personalized comfort prediction has improved performance compared to when the subject's ID is not provided, which was 63% in cooling and 68% in heating, while Fanger's PMV method had a prediction accuracy of less than 65%. Researchers have also developed a real-time feedback system using the FlirA35 thermal camera and a depth sensor to analyze both the face temperature and the body pose of the occupants [28]. Further research has revealed the possibility of replacing the previous cameras with a less expensive and smaller infrared camera capable of predicting skin temperature with an acceptable accuracy of 85 percent [29]. This study has further investigated the possibility of developing a smart thermostat based on the developed prediction algorithms [30]. Thermal cameras have also been integrated with

visual RGB cameras for landmark detection and higher accuracy, [31]. Studies have also assessed the effectiveness of several facial feature detection algorithms in identifying areas of interest (ROIs) [32]. In this regard, research has compared the accuracy of three distinct sensor types, including air temperature sensors, wristband-based skin temperature monitoring, and thermal imaging-based facial temperature monitoring. This development proves the marginal improvement in accuracy when physiological sensors are combined with environmental sensors and casts doubt on the efficacy of physiological sensors as a consequence of this marginal improvement in accuracy (3% to 4%)[33] . Li et al. proved successful in monitoring and recording the skin temperature of two inhabitants concurrently utilizing two thermal camera nodes, each camera catching sections of their faces [34]. Although facial skin temperature is used as the primary physiological factor for thermal comfort prediction, other studies have considered several other body parts, including hands, shoulders, and torso [35, 36, 37] Thermal cameras have also been shown to be a promising tool for the non-invasive prediction of elderly thermal comfort in nursing homes [37].

Table 4.1: State of the art research overview

Study	Region*							Thermal condition	Duration	Temperature	Camera	Distance	Head Position	ROI	Prediction Method
	W	L	Ch	Cn	N	F	E								
[27] 2016		*	*	*		*		Uncontrolled	Twice/day Five weeks	23-26°C	Thermal FLIR A655	-	Frontal Face	Manual Rectangle	Rotation Forest
[28] 2018		*	*	*	*	*		Transient Cooling	60 minutes	25-17°C	Thermal FLIR A35 Depth Microsoft Kinect	1.40 m	Frontal Face	Active Appearance Model	No Prediction Sensor Fusion Techniques
[29] 2018		*	*		*	*	*	Transient Heating Cooling	3 Hours	22-28°C	Thermal FLIR Lepton	1 m	Frontal Face	Haar Cascade Rectangular	Random Forest
[35] 2018	*							Transient Heating	40 minutes	21.11 27.78 °C.	Thermal: FLIR Lepton Depth-Visual: Kinect	2 m	Frontal Face	Facial Patch by joint detection	No prediction ANOVA Test
[31] 2019		*	*	*	*	*	*	Constant Transient: Heating Cooling	2.5 hours	Constant: 20/24/28°C Transient: 20-28°C	Thermal: FLIR Lepton Visual: Pi Camera	Close Up	Frontal Face	Haar-Like Features Contrast in heatmap	Random Forest Support Vector Machine
[34] 2019	*							Transient Heating	50 minutes	23-27 °C.	Thermal: FLIR Lepton Depth-Visual: Kinect	1-1.30 m	Frontal Profile	Haar Cascade Dual camera nodes	No prediction ANOVA Test
[108] 2019			*			*	*	Transient: Heating Cooling	1-1.5 hours	24-19°C 22-29°C	Thermal: FLIR Lepton Visual: RGB	1-2 m	Free Frontal Face	Haar-Cascade dlib	Random Forest SVM KNN
[36] 2019	*							Transient Heating	2 hours 14 Sessions	17-30 °C.	Thermal: FLIR B8400	1 m	Semi-Profile	Manual Flir tools	Random Forest SVM
[37] 2020			*	*	*	*		Uncontrolled	5 minutes	19-25 °C.	Thermal: FLIR E60bx	0.5 m	Frontal Face	Facial Patch by joint detection	PMV PPD

* W: Whole Face, L: Lips, Ch: Cheeks, Cn: Chin, N: Nose, F: Forehead, E: Ears

The presented review shows that although the initial results are promising, the plat-

form's application in actual buildings has been limited by a number of major short-comings. Firstly, the greatest subject-to-camera distance in the present investigations is two meters, making the platform appropriate for relatively small spaces. In addition, it has been proven that one of the major factors that influences Thermal Infrared Reading (TIR) is the shooting distance, which is defined as the distance between the object and the thermal camera. This measure becomes more important in remote thermal readings, where the shooting distance is well over one meter. Although there is awareness of this factor's influence on thermal readings, there has been very little research conducted on this area until recently. Most of the previous researchers had performed their studies at equal distances from the camera to avoid this inconsistency. One main study on the influence of distance on TIR of living organisms was performed in 2016, which studied the shooting distance range from 0.3 to 80 meters. The study showed the powerful influence of the measuring distance on the first 20 meters of the subject. A non-linear decrease has resulted in an underestimation of the surface temperature [38]. Other studies on the influence of distance on human facial (inner-canthi of the eye) TIR have shown a measurement error in distances larger than 80 cm from the camera [39]. The findings from other recent research align with the previous studies on the distance variation effect. This field application of thermography has shown the strong influence of spot size and shooting distance on the surface temperature of both calibrated temperature sources and wild birds. The decrease in temperature can be as high as 6°C at a 10 m distance from the subject [40]. Secondly, required Regions of Interest (ROIs) for thermal measurements are often selected manually or with insufficient detection precision. Therefore, in the majority of current research, participants are instructed to keep a frontal face posture or have minimal head position movements due to the limitations of their landmark identification approach. Any change in the human head position will result in a change in the degree between the camera and the facial area. Research has shown that the influence of object position on the camera alters the TIR by affecting the

apparent emissivity[40]. This effect may result in errors as high as 8 °C if the angle is 90 degrees to the camera in comparison to 0 °, which also depends on the target area emissivity. Additional research has also studied the influence of the angle of the camera on the inner-canthi of the eye temperature, which also aligns with the previous findings. The mean temperature of the inner-canthi of the eye has decreased by 0.5 °C at 75 degrees to the camera [39]. As mentioned previously, the contribution of our study in this area is to develop a more advanced thermal comfort assessment from a distance through the integration of thermal and visual images. This includes performing several readings at different distances and head positions. One main objective of this study is the collection of facial skin temperature data in a completely non-intrusive approach through thermal cameras. In addition, this research creates a platform for a more precise reading from larger distances, which makes it a great fit for real-time applications in the actual world. This is accomplished by leveraging both visual and thermal cameras to create a multi-modal sensing platform. Through this integrated system, we will use visual cameras for localizing facial areas and thermal cameras to measure the thermal values of those areas, which will enhance the accuracy and robustness of sensing and measurement. The proposed system performs fine-tuning and calibration based on the actual physical properties, including the subject's distance to the camera and head position. The collected physiological and environmental data can then be utilized for predicting and controlling each occupant's thermal conditions in the built environment through personalized comfort models.

4.3   Deep-Comfort Methodology

Based on the literature, it has been found that there is a gap in utilizing these influencing factors in facial skin temperature readings for developing thermal comfort models. As mentioned previously, the contribution of our study in the thermal infrared imaging area is to develop a more advanced thermal comfort prediction platform from a distance through the integration of thermal and visual images. This includes performing several

readings at different distances and head positions to create the training dataset. As Figure 4.1 displays the methodology section consists of three main phases: data collection, data preparation, and comfort prediction.
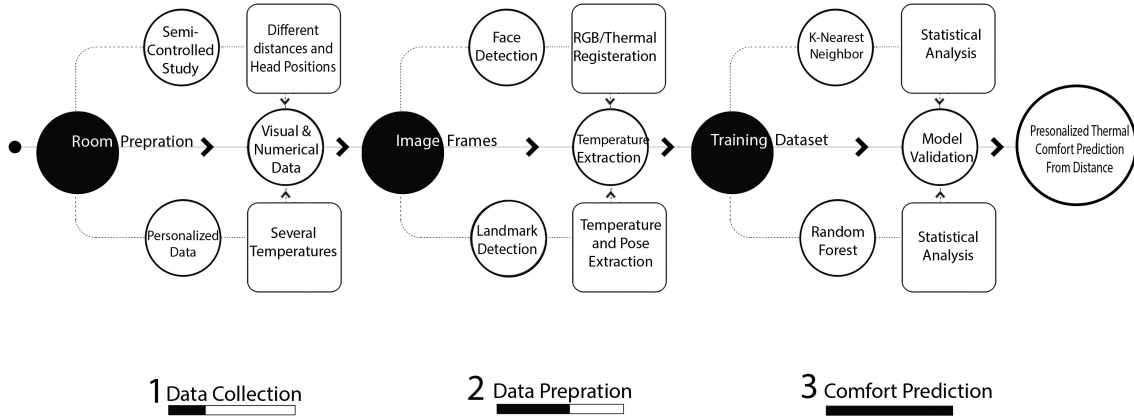
Figure 4.1: The Methodology Phases and Process

4.3.1   Data Collection

We have designed the data gathering process with the objective of creating a dataset that includes thermal and visual images in several thermal conditions and at several different distances from the camera and head positions. The Office of Research Protection and Integrity (UNCC-IRB 183845 has approved this study. The data collection process took place in June 2021. We collected the data in a one-day long session or two shorter sessions over two days based on the subject's preference. Participants are five males and five females, healthy adults. We made certain that the subjects were not suffering from any thermoregulatory illnesses, heat intolerance, colds, flu, or infections. The participants did not use any makeup or facial cream and removed their glasses for the recordings. All participants wore light-colored short-sleeve shirts and pants. Two of the male participants had facial hair. Table4.2 shows the information for each subject in detail.

The test room arrangement is shown in Figure 4.2, along with the locations of the following items: (1) thermal camera, (2) subject stations, (3) data loggers, (4) temperature and relative humidity sensors, and (5) air diffuser and airflow sensor. The tem-

Table 4.2: Subjects' Information

ID	Sex	Age	Height(cm)	Weight(kg)	BMI(kg/m²)
1	Female	34	168	69	24.4
2	Male	42	170	87	30.1
3	Female	30	170	54	18.7
4	Male	33	173	70	23.4
5	Female	34	163	57	21.5
6	Female	35	171	89	29.4
7	Male	32	168	70	24.8
8	Male	34	183	78	23.3
9	Female	33	168	72	25.5
10	Male	27	175	72	23.5
AVG	-	33.4	170.9	71.8	23.3

perature and humidity sensors are set at the number(4) and fixed on a pole at three different heights, as shown in this diagram (0.1, 1.1, and 1.7 meters). The recordings were made at 10 various relative distances ranging from 1 to 6.6 meters, as seen in this graph (2). After taking the informed consent, researchers recorded the participant's age,

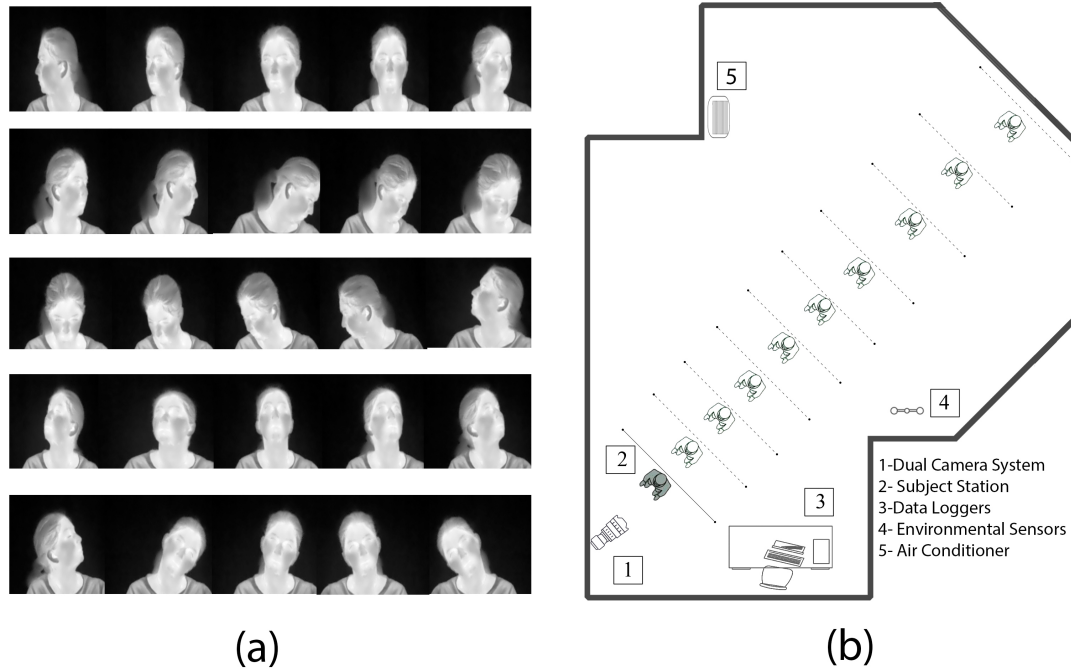(a)   (b)

Figure 4.2: Test Room (a) Head Positions (b) Recording Stations' Layout

gender, height, and weight. The participants had entered the test room and stayed in a seated position for 60 minutes before the test, so their metabolic rate had reached a stable state, and to eliminate any influence of the prior outdoor temperature, which

was eliminated. The data collection was performed in semi-controlled setups. The experiment for each participant was a combination of at least four sub-sessions in an approximately 90-minute time frame for each sub-session. The recording was initiated at a temperature of 21°C while the thermostat held the ambient temperature constant with a 1°C fluctuation allowance in each steady state session. Each subsequent session started at a 1.5°C higher temperature in the same one-hour time frame. The airflow was under 0.2 m3/s for all the sessions except the first session, which was the coolest, and as the experiment was conducted in the summertime, we needed the air conditioning to keep the temperature constant. Participants were seated in front of the camera during the study and changed their head positions as instructed while recording RGB and thermal frame pairs. The researchers performed the recordings in each station from the camera and in 25 different head positions instructed to the subjects (Figure 4.2). The user logged the thermal sensation in each station from the camera through a "Google Form" with standard levels. The thermal sensation scale is similar to the ASHRAE 7-point scale (3- "hot",2-"warm",1-"slightly warm",0-"neutral", -1-"slightly cool",-2-"cool", -3- "cold") and the thermal preference is the 5-point scale (slightly cooler, no change, slightly warmer, much warmer). An approximate number of 1,000 frames were captured for each subject, with a total of 10,903 thermal frames for the dataset. Table 4.3 shows the recorded variables and recording sensors' information in more detail. The air temperature and relative humidity are measured with HOBO Pro v2 temperature and relative humidity data logger sensors, which were calibrated with ice water before the experiments. The airspeed is recorded at the air diffuser proximity with an average distance of 3 meters from the subject's station. The data collected can be found at citeTeCSAR-UNCC/UNCC-ThermalFace. UNCC-ThermalFace is the first public thermal database annotated with each subject's thermal sensation at various temperatures. It also provides raw data frames with radiometric capabilities.

Table 4.3: List of Data Acquisition Devices

Variable	Device Brand	Model	Accuracy	Resolution
Indoor Air Temperature	Onset	S-THB-M008	+/- 0.21°C from 0° to 50°C	0.02°C at 25°C
Relative Humidity	Onset	S-THB-M008	+/- 2.5% from 10% to 90% RH	0.1% RH
Air Velocity	Fluke	922 Airflow Meter	±2.5% of reading 10.00 m/s)	0.001 m/s

4.3.2   Data Extraction

We have extracted the skin temperature from the thermal images through the following steps, as Figure 4.4 displays. 1,2. In both thermal and visual frames, the face region is cropped by the detected facial area in the visual image. After using several face identification methods, we cropped the facial region using a Dlib-based face recognition model. This model is built on a Residual Networks ResNet layer with 29 convolutional layers [203]. 3. Two masked images are generated from thermal and visual RGB frames in order to calibrate the two images together accurately. The masking of the thermal images is conducted by assigning black or white values to pixels with less than or more than a threshold value. For the visual images, we have utilized the deep learning-based segmentation code by HrNet [42]. 4.The Homography matrix is constructed by using the orientated fast and rotated BRIEF (ORB) properties between the two masked frames [214]. 5.Facial landmarks are identified from the visual frame, and required ROIs are computed based on these facial landmarks. In each RGB picture, 68 face landmark coordinates are recognized and converted to the thermal image using the homography matrix established in the previous stage. 6.Based on the specified ROIs and the thermal image type, we can read the skin temperature of the desired facial areas.

The authors have utilized the estimated facial landmarks to define the selected facial areas, as shown in Figure 4.4. Since the recorded frames are raw radiometric data, the value of each pixel presents the temperature of the pixel's representing area in the actual world. According to the Flir camera's datasheet, when using the TemperatureLinear (TLinear) option, the temperature of each pixel in degrees of Kelvin can be defined with Formula 4.1. It is also very important to set the emissivity of the measuring target to the
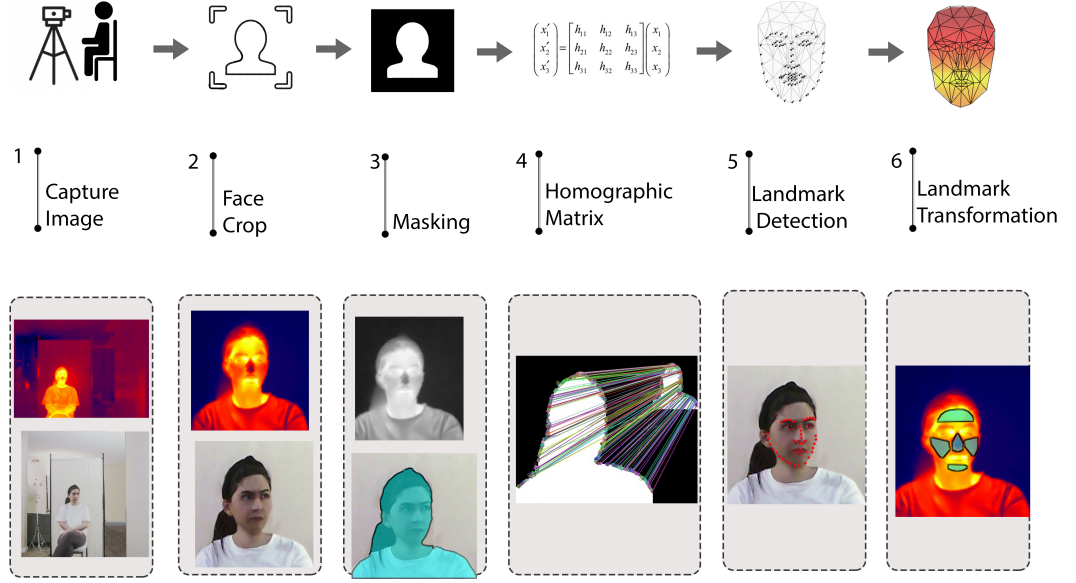
Figure 4.3: Identified Facial Areas Based on Landmarks In Three Different Facial Positions

correct number before the capture, which is 0.98 for the human skin. We have set the TLinear resolution is set to 100 mK(millikelvins) in our recordings [140].

$$SkinTemperature = (PixelValue/Tlinearresolution - 273.15K) \qquad (4.1)$$
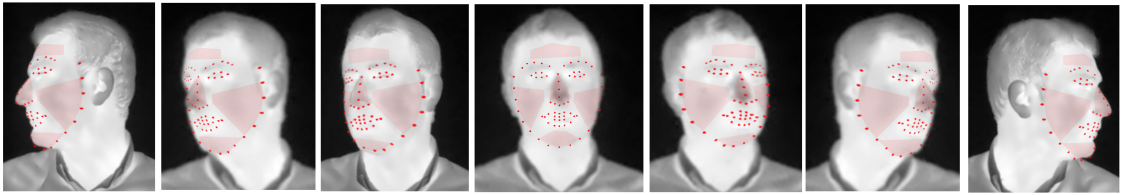
Figure 4.4: ROI Detection Based on Facial Landmarks in Some Head Positions

The physical variables include the distance from the camera and head position variables. We have calculated three independent variables based on the facial landmark

status to present the head position, which includes yaw, pitch, and roll. As figure 4.5 presents yaw variable is the rotation of the head along the Y axis (horizontal rotation) and the pitch variable presents the rotation along the X axis (vertical rotation). The face roll presents the face rotation in the XY plane. Table 4.4 presents the recorded dependent and independent variables, including environmental, physical, physiological, and psychological features.

Table 4.4: Recorded Variables
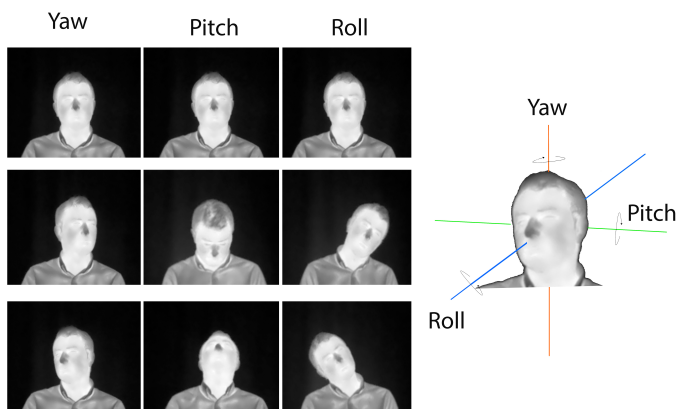
Category	Feature
Survey	Thermal preference
	Thermal sensation
Environmental properties	Indoor Air temperature
	Relative humidity
	Globe temperature
	Airflow
	Illuminance level
	Outdoor Temperature
Physical Properties	Distance to camera
	Head Position
Infrared Thermal Reading	forehead
	cheeks
	Nose
	Chin

4.3.3   Comfort Prediction

We have prepared all three types of environmental, physiological, and psychological data to investigate the accuracy of different machine learning algorithms in predicting subjects' thermal preferences. In addition, we have studied the influence of independent variables, including room temperature, distance from the camera, and head position on the skin temperature-dependent variables. This section includes an initial investigation of all environmental and physiological data and the correlation of facial skin temperature in different regions with room temperature. To that end, we have calculated the correlation factors between room temperature and skin temperature values based on the Pearson Correlation Coefficient. The Pearson correlation coefficient indicates the strength and direction of a linear relationship between variables and is relevant for our calculations. The main part of the analysis section is the machine learning-based thermal comfort prediction. In this study, thermal preference is a state, which makes our case a classification problem. We have gathered two types of subjective thermal votes, including thermal preference and thermal sensation. Considering the final objective of these predictions, which is the personalized thermal environment control in smart buildings, we have utilized the thermal preference variable for our machine learning problem. We have trained two supervised machine learning algorithms to test the accuracy of the prediction of the thermal preference based on the provided input variables. We have selected the Random Forest (RF) and K-Nearest-Neighbor (KNN) algorithms among all others due to our prior findings in our previous study. Based on our research, these two algorithms perform better than the Support Vector Machine algorithm in thermal comfort prediction based on personalized thermal images [165]. Other researchers have also studied different machine learning algorithms for thermal comfort prediction, concluding the successful performance of Random Forest [29], Support Vector Machine [36], and K-Nearest Neighbor [18]. The KNN is a classifier algorithm that works based on the close proximity of similar data points, which has a wide application

in recommender systems. An essential task in utilizing this classifier is selecting the best number for the K hyperparameter, which provides us with the most accurate results. To select the best K number for each subject, we have compared the accuracy of the classification with K numbers from 1 to 30 and selected the best K for each. Figure 4.6 displays a visualization of the KNN classification when K=5 and with just two features of "Nose Minimum Temperature" and "Right Cheek Minimum Temperature".
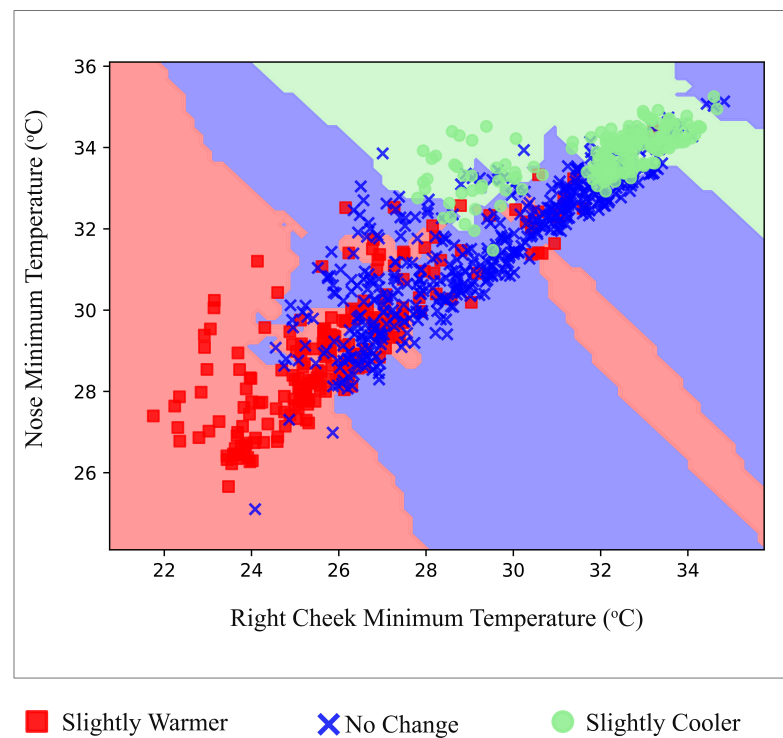
Figure 4.6: KNN Classification Visualization With Two Features for a Subject

The RF classifier is another supervised machine learning algorithm which works based on several decision tree algorithms and subsets of data. RF employs several hyperparameters to either improve the performance and prediction accuracy or speed up the model-making process. Therefore, it is essential to select the right combination of hyperparameters based on the provided data to achieve an acceptable level of accuracy. For the RF algorithm, we have conducted a grid search for tuning the hyperparameters by testing the accuracy of unique each configuration. The available op-

tions include 'max-depth': (40,60,80,100,110), 'max-features': ('auto','sqrt', 'log2');'min-samples-leaf': (2,3,5);'min-samples-split': (2, 5, 10), 'n-estimators': (300,500,700, 1000). Table 4.5 presents the selected hyperparameter combinations for each subject. Another essential step in preparing our prediction models is *feature selection* process, which helps us with choosing the most important input variables to reduce overfitting, improve performance, and decrease computation time. Based on the data types, we have selected the Chi-Squared method for our feature selection task. We have selected a limited number of features for each subject based on the chi-squared feature selection approach. Using this method, we could identify the dataset attributes that contribute the most to our prediction variable, thermal preference. To increase the score of the model, we require a dataset with high chi-squared statistics; thus, it would be advantageous if we could choose features from the dataset that have high chi-squared statistics. Also, the chance of data overfitting would go down if we chose 12 variables from the factors given. We need to highlight that the total number of input variables is 22, which includes 18 skin temperature variables, 3 variables related to head position, and 1 variable for the distance to the camera.
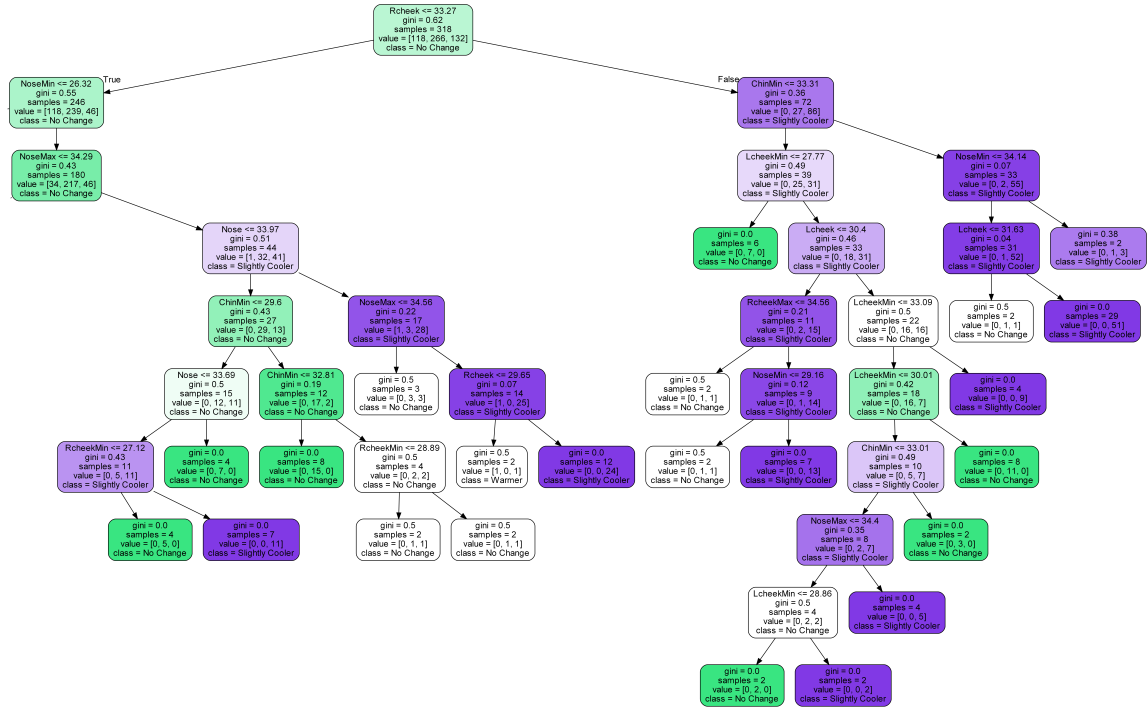
Figure 4.7: A part of a Tree in the Random Forest Classification for a Subject

Moreover, we have used the K-fold cross-validation method to limit the likelihood of over-fitting the model to the training set and produce a model that is more generally applicable. That would be using a small sample to see how well the model is expected to work when used to make predictions on data that wasn't used during training. Both algorithms were investigated using 10-fold cross-validation, in which the dataset was randomly divided into 10 groups. Cross-validation performs the fitting operation ten times, with each fit being conducted on a training set comprised of 90 percent of the entire training set, with the remaining 10 percent being utilized as a holdout set for validation.

4.4   Results and Evaluation

4.4.1   Initial Analysis

A total of 10,930 image pairs were captured from 10 subjects. As the facial landmarks are detected in the visual RGB images, we first need to look into the performance of the

Table 4.5: Selected Random Forest Hyper-parameters For Each Subject

	max_depth	max_features	min_samples_leaf	min_samples_split	n_estimators
S1	110	log2	3	10	300
S2	80	sqrt	2	5	1000
S3	40	auto	2	2	500
S4	60	auto	2	2	300
S5	100	sqrt	2	5	500
S6	60	sqrt	2	2	700
S7	40	auto	2	2	1000
S8	40	log2	2	2	300
S9	40	sqrt	3	5	300
S10	80	auto	2	5	300

landmark detection algorithm. Table 4.6 presents in detail the total number of recorded frames for each subject, in addition to the number of frames that their facial landmarks could be detected. All the subjects have participated in at least four experimental sessions. Subject 3 and subject 5 have participated in five sessions. The number of captured images for subject 1 is slightly less than the other subjects due to some damaged recorded frames, which were deleted. The highest number of captured frames is 1340 frames for subject 5. As shown in Figure 4.8 the percentage of detectable frames decreases as the distance from the camera increases. This decrease in face detection algorithm performance is expected as by going farther from the camera, the image resolution decreases as well. Although the integrated RGB camera has a resolution of 1280x960 pixels, the face recognition algorithms depend on the resolution of the facial frame detected in the image. In addition, the face position influences the facial detection algorithm performance. As an instance, the performance of a recent facial recognition algorithm was 98% in the frontal view, 84% for profile position, and 57% for half profile position. [215]. Distance from the camera has also been shown to impact the performance of landmark detection algorithms (reference). Figure 4.8 displays that the lowest amount of facial landmark detection for the whole dataset is 33% detection rate at 6.6 meters distance from the camera, and the highest detection rate is 85% at the distance of 1.8 meters.

For each facial region, three measures of mean, maximum, and minimum are calculated in each frame. The initial results from our previous experiment have shown that

Table 4.6: Recorded Frames and Detected Faces For All Subjects

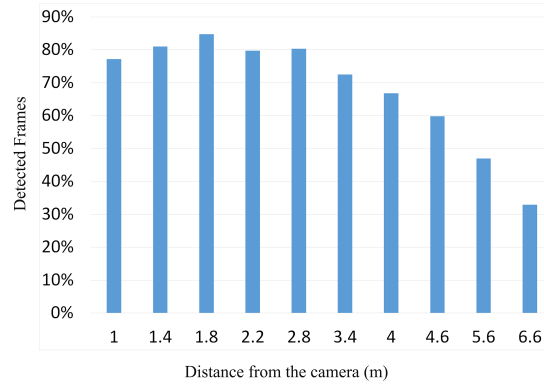|	Total	Detected	Percentage
S1	858	506	59%
s2	1050	736	70%
S3	1340	852	64%
S4	1071	641	60%
S5	1340	1036	77%
S6	1083	817	75%
S7	1084	636	59%
S8	1083	785	72%
S9	945	636	67%
S10	1076	669	62%
	10930	6645	61%

Figure 4.8: Skin Temperature Range For Each Facial Location

there are some inconsistencies in the thermal camera readings. This change in thermal measurements is due to the camera's Fast Field Correction (FFC) action, which is executed every 3 minutes to re-calibrate the camera. We have removed this thermal drift by calibrating all the thermal values in each image frame with a reference point in the background. We have used an IButton sensor to record the accurate temperature of the subjects' background partition and used this temperature value and its corresponding pixels in the thermal images to calibrate all the other pixels' thermal values. IButton sensors have an accuracy range of ±0.5°C, and the resolution of this device is 0.125°C [216]. For removing the outliers, we have only deleted the data with skin temperature less than 20 °C and more than 37°C. We have not used any other smoothing filter on the data as the previous research in this area [34, 18]. The reason for this decision is that

our data includes image frames with sudden changes in the head position, which we expect to influence the thermal readings to a high extent. Applying any filter to this data for smoothing the data points may result in an inaccurate investigation of how changing the head position changes the infrared temperature. To have an initial presentation of the extracted data, Figure 4.9 displays the room temperature, calculated minimum, maximum, and mean for the nose and cheek area for subject 3. This figure includes both the right and left cheek in addition to the average of these two in each frame. The cheek average is calculated based on the head's rotation degree and the visibility of each side in the thermal frame. As it was mentioned in the literature and will be explained in the next section. The thermal readings change as the head position changes in front of the camera. This makes the thermal readings of some facial areas, such as the cheeks, unrealistic at high rotation degrees. We have decided to add the cheek's average factor based on the readings from both cheeks and the rotation degree of the head as it is shown in conditional Equation 1:

Rotation < 30 : Cheeks Average Value = Average (Right Cheek, Left Cheek)

Rotation > 30 AND Yaw > 0 : Cheeks Average Value = Right Cheek

Rotation > 30 AND Yaw < 0 : Cheeks Average Value = Left Cheek

By comparing graphs (a) and (b) with graphs (c) and (d), we can see that the noise resulting from changing the head position is much less in the nose area than the noise in the right and left cheek. This shows that when the thermal reading in one cheek is impacted due to the change in head position, the thermal reading of the other cheek is also changed in the opposite way, which results in a more stable cheek average temperature. Moreover, as the room temperature in this figure shows, the experiment successfully is a

combination of constant and transient conditions. The whole section is transient thermal heating, while the thermal condition in each sub-section was kept constant with the thermal range allowance of 1°C.
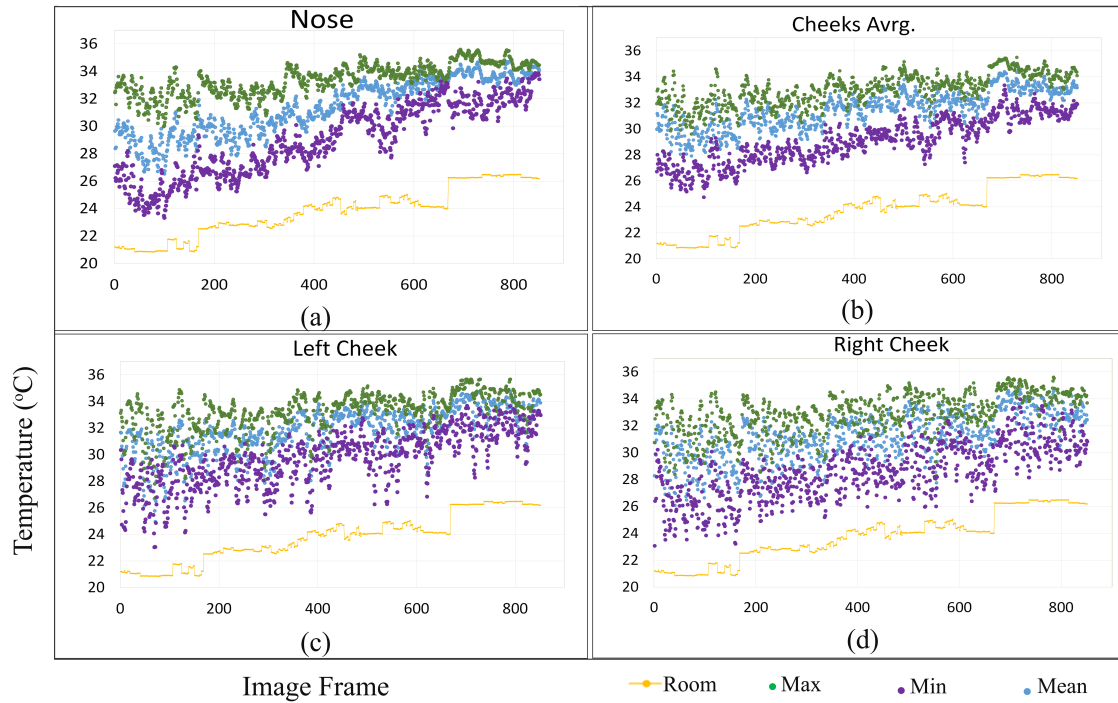
Figure 4.9: Skin Temperature Range at Nose and Cheeks Area for Subject 3

The covered thermal conditions and subjective thermal preference votes for all subjects are presented in Figure 4.10. As the experiment covers a wide range of room air temperatures, all the subjects have experienced at least three different thermal preferences. In addition, subjects 2, 4,6,9, and 10 have experienced another level of preferringring "much colder". In addition, the total number of both thermal sensation and thermal preference and the percentage of each vote are presented in the table 4.7. The thermal preference measure was used in the prediction process as it was shown to be a better predictor of thermal comfort [17].

Table 4.7: Thermal Sensation and Thermal Preference Scaled Votes For All Subjects

|	Thermal Sensation				Thermal Preference				Total
	Slightly Cool	Neutral	Slightly Warm	Warm	Slightly Warmer	No Change	Slightly Cooler	Much Cooler	
S1	170	155	182	0	182	170	155	0	507
	34 %	31 %	36 %	0 %	36 %	34 %	31 %	0 %	
S2	61	488	137	49	367	182	55	131	735
	8 %	66 %	19 %	7 %	50 %	25 %	7 %	18 %	
S3	214	463	183	0	214	463	183	0	860
	25 %	54 %	21 %	0 %	25 %	54 %	21 %	0 %	
S4	154	118	244	124	154	190	172	124	640
	24 %	18 %	38 %	19 %	24 %	30 %	27 %	19 %	
S5	109	269	659	0	109	456	472	0	1037
	11 %	26 %	64 %	0 %	11 %	44 %	46 %	0 %	
S6	139	458	141	78	340	257	83	136	816
	17 %	56 %	17 %	10 %	42 %	31 %	10 %	17 %	
S7	248	230	157	0	248	230	157	0	635
	39 %	36 %	25 %	0 %	39 %	36 %	25 %	0 %	
S8	94	398	212	0	340	212	152	0	704
	13 %	57 %	30 %	0 %	48 %	30 %	22 %	0 %	
S9	37	270	184	204	15	86	243	351	695
	5 %	39 %	26 %	29 %	2 %	12 %	35 %	51 %	
S10	218	276	174	0	77	114	174	303	668
	33 %	41 %	26 %	0 %	12 %	17 %	26 %	45 %	
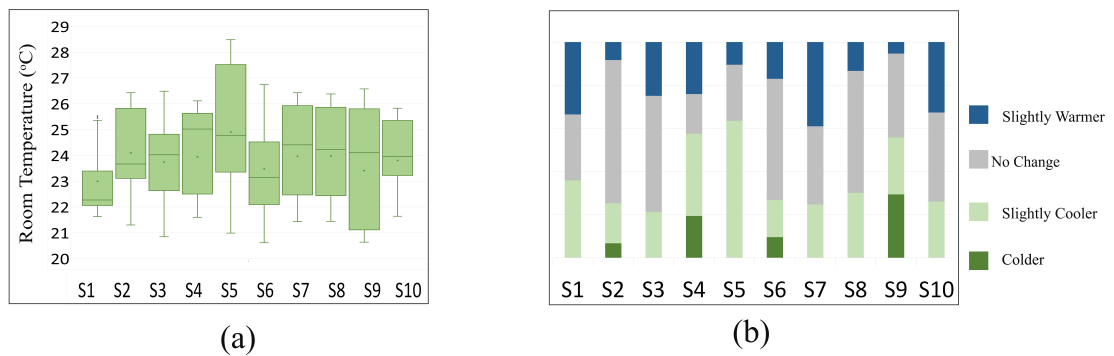
Figure 4.10: Skin Temperature Range For Each Facial Location

The correlation factors between room temperature and skin temperature values are calculated based on the Pearson Correlation Coefficient to better understand the influence of room air temperature on the skin temperature in different facial areas. The Pearson correlation coefficient indicates the strength and direction of a linear relationship between variables and is relevant for our calculations. As presented in Figure 3.9 the correlation value is calculated for all the subjects, and the average value is calculated in the last row. Regarding the average amounts of correlation among all subjects, the cheeks' average had the highest correlation of 0.75 with the room temperature. This amount is followed by the nose area with a 0.63 and the chin area with a 0.54 correlation number. The lowest correlation factors are for the left cheek, right cheek, and forehead area, which is 0.46 for all of them. The comparison of the correlation of minimum, maximum, and mean temperature values in each region shows that the mean temperatures have a higher correlation with the room temperature. Compared to the average correlation values of the right and left cheeks, they show the same number of 0.46 for the mean value and 0.31 for the maximum value.

By looking into the values for each subject, we can learn that for almost all the subjects, the correlation values are highest in the average of the cheeks and the nose area. However, for some subjects, such as subjects 6 and 7, the cheek average is the highest, with

correlation numbers of 0.91 and 0.84, while for subjects 3 and 4, the nose region has a higher correlation of 0.80 and 0.83. Subject 9 shows approximately similar and high correlation numbers of 0.81 and 0.84 for the nose and cheek average, respectively. A more detailed investigation into the correlation of nose and cheek average among all subjects shows that the highest amount is for subject 6, with 0.91 for the cheeks and 0.83 for the nose area. The lowest correlation numbers are for subject 2 due to the subject's unnoticed facial perspiration. Since the subject has a lower thermal tolerance, he perspires more readily when temperatures rise. When it came to the experiment, however, the amount of sweat was so small that it was hardly detectable to researchers or the participant. In light of this behavior, it is essential to consider the sweating factor in a whole other study as we change the emissivity of the skin temperature and apply other essential changes. However, we did not eliminate these subjects from this paper to have an initial look at the impact of sweating behavior on the results. Another conclusion from this table is that the cheek average correlation values have more consistency among all subjects. Although the correlation in the nose area is as high as 0.83, for some subjects, such as subject 10, it is only 0.35, which is low. However, the cheek average correlation numbers are approximately high among all subjects, with a minimum value of 0.61 for subject 1, which is still meaningful.

	Nose	Nose Max	Nose Min	Lcheek	Lcheek Max	Lcheek Min	Rcheek	Rcheek Max	Rcheek Min	Cheek Avrg.	Cheek Avrg. Max	Cheek Avrg. Min	Forehead	Forehead Max	Forehead Min	Chin	Chin Max	Chin Min
S1	0.37	0.30	0.39	0.32	0.16	0.23	0.39	0.19	0.31	0.61	0.29	0.33	0.39	0.43	0.18	0.30	0.22	0.25
S2	0.23	0.26	0.15	0.37	0.15	0.39	0.32	0.18	0.35	0.62	0.32	0.45	0.00	-0.04	0.14	0.53	0.60	0.29
S3	0.80	0.67	0.75	0.53	0.43	0.53	0.50	0.40	0.54	0.78	0.67	0.65	0.42	0.50	0.28	0.61	0.65	0.38
S4	0.83	0.61	0.73	0.41	0.29	0.37	0.51	0.36	0.52	0.77	0.62	0.58	0.55	0.61	0.32	0.58	0.58	0.39
S5	0.67	0.50	0.65	0.54	0.42	0.56	0.50	0.32	0.56	0.73	0.61	0.63	0.49	0.48	0.46	0.55	0.57	0.52
S6	0.83	0.72	0.73	0.70	0.50	0.61	0.70	0.56	0.64	0.91	0.80	0.75	0.75	0.75	0.43	0.80	0.77	0.53
S7	0.76	0.65	0.61	0.55	0.37	0.51	0.44	0.28	0.48	0.81	0.62	0.63	0.59	0.65	0.33	0.61	0.67	0.37
S8	0.65	0.54	0.40	0.38	0.21	0.38	0.35	0.22	0.34	0.72	0.44	0.42	0.60	0.60	0.31	0.50	0.37	0.40
S9	0.81	0.73	0.67	0.53	0.41	0.51	0.53	0.42	0.53	0.84	0.72	0.68	0.62	0.70	0.40	0.63	0.72	0.45
S10	0.35	0.35	0.39	0.30	0.17	0.34	0.36	0.20	0.36	0.65	0.37	0.44	0.15	0.21	0.14	0.33	0.29	0.26
AVRG.	0.63	0.53	0.55	0.46	0.31	0.44	0.46	0.31	0.46	0.75	0.54	0.56	0.46	0.49	0.30	0.54	0.54	0.38

Figure 4.11: Correlation of Different Facial Areas With Room Temperature For All Subjects

Figure 4.12 shows the whole considered temperature data for subject 3 from five experiment sessions. This figure displays a better visual understanding of how the temperature in each facial region changes with the change in the room air temperature. The linear trend line calculated for each facial area shows that the nose area has the most changing range with a slope of 0.98 for the linear trend. The forehead temperature changes the least, which is in line with the previous findings of our studies and other literature [217]. The high amount of change in the cheek temperature is displayed in this figure again. This shows that although the cheek temperatures increase as the room temperature increases, the thermal readings vary to a high extent for the images recorded at a constant temperature, which is due to the change in head position. This variation is much lower when we calculate the average temperature of the two cheeks in each frame.
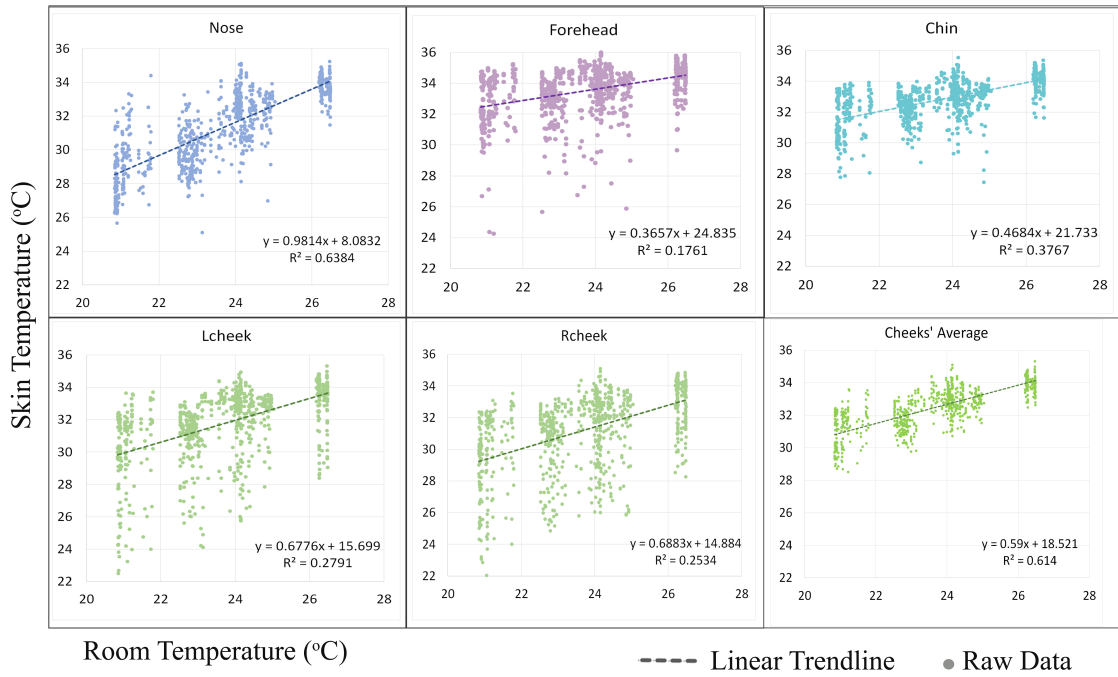
Figure 4.12: Skin Temperature Range For Each Facial Location

To have a better understanding of the influence of distance from the camera on the thermal infrared readings, Figure 4.13 presents the range of maximum recorded values at the forehead in each station for the whole dataset. The number of data points for this chart is 7,260 thermal readings, which is the maximum recorded temperature of the forehead in each data frame. The forehead area is selected for this purpose for two main reasons. First, as it was said previously, the forehead temperature has more stability, which makes it a better feature for looking into the influence of other factors. Second, by changing the head position, some facial areas become invisible to the camera. However, the forehead temperature is always visible in the thermal images. As Figure 4.13 shows, the mean and median of the skin temperature decrease as the subjects get farther from the thermal camera. The upper and lower quartile of the thermal readings also have a decreasing pattern with the maximum amounts of (36.22°C, 34.96°C) at a 1-meter distance from the camera and a minimum of (35.5°C, 34.19°C) at 6.6 meters from the camera. Moreover, Figure 4.13 shows the changes in maximum reading of the forehead area as the subjects change their head position. As we have mentioned in the literature

review, the angle to the camera was proven to influence the skin thermal readings [39]. This change in the thermal readings was around 2°C for the eye area when we compared the full frontal face and full profile images. In our experiment, we have recorded several readings at various distances from the camera and at various temperatures, which makes the temperature range in different head positions less. However, the increase in the thermal readings' mean temperature from full profile (35.13°C) to full frontal face (35.38°C) , followed by a decrease to the profile face at the other side (35.15°C), is shown in this figure.
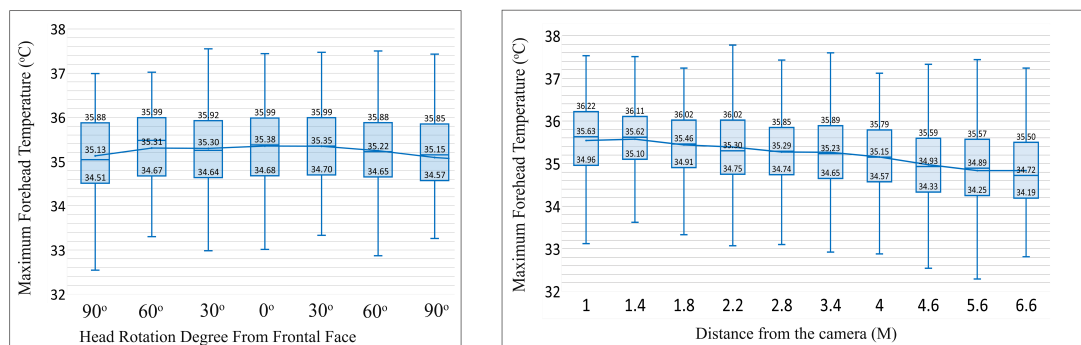

Figure 4.13: Skin Temperature Reading Change with Distance From the Camera

4.4.2   Thermal Comfort Prediction

The objective of this phase was to compare the performance of two selected algorithms on the prediction of thermal preference in a personalized approach. We have analyzed the results using the two selected prediction algorithms, Random Forest (RF) and K-Nearest-Neighbor (KNN). As mentioned in the methodology section, we have used the chi-squared feature selection to select a limited number of features for each subject. Therefore, we could identify the dataset attributes that contribute the most to our prediction variable, thermal preference. To avoid the problem of overfitting, we have modified the number of selected features to ten variables. Moreover, for both algorithms, we have utilized k-fold cross-validation to limit the likelihood of over-fitting the

model to the training set and produce a model that is more generally applicable. That would be using a small sample to assess how well the model is predicted to perform when used to generate predictions on data that was not included during training. For the RF algorithm, we have conducted a grid search for tuning the hyper-parameters in order to exhaustively test the accuracy of each configuration for performance improvement. Through this grid search, we have selected the best combination of hyperparameters for each subject, which includes: max-depth, max-features, min-samples-leaf, min-samples-split, and n-estimators. Table 4.5 shows the selected hyperparameters for each subject. A grid search was also applied to the KNN algorithm to select the number of neighbors from 1 to 30. The prediction results for the RF algorithm are presented in Table 4.9, and the results of the KNN method are shown in Table 4.10. In addition, we have compared the accuracy of these algorithms for all subjects in Figure 4.14. As this figure shows, the RF algorithm performed much better than KNN for all the subjects. The highest accuracy for the RF algorithm is 92.2% for subjects 8 and 9; for the KNN algorithm, the highest accuracy is 85.2% for subject 5. Although in our previous studies, the accuracy of the RF algorithm and the KNN algorithm was approximately similar [217], the RF had better accuracy numbers in this experiment. This can result from introducing new features to the training process, including head position and distance from the camera. In regards to the precision values of each classifier, the average of precision values in RF is approximately the same for "Slightly Warmer": 84.7%, "No Change": 84.7%, and "Slightly Cooler": 86.4%, while the "Much Cooler": 92.8% has higher accuracy. The KNN algorithm precision values are lower in all classes, with the highest precision of 76.1% for the "Slightly Warmer" class.

Table 4.8: Ten Most Important Selected Features for Each Subject

|	
S1	'Roll', 'Yaw', 'Pitch', 'RcheekMin', 'Rcheek', 'NoseMin', 'ForeheadMin', 'Forehead', 'ForeheadMax', 'NoseMax'
S2	'Yaw', 'Pitch', 'Distance', 'LcheekMin', 'RcheekMin', 'ChinMin', 'Rcheek', 'Roll', 'ForeheadMax', 'Chin'
S3	'Pitch', 'Roll', 'NoseMin', 'Nose', 'ChinMin', 'Yaw', 'Lcheek', 'Distance', 'RcheekMin', 'Forehead'
S4	'NoseMin', 'Pitch', 'Distance', 'RcheekMin', 'Roll', 'Nose', 'ChinMin', 'Rcheek', 'LcheekMin', 'ForeheadMin'
S5	'Yaw', 'RcheekMin', 'LcheekMin', 'ChinMin', 'NoseMin', 'Rcheek', 'Lcheek', 'Nose', 'ForeheadMin', 'Chin'
S6	'Yaw', 'NoseMin', 'RcheekMin', 'Rcheek','LcheekMin', 'Nose', 'Lcheek', 'Distance', 'ChinMin', 'RcheekMax'
S7	'NoseMin', 'Pitch', 'Distance', 'Nose', 'LcheekMin', 'Roll', 'ChinMin', 'Lcheek', 'ForeheadMin', 'LcheekMax'
S8	'Pitch', 'Yaw', 'NoseMin', 'LcheekMin', 'ChinMin', 'RcheekMin', 'Distance', 'Nose', 'Lcheek', 'ForeheadMin'
S9	'NoseMin', 'Yaw', 'RcheekMin', 'Nose', 'LcheekMin', 'ChinMin', 'Rcheek', 'Lcheek', 'Distance', 'ForeheadMin'
S10	'Roll', 'NoseMin', 'Distance', 'RcheekMin', 'Nose', 'ChinMin', 'Rcheek', 'RcheekMax', 'ForeheadMin', 'NoseMax'
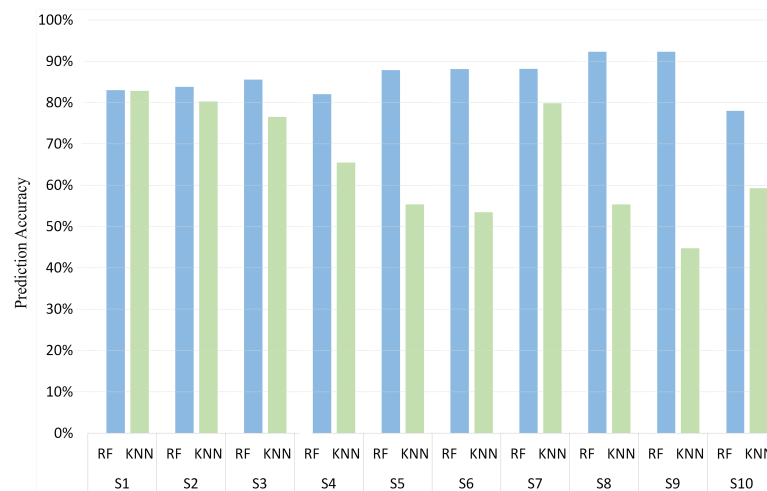
Figure 4.14: Prediction Accuracy of RF and KNN algorithms for All Subjects

Table 4.9: Prediction Accuracy and Precision of RF Algorithm For Each Subject

	Accuracy	Precision			
		Slightly Warmer	No Change	Slightly Cooler	Much Cooler
S1	83.0%	91.5%	74.0%	82.1%	-
S2	83.8%	94.7%	83.3%	79.8%	88.9%
S3	85.6%	87.8%	84.7%	85.9%	-
S4	82.0%	82.2%	80.2%	80.1%	88.7%
S5	87.8%	60.0%	87.5%	91.2%	-
S6	88.1%	83.0%	86.9%	90.3%	98.7%
S7	88.2%	85.8%	90.2%	89.8%	-
S8	92.3%	90.6%	93.0%	91.8%	-
S9	92.3%	90.6%	93.0%	91.8%	94.9%

Table 4.10: Prediction Accuracy and Precision of KNN Algorithm For Each Subject

	Accuracy	Precision			
		Slightly Warmer	No Change	Slightly Cooler	Much Cooler
S1	67.3%	82.8%	49.1%	69.6%	-
S2	76.5%	80.3%	80.0%	57.8%	40.0%
S3	77.3%	76.5%	76.5%	80.2%	-
S4	66.3%	65.5%	60.6%	69.4%	65.2%
S5	85.2%	55.4%	87.3%	86.8%	-
S6	74.6%	53.5%	81.1%	79.7%	63.2%
S7	77.2%	79.9%	68.3%	89.7%	-
S8	77.3%	55.3%	80.7%	81.7%	-
S9	77.3%	44.7%	78.2%	72.3%	86.1%
S10	64.5%	59.3%	62.9%	73.4%	-
AVRG.	74.3%	65.3%	72.5%	63.6%	63.6%

Considering the better performance of RF, we have continued the next phase just with this classifier. The confusion matrices for all the subjects were calculated, and the results are displayed in Figure 4.15. Based on these matrices, "Warmer" is the hardest class to predict for most subjects. The percentage of wrong predictions in this class goes as high as 37% which means 63% of the time, the classifier confuses wanting "No Change" with preferring " Warmer" or even "Slightly Cooler". Although this subject participated in an additional sub-session for the experiment and the number of data points was a total of 1037 image frames for this subject, the percentage of "Warmer" votes was 10% of the whole dataset. The fifth session for this subject was on the hotter side of the thermal spectrum, which has added additional "cooler" votes. We can conclude from this experiment that, in addition to the total number of data points, the inconsistent number of thermal votes will result in low accuracy. The low performance of the "Warmer" classifier is shown in other subjects as well, including Subject 6: 51% true positives, Subject 8: 64% true positives, Subject 9 : 50% true positives, and Subject 10 : 61% true posi-

tives. This can be explained by the lower number of "warmer" votes and the absence of colder thermal conditions. As the clothing level of all the subjects were one short sleeve shirt with pants, and due to the health concerns, we had decided to keep the minimum temperature of all experiments at approximately 21°C. The best performance of the RF classifier for the "Warmer" class is for subjects 1 and 7, with 90% correct predictions. The most correct prediction is for the "Slightly Cooler" class, which goes as high as 97% true predictions for subject 7. The predictions for subject 2 are the worst performance of this classifier in all the classes, which is due to the unnoticed sweating of this subject at the higher temperatures, which was previously explained in the previous section. Although sweat changes the whole path of how a thermal image needs to be studied for thermal comfort prediction, we have included this case as an example of the reasons for an unsuccessful prediction process.
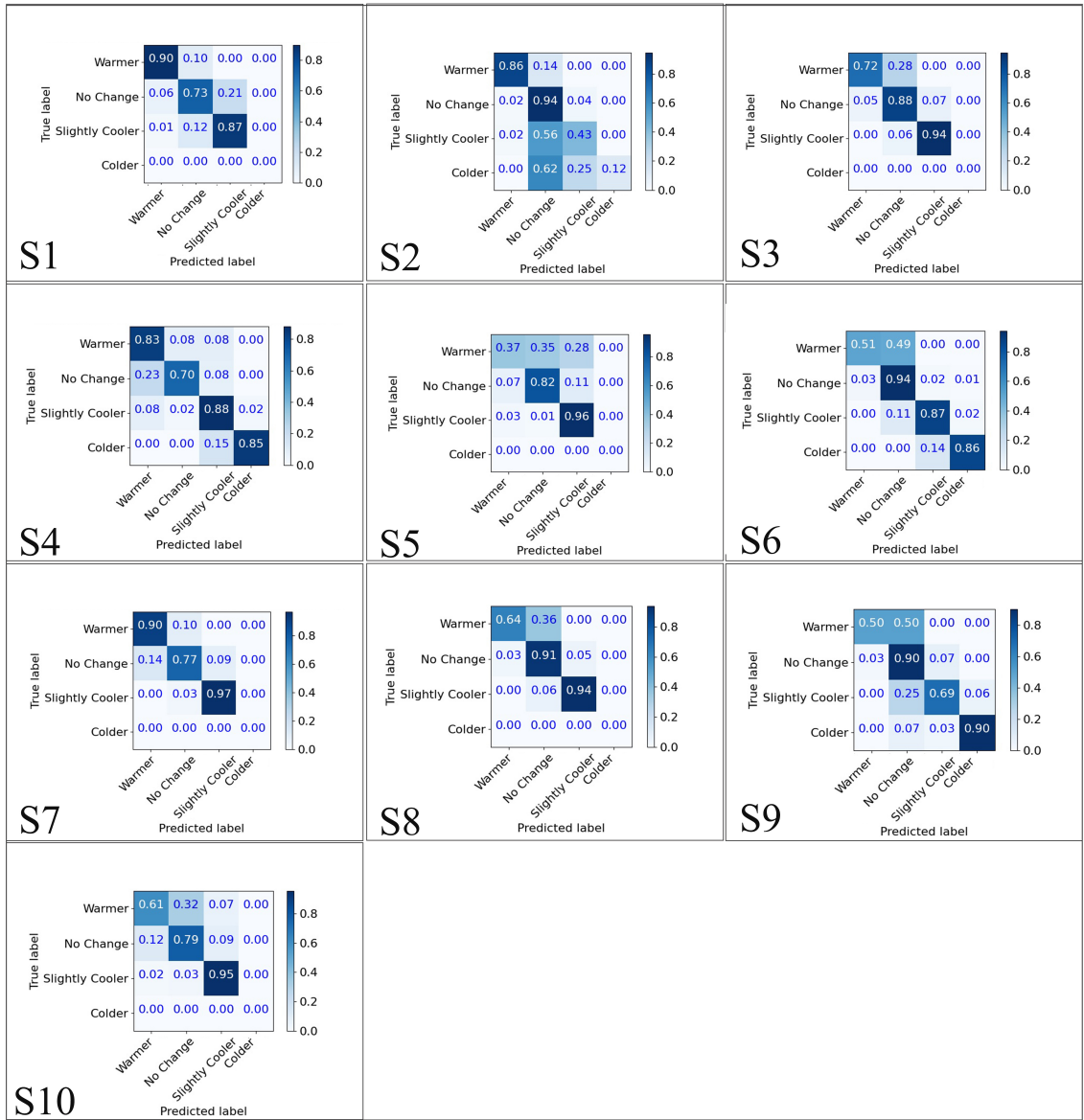
Figure 4.15: Confusion Matrices for RF Classifier

4.5 Conclusion and Future Work

An automated infrared thermal reading platform was investigated to predict the individual's thermal preference at a farther distance from the camera. The advantage of this system is the automated calibration of thermal and RGB data frames without manual registration or information about the distance between the camera and the subject. The framework allowed the investigation of the influence of distance from the camera and angle to the camera on thermal readings for the whole dataset. The experimental results

confirmed that changes in all three variables, including the environmental temperature, distance from the camera, and head positions, change the thermal readings. While the changes in temperature readings in different thermal sessions are due to changes in facial skin temperature, distance and head position do not change the skin temperature but just the thermal reading through the thermal camera. It was highlighted that the thermal readings from the subjects' facial skin decreased in value while they increased their distance from the camera. Head rotation was also proven to decrease the thermal readings compared to the full frontal face position. Furthermore, all the facial areas have shown a strong correlation with the room air temperature, while the cheek has the highest correlation with the environmental temperature, followed by the nose area. A new variable was also introduced as the average present value of both cheeks that could eliminate the noise in the data while the head position changes. Another significance of this study is the combination of at least four sub-sessions, each continuing for 90 minutes at an approximately constant temperature. The gradual increase in the constant thermal environment of each sub-session could create several unique and realistic data points. All the previous studies were conducted in transient heating or cooling sessions with a fast rate of change in the air temperature, which is unrealistic compared to the conditions in an actual office setting. We have introduced a new value for the average of the two cheeks based on the face rotation value, which has higher consistency while the head position changes. Moreover, we have examined the correlation of the skin temperature in different facial areas with the room temperature. Our results indicate a higher correlation of nose and cheek averages with the room temperature. However, the cheek average correlation numbers have a higher consistency among all subjects. In addition, we have investigated the potential of predicting an individual's thermal comfort. We have studied the accuracy and precision of the Random Forest and K-Nearest Neighbor prediction algorithms. The result highlighted an average accuracy of 86% for the Random Forest algorithm and 74% for the K-Nearest Neighbor algorithm. We can conclude

from this experiment that, in addition to the total number of data points, the inconsistent number of thermal votes will result in low accuracy. This research has some limitations in regards to both data collection and analysis. Firstly, although we have considered personalized thermal comfort, which does not require many subjects, it would be best to include subjects from diverse skin colors, ages, and body mass index (BMI) conditions. With regard to the prediction process, we have included supervised algorithms, which are not always the best option for online applications. In our next studies, we will focus on the online prediction process and related approaches such as reinforcement learning.

CHAPTER 5: CONCLUSIONS

5.1   Dissertation Highlights

An automated infrared thermal reading platform was investigated to predict the individuals' thermal preferences at a farther distance from the camera. The advantage of this system is the automated calibration of thermal and RGB data frames without manual registration. The framework allowed the investigation of the influence of distance from the camera and angle to the camera on thermal readings for the whole dataset. To create a holistic database for the experiment, we have developed and published the Charlotte-Thermal Face dataset. This publicly available dataset includes facial thermal images with variations in environmental properties, distance from the camera, and head position in raw 16-bit data frames. The data is annotated with each person's environmental conditions, facial landmarks, and thermal sensations at the time of recording each frame. The subjective thermal sensation annotations are a new addition to the face thermal image datasets. The comparative study of the temperature in different facial areas shows the importance of environmental temperature in facial thermography. To investigate the reliability of the dataset, we have looked into the temperature range of the images and the correlation of ambient temperature with the skin temperature of each subject. The experimental results confirmed that changes in all three variables, including the environmental temperature, distance from the camera, and head positions, change the thermal readings. While the changes in temperature readings in different thermal sessions are due to changes in facial skin temperature, distance and head position do not change the skin temperature but just the thermal reading through the infrared camera. It was highlighted that the thermal readings from the subjects' facial skin decreased in value while they increased their distance from the camera. Head rotation

was also proven to decrease the thermal readings compared to the full frontal face position. Furthermore, all the facial areas have shown a strong correlation with the room air temperature, while the cheek thermal value has the highest correlation with the environmental temperature, followed by the nose area. A new variable was also introduced as the average present value of both cheeks that could eliminate the noise in the data while the head position changes. Additionally, significant to this study is the combination of at least four sub-sessions, each continuing for 90 minutes at an approximately constant temperature. The gradual increase in the constant thermal environment of each sub-session could create several unique and realistic data points. Most of the previous studies were conducted in transient heating or cooling sessions with a fast rate of change in the air temperature, which is unrealistic compared to the conditions in an actual office setting. In addition, we have investigated the potential of predicting an individual's thermal comfort. We have studied the accuracy and precision of the Random Forest and K-Nearest Neighbor prediction algorithms. The result highlighted an average accuracy of 86% for the Random Forest algorithm and 74% for the K-Nearest Neighbor algorithm. We can conclude from this experiment that, in addition to the total number of data points, the inconsistent number of thermal votes will result in low accuracy. Utilizing thermal cameras, this research provides encouraging findings for the establishment of automated thermal comfort prediction from a distance.

5.2 Future Work

Utilizing thermal cameras, this research provides encouraging findings for the establishment of automated thermal comfort prediction from a distance. Personalized thermal comfort modeling is a growing and promising approach due to the potential for decreasing the necessity for long-term feedback collection from occupants. This research has some limitations in regards to both data collection and analysis. Personal characteristics obtained through physiological sensing technologies might be investigated further following the recent accelerated development of infrared camera technologies. In

addition, the participants of the studies can be more diverse in future research in terms of including different age groups, gender types, ethnicity, skin color, and health status. In this regard, skin color is particularly important for the non-contact camera-based thermal comfort prediction methods as it results in changing the emissivity of the target area and impacts the thermal readings. There are currently several thermal comfort scales utilized for reporting occupants' subjective thermal votes. Most of the researchers are using the thermal sensation scale. In this research, we have utilized thermal sensation and thermal preference. However, other thermal scales could be studied further to be applied in the building control systems. Different thermal scales of application and performance need more investigation for improved future research. Although supervised learning algorithms, especially RF and KNN, have resulted in good accuracy, reinforcement learning RL-based research still needs more research. One main reason for the limited RL research is the difficulty of application and performance validation of an online system, forcing researchers to use offline simulated test beds for this objective. Future research on online learning approaches for personalized thermal comfort would be helpful for the field.

REFERENCES

[1] L. t. Graham, T. parkinson, and S. schiavon, "Lessons learned from 20 years of CBE's occupant surveys," *Buildings and Cities*, vol. 2, no. 1, pp. 166–184, 2021.

[2] C. Karmann, S. Schiavon, and E. Arens, "Percentage of commercial buildings showing at least 80% occupant satisfied with their thermal comfort," *10th Windsor Conference: rethinking comfort*, pp. 0–7, 2018.

[3] A. Ghaffarianhoseini, H. AlWaer, H. Omrany, A. Ghaffarianhoseini, C. Alalouch, D. Clements-Croome, and J. Tookey, "Sick building syndrome: are we doing enough?," *Architectural Science Review*, vol. 61, no. 3, pp. 99–121, 2018.

[4] T. Hong, D. Yan, S. D'Oca, and C. f. Chen, "Ten questions concerning occupant behavior in buildings: The big picture," *Building and Environment*, vol. 114, pp. 518–530, 3 2017.

[5] B. Ruoxi Jia, B. Jin, M. Jin, Y. Zhou, I. C. Konstantakopoulos, H. Zou, J. Kim, R. Arghandeh, S. Member IEEE, P. Nuzzo, M. Ieee, S. Schiavon, A. L. Sangiovanni-vincentelli, F. Ieee, C. J. Spanos, R. Jia, B. Jin, M. Jin, Y. Zhou, I. C. Konstantakopoulos, H. Zou, A. L. Sangiovanni-Vincentelli, C. J. Spanos, J. Kim, S. Schiavon, D. Li, W. Gu, R. Arghandeh, and P. Nuzzo, "Design Automation for Smart Building Systems," 2018.

[6] C. Ma, N. T. Trung, H. Uchiyama, H. Nagahara, A. Shimada, and R.-i. Taniguchi, "Mixed features for face detection in thermal image," *Thirteenth International Conference on Quality Control by Artificial Vision 2017*, vol. 10338, no. May 2017, p. 103380E, 2017.

[7] S. Sumriddetchkajorn and A. Somboonkaew, "Face detection in thermal imagery using an Open Source Computer Vision library," *Thermosense XXXI*, vol. 7299, no. April 2009, p. 729906, 2009.

[8] M. Kowalski, A. Grudzień, and W. Ciurapiński, "Detection of human faces in thermal infrared images," *Metrology and Measurement Systems*, vol. 28, no. 2, pp. 307–321, 2021.

[9] V. Espinosa-Duró, M. Faundez-Zanuy, and J. Mekyska, "A New Face Database Simultaneously Acquired in Visible, Near-Infrared and Thermal Spectrums," *Cognitive Computation*, vol. 5, no. 1, pp. 119–135, 2013.

[10] M. Peng, C. Wang, T. Chen, and G. Liu, "NIRFaceNet: A convolutional neural network for near-infrared face identification," *Information (Switzerland)*, vol. 7, no. 4, pp. 1–14, 2016.

[11] M. Kopaczka, R. Kolk, and D. Merhof, "A fully annotated thermal face database and its application for thermal facial expression recognition," *I2MTC 2018 -*

2018 IEEE International Instrumentation and Measurement Technology Conference: Discovering New Horizons in Instrumentation and Measurement, Proceedings, pp. 1–6, 2018.

[12] C. Goulart, C. Valadão, D. Delisle-Rodriguez, D. Funayama, A. Favarato, G. Baldo, V. Binotte, E. Caldeira, and T. Bastos-Filho, "Visual and thermal image processing for facial specific landmark detection to infer emotions in a child-robot interaction," *Sensors (Switzerland)*, vol. 19, no. 13, 2019.

[13] C. Ordun, E. Raff, and S. Purushotham, "The Use of AI for Thermal Emotion Recognition: A Review of Problems and Limitations in Standard Design and Data," 2020.

[14] Z. Jiang, M. Hu, L. Fan, Y. Pan, W. Tang, G. Zhai, and Y. Lu, "Combining Visible Light and Infrared Imaging for Efficient Detection of Respiratory Infections such as COVID-19 on Portable Device," no. 19, 2020.

[15] S. N. Al-Humairi and A. A. A. Kamal, "Opportunities and challenges for the building monitoring systems in the age-pandemic of COVID-19: Review and prospects," *Innovative Infrastructure Solutions*, vol. 6, no. 2, pp. 1–10, 2021.

[16] M. Wigginton and J. Harris, *Intelligent skins.* Oxford: Butterworth-Heinemann, 2002.

[17] Z. Qavidel Fard, Z. Sadat Zomorodian, and S. Sadat Korsavi, "Application of Machine Learning in Thermal Comfort Studies: A Review of Methods, Performance and Challenges," *Energy and Buildings*, vol. 256, p. 111771, 2021.

[18] A. Aryal and B. Becerik-Gerber, "Thermal comfort modeling when personalized comfort systems are in use: Comparison of sensing and learning methods," *Building and Environment*, vol. 185, p. 107316, 11 2020.

[19] D. Poster, M. Thielke, R. Nguyen, S. Rajaraman, X. Di, C. N. Fondje, V. M. Patel, N. J. Short, B. S. Riggan, N. M. Nasrabadi, and S. Hu, "A Large-Scale, Time-Synchronized Visible and Thermal Face Dataset," in *2021 IEEE Winter Conference on Applications of Computer Vision (WACV)*, pp. 1558–1567, IEEE, 1 2021.

[20] A. Kwasniewska, J. Ruminski, M. Szankin, and M. Kaczmarek, "Super-resolved thermal imagery for high-accuracy facial areas detection and analysis," *Engineering Applications of Artificial Intelligence*, vol. 87, no. October 2019, p. 103263, 2020.

[21] Y. Cheng, J. Niu, and N. Gao, "Thermal comfort models: A review and numerical investigation," *Building and Environment*, vol. 47, pp. 13–22, 1 2012.

[22] T. Hong, D. Yan, S. D'Oca, and C. f. Chen, "Ten questions concerning occupant behavior in buildings: The big picture," *Building and Environment*, vol. 114, pp. 518–530, 3 2017.

[23] R. d. Dear, G. S. Brager, and D. Cooper, "Developing an adaptive model of thermal comfort and preference. Final report," *"Results of Cooperative Research between the American Society of Heating, Refrigerating and Air Conditioning Engineers, Inc., and Macquarie Research, Ltd.",* vol. 104, no. March, pp. 1–18, 1997.

[24] M. Luo, E. Arens, H. Zhang, A. Ghahramani, and Z. Wang, "Thermal comfort evaluated for combinations of energy-efficient personal heating and cooling devices," *Building and Environment,* vol. 143, pp. 206–216, 10 2018.

[25] S. Shahzad, J. K. Calautit, K. Calautit, B. Hughes, and A. I. Aquino, "Advanced personal comfort system (APCS) for the workplace: A review and case study," *Energy and Buildings,* vol. 173, pp. 689–709, 8 2018.

[26] W. Jung and F. Jazizadeh, "Human-in-the-loop HVAC operations: A quantitative review on occupancy, comfort, and energy-efficiency dimensions," *Applied Energy,* vol. 239, pp. 1471–1508, 4 2019.

[27] J. Ranjan and J. Scott, "ThermalSense: Determining Dynamic Thermal Comfort Preferences using Thermographic Imaging," 2016.

[28] H. Metzmacher, D. Wölki, C. Schmidt, J. Frisch, and C. van Treeck, "Real-time human skin temperature analysis using thermal image recognition for thermal comfort assessment," *Energy and Buildings,* vol. 158, pp. 1063–1078, 1 2018.

[29] D. Li, C. C. Menassa, and V. R. Kamat, "Non-intrusive interpretation of human thermal comfort through analysis of facial infrared thermography," *Energy and Buildings,* vol. 176, pp. 246–261, 10 2018.

[30] D. Li, C. C. Menassa, V. R. Kamat, and E. Byon, "HEAT - Human Embodied Autonomous Thermostat," *Building and Environment,* vol. 178, no. April, 2020.

[31] A. C. Cosma and R. Simha, "Machine learning method for real-time non-invasive prediction of individual thermal preference in transient conditions," *Building and Environment,* vol. 148, no. July 2018, pp. 372–383, 2019.

[32] A. Aryal and B. Becerik-Gerber, "A comparative study of predicting individual thermal sensation and satisfaction using wrist-worn temperature sensor, thermal camera and ambient temperature sensor," *Building and Environment,* vol. 160, 8 2019.

[33] A. Aryal and B. Becerik-Gerber, "Skin Temperature Extraction Using Facial Landmark Detection and Thermal Imaging for Comfort Assessment," pp. 71–80, 2019.

[34] D. Li, C. C. Menassa, and V. R. Kamat, "Robust non-intrusive interpretation of occupant thermal comfort in built environments with low-cost networked thermal cameras," *Applied Energy,* vol. 251, p. 113336, 10 2019.

[35] A. C. Cosma and R. Simha, "Thermal comfort modeling in transient conditions using real-time local body temperature extraction with a thermographic camera," *Building and Environment*, vol. 143, pp. 36–47, 10 2018.

[36] S. Lu, W. Wang, S. Wang, and E. Cochran Hameen, "Thermal Comfort-Based Personalized Models with Non-Intrusive Sensing Technique in Office Buildings," *Applied Sciences*, vol. 9, p. 1768, 4 2019.

[37] B. Tejedor, M. Casals, M. Gangolells, M. Macarulla, and N. Forcada, "Human comfort modelling for elderly people by infrared thermography: Evaluating the thermoregulation system responses in an indoor environment during winter," *Building and Environment*, vol. 186, 12 2020.

[38] E. Faye, O. Dangles, and S. Pincebourde, "Distance makes the difference in thermography for ecological studies," *Journal of Thermal Biology*, vol. 56, pp. 1–9, 2016.

[39] R. Vardasca, A. R. Marques, J. Diz, A. Seixas, J. Mendes, and E. F. J. Ring, "The influence of angles and distance on assessing inner-canthi of the eye skin temperature," tech. rep., 2017.

[40] N. Playà-Montmany and G. J. Tattersall, "Spot size, distance and emissivity errors in field applications of infrared thermography," *Methods in Ecology and Evolution*, pp. 2041–210, 2 2021.

[41] H. Zhang, B. S. Riggan, S. Hu, N. J. Short, and V. M. Patel, "Synthesis of High-Quality Visible Faces from Polarimetric Thermal Faces using Generative Adversarial Networks," *International Journal of Computer Vision*, vol. 127, no. 6-7, pp. 845–862, 2019.

[42] J. Wang, K. Sun, T. Cheng, B. Jiang, C. Deng, Y. Zhao, D. Liu, Y. Mu, M. Tan, X. Wang, W. Liu, and B. Xiao, "Deep High-Resolution Representation Learning for Visual Recognition," *IEEE Transactions on Pattern Analysis and Machine Intelligence*, no. March, pp. 1–1, 2020.

[43] "GitHub - HRNet/HRNet-Facial-Landmark-Detection."

[44] Y. Cheng, J. Niu, and N. Gao, "Thermal comfort models: A review and numerical investigation," *Building and Environment*, vol. 47, pp. 13–22, 1 2012.

[45] B. Qolomany, G. Student Member, A. Al-Fuqaha, S. Member, A. Gupta, D. Benhaddou, S. Alwajidi, J. Qadir, and A. C. Fong, "Leveraging Machine Learning and Big Data for Smart Buildings: A Comprehensive Survey," tech. rep.

[46] Y. Feng, S. Liu, J. Wang, J. Yang, Y. L. Jao, and N. Wang, "Data-driven personal thermal comfort prediction: A literature review," *Renewable and Sustainable Energy Reviews*, vol. 161, no. September 2021, p. 112357, 2022.

[47] G. Halhoul Merabet, M. Essaaidi, M. Ben Haddou, B. Qolomany, J. Qadir, M. Anan, A. Al-Fuqaha, M. R. Abid, and D. Benhaddou, "Intelligent building control systems for thermal comfort and energy-efficiency: A systematic review of artificial intelligence-assisted techniques," *Renewable and Sustainable Energy Reviews*, vol. 144, no. April, p. 110969, 2021.

[48] A. Čulić, S. Nižetić, P. Šolić, T. Perković, and V. Čongradac, "Smart monitoring technologies for personal thermal comfort: A review," *Journal of Cleaner Production*, vol. 312, no. May, 2021.

[49] J. Xie, H. Li, C. Li, J. Zhang, and M. Luo, "Review on occupant-centric thermal comfort sensing, predicting, and controlling," *Energy and Buildings*, vol. 226, p. 110392, 2020.

[50] L. Arakawa Martins, V. Soebarto, and T. Williamson, "A systematic review of personal thermal comfort models," *Building and Environment*, vol. 207, no. PA, p. 108502, 2022.

[51] Y. Peng, Z. Nagy, and A. Schlüter, "Temperature-preference learning with neural networks for occupant-centric building indoor climate controls," *Building and Environment*, vol. 154, pp. 296–308, 5 2019.

[52] J. Xiong, A. Tzempelikos, I. Bilionis, and P. Karava, "A personalized daylighting control approach to dynamically optimize visual satisfaction and lighting energy use," *Energy and Buildings*, vol. 193, pp. 111–126, 6 2019.

[53] M. Zang, Z. Xing, and Y. Tan, "IoT-based personal thermal comfort control for livable environment," *International Journal of Distributed Sensor Networks*, vol. 15, no. 7, 2019.

[54] B. Yang, X. Cheng, D. Dai, T. Olofsson, H. Li, and A. Meier, "Real-time and contactless measurements of thermal discomfort based on human poses for energy efficient control of buildings," *Building and Environment*, vol. 162, no. July, p. 106284, 2019.

[55] J. Guenther and O. Sawodny, "Feature selection and Gaussian Process regression for personalized thermal comfort prediction," *Building and Environment*, vol. 148, pp. 448–458, 1 2019.

[56] M. Javed, N. Li, and S. Li, "Personalized thermal comfort modeling based on Support Vector Classification," *Chinese Control Conference, CCC*, pp. 10446–10451, 2017.

[57] F. Auffenberg, S. Snow, S. Stein, and A. Rogers, "A comfort-based approach to smart heating and air conditioning," *ACM Transactions on Intelligent Systems and Technology*, vol. 9, no. 3, 2017.

[58] W. Liu, Z. Lian, and B. Zhao, "A neural network evaluation model for individual thermal comfort," *Energy and Buildings*, vol. 39, no. 10, pp. 1115–1122, 2007.

[59] H. Zhang, E. Arens, and Y. Zhai, "A review of the corrective power of personal comfort systems in non-neutral ambient environments," *Building and Environment*, vol. 91, pp. 15–41, 2015.

[60] J. Kim, Y. Zhou, S. Schiavon, P. Raftery, and G. Brager, "Personal comfort models: Predicting individuals' thermal preference using occupant heating and cooling behavior and machine learning," *Building and Environment*, vol. 129, pp. 96–106, 2 2018.

[61] J. Kim, S. Schiavon, and G. Brager, "Personal comfort models – A new paradigm in thermal comfort for occupant-centric environmental control," 2018.

[62] D. He, N. Li, Y. He, M. He, C. Song, and H. Chen, "Experimental Study on Thermal Sensation of Radiant Cooling Workstation and Desktop Fan in Hot-humid Environment," *Procedia Engineering*, vol. 205, pp. 757–764, 2017.

[63] M. He, N. Li, Y. He, D. He, and C. Song, "The influence of personally controlled desk fan on comfort and energy consumption in hot and humid environments," *Building and Environment*, vol. 123, pp. 378–389, 10 2017.

[64] C. Du, B. Li, H. Liu, Y. Ji, R. Yao, and W. Yu, "Quantification of personal thermal comfort with localized airflow system based on sensitivity analysis and classification tree model," *Energy and Buildings*, vol. 194, pp. 1–11, 2019.

[65] K. Katić, R. Li, J. Verhaart, and W. Zeiler, "Neural network based predictive control of personalized heating systems," *Energy and Buildings*, vol. 174, pp. 199–213, 9 2018.

[66] K. Katić, R. Li, and W. Zeiler, "Machine learning algorithms applied to a prediction of personal overall thermal comfort using skin temperatures and occupants' heating behavior," *Applied Ergonomics*, vol. 85, p. 103078, 5 2020.

[67] L. Pérez-Lombard, J. Ortiz, and C. Pout, "A review on buildings energy consumption information," *Energy and Buildings*, vol. 40, no. 3, pp. 394–398, 2008.

[68] H. Zhang, E. Arens, and Y. Zhai, "A review of the corrective power of personal comfort systems in non-neutral ambient environments," *Building and Environment*, vol. 91, pp. 15–41, 9 2015.

[69] J. Ngarambe, G. Y. Yun, and M. Santamouris, "The use of artificial intelligence (AI) methods in the prediction of thermal comfort in buildings: energy implications of AI-based thermal comfort controls," *Energy and Buildings*, vol. 211, p. 109807, 2020.

[70] N. Morresi, S. Casaccia, M. Sorcinelli, M. Arnesano, A. Uriarte, J. I. Torrens-Galdiz, and G. M. Revel, "Sensing physiological and environmental quantities to measure human thermal comfort through machine learning techniques," *IEEE Sensors Journal*, vol. 21, no. 10, pp. 12322–12337, 2021.

[71] E. Arens, H. Zhang, and C. Huizenga, "Partial- and whole-body thermal sensation and comfort - Part I: Uniform environmental conditions," *Journal of Thermal Biology*, vol. 31, no. 1-2 SPEC. ISS., pp. 53–59, 2006.

[72] S. Liu, S. Schiavon, H. P. Das, M. Jin, and C. J. Spanos, "Personal thermal comfort models with wearable sensors," *Building and Environment*, vol. 162, p. 106281, 9 2019.

[73] C. Dai, H. Zhang, E. Arens, and Z. Lian, "Machine learning approaches to predict thermal demands using skin temperatures: Steady-state conditions," *Building and Environment*, vol. 114, pp. 1–10, 3 2017.

[74] S. Lu, W. Wang, S. Wang, and E. Cochran Hameen, "Thermal Comfort-Based Personalized Models with Non-Intrusive Sensing Technique in Office Buildings," *Applied Sciences*, vol. 9, p. 1768, 4 2019.

[75] D. Li, C. C. Menassa, and V. R. Kamat, "Robust non-intrusive interpretation of occupant thermal comfort in built environments with low-cost networked thermal cameras," *Applied Energy*, vol. 251, p. 113336, 10 2019.

[76] S. Liu, S. Schiavon, H. P. Das, M. Jin, and C. J. Spanos, "Personal thermal comfort models with wearable sensors," *Building and Environment*, vol. 162, p. 106281, 9 2019.

[77] W. Jung and F. Jazizadeh, "Vision-based thermal comfort quantification for HVAC control," *Building and Environment*, vol. 142, pp. 513–523, 9 2018.

[78] C. Dai, H. Zhang, E. Arens, and Z. Lian, "Machine learning approaches to predict thermal demands using skin temperatures: Steady-state conditions," *Building and Environment*, vol. 114, pp. 1–10, 3 2017.

[79] J.-H. Choi and D. Yeom, "Study of data-driven thermal sensation prediction model as a function of local body skin temperatures in a built environment," *Building and Environment*, vol. 121, pp. 130–147, 8 2017.

[80] N. Von Frankenberg, P. Ruoff, B. Bruegge, and V. Loftness, "LATEST: A learning-based automated thermal environment control system," *UbiComp/ISWC 2020 Adjunct - Proceedings of the 2020 ACM International Joint Conference on Pervasive and Ubiquitous Computing and Proceedings of the 2020 ACM International Symposium on Wearable Computers*, pp. 573–579, 2020.

[81] M. Rafaie, M. Tesfay, and F. Alsaleem, "Utilizing wearable devices to design personal thermal comfort model," *International High Performance Buildings Conference*, no. July, p. 246, 2018.

[82] Z. Wang, H. Onodera, and R. Matsuhashi, "Proposal of Relative Thermal Sensation: Another Dimension of Thermal Comfort and Its Investigation," *IEEE Access*, vol. 9, pp. 36266–36281, 2021.

[83] X. Shan and E. H. Yang, "Supervised machine learning of thermal comfort under different indoor temperatures using EEG measurements," *Energy and Buildings*, vol. 225, p. 110305, 2020.

[84] F. Alsaleem, M. K. Tesfay, M. Rafaie, K. Sinkar, D. Besarla, and P. Arunasalam, "An IoT Framework for Modeling and Controlling Thermal Comfort in Buildings," *Frontiers in Built Environment*, vol. 6, no. June, pp. 1–14, 2020.

[85] F. Salamone, L. Belussi, C. Currò, L. Danza, M. Ghellere, G. Guazzi, B. Lenzi, V. Megale, and I. Meroni, "Integrated method for personal thermal comfort assessment and optimization through users' feedback, IoT and machine learning: A case study," *Sensors (Switzerland)*, vol. 18, no. 5, 2018.

[86] A. Youssef, A. Y. A. Amer, N. Caballero, and J. M. Aerts, "Towards online personalized-monitoring of human thermal sensation using machine learning approach," *Applied Sciences (Switzerland)*, vol. 9, no. 16, 2019.

[87] J. Lee and Y. Ham, "Physiological sensing-driven personal thermal comfort modelling in consideration of human activity variations," *Building Research and Information*, 2020.

[88] A. Kirimtat, O. Krejcar, A. Selamat, and E. Herrera-Viedma, "FLIR vs SEEK thermal cameras in biomedicine: Comparative diagnosis through infrared thermography," *BMC Bioinformatics*, vol. 21, no. Suppl 2, pp. 1–10, 2020.

[89] R. Hughes, "Non-Contact Thermometers for Detecting Fever: A Review of Clinical Effectiveness," *Journal of Chemical Information and Modeling*, vol. 53, no. 9, p. 287, 2008.

[90] M. U. Selent, N. M. Molinari, A. Baxter, A. V. Nguyen, H. Siegelson, C. M. Brown, A. Plummer, A. Higgins, S. Podolsky, P. Spandorfer, N. J. Cohen, and D. B. Fishbein, "Mass screening for fever in children: a comparison of 3 infrared thermal detection systems.," *Pediatric emergency care*, vol. 29, pp. 305–313, 3 2013.

[91] M. Han, R. May, X. Zhang, X. Wang, S. Pan, Y. Da, and Y. Jin, "A novel reinforcement learning method for improving occupant comfort via window opening and closing," *Sustainable Cities and Society*, vol. 61, no. April, 2020.

[92] F. Salamone, L. Belussi, C. Currò, L. Danza, M. Ghellere, G. Guazzi, B. Lenzi, V. Megale, and I. Meroni, "Application of IoT and Machine Learning techniques for the assessment of thermal comfort perception.," *Energy Procedia*, vol. 148, no. Ati, pp. 798–805, 2018.

[93] S. S. Shetty, D. C. Hoang, M. Gupta, and S. K. Panda, "Learning desk fan usage preferences for personalised thermal comfort in shared offices using tree-based methods," *Building and Environment*, vol. 149, pp. 546–560, 2 2019.

[94] W. Jung, F. Jazizadeh, and T. E. Diller, "Heat flux sensing for machine-learning-based personal thermal comfort modeling," *Sensors (Switzerland)*, vol. 19, no. 17, 2019.

[95] F. Salamone, A. Bellazzi, L. Belussi, G. Damato, L. Danza, F. Dell'aquila, M. Ghellere, V. Megale, I. Meroni, and W. Vitaletti, "Evaluation of the visual stimuli on personal thermal comfort perception in real and virtual environments using machine learning approaches," *Sensors (Switzerland)*, vol. 20, no. 6, 2020.

[96] L. Xiong and Y. Yao, "Study on an adaptive thermal comfort model with K-nearest-neighbors (KNN) algorithm," *Building and Environment*, vol. 202, no. May, p. 108026, 2021.

[97] A. Ghahramani, C. Tang, and B. Becerik-Gerber, "An online learning approach for quantifying personalized thermal comfort via adaptive stochastic modeling," *Building and Environment*, vol. 92, pp. 86–96, 10 2015.

[98] C. C. J. Huang, R. Yang, and M. W. Newman, "The potential and challenges of inferring thermal comfort at home using commodity sensors," *UbiComp 2015 - Proceedings of the 2015 ACM International Joint Conference on Pervasive and Ubiquitous Computing*, pp. 1089–1100, 2015.

[99] L. Jiang and R. Yao, "Modelling personal thermal sensations using C-Support Vector Classification (C-SVC) algorithm," *Building and Environment*, vol. 99, pp. 98–106, 2016.

[100] E. Laftchiev and D. Nikovski, "An IoT system to estimate personal thermal comfort," *2016 IEEE 3rd World Forum on Internet of Things, WF-IoT 2016*, pp. 672–677, 2017.

[101] T. Chaudhuri, D. Zhai, Y. C. Soh, H. Li, and L. Xie, "Random forest based thermal comfort prediction from gender-specific physiological parameters using wearable sensing technology," *Energy and Buildings*, vol. 166, pp. 391–406, 5 2018.

[102] A. Ghahramani, G. Castro, S. A. Karvigh, and B. Becerik-Gerber, "Towards unsupervised learning of thermal comfort using infrared thermography," *Applied Energy*, vol. 211, pp. 41–49, 2 2018.

[103] K. N. Nkurikiyeyezu, Y. Suzuki, and G. F. Lopez, "Heart rate variability as a predictive biomarker of thermal comfort," *Journal of Ambient Intelligence and Humanized Computing*, vol. 9, no. 5, pp. 1465–1477, 2018.

[104] W. Hu, Y. Luo, Z. Lu, and Y. Wen, "Heterogeneous transfer learning for thermal comfort modeling," *BuildSys 2019 - Proceedings of the 6th ACM International Conference on Systems for Energy-Efficient Buildings, Cities, and Transportation*, pp. 61–70, 2019.

[105] A. C. Cosma and R. Simha, "Using the contrast within a single face heat map to assess personal thermal comfort," *Building and Environment*, vol. 160, 8 2019.

[106] S. Lu, W. Wang, C. Lin, and E. C. Hameen, "Data-driven simulation of a thermal comfort-based temperature set-point control with ASHRAE RP884," *Building and Environment*, vol. 156, pp. 137–146, 6 2019.

[107] G. Gao, J. Li, and Y. Wen, "Energy-Efficient Thermal Comfort Control in Smart Buildings via Deep Reinforcement Learning," tech. rep., 2019.

[108] A. Aryal and B. Becerik-Gerber, "A comparative study of predicting individual thermal sensation and satisfaction using wrist-worn temperature sensor, thermal camera and ambient temperature sensor," *Building and Environment*, vol. 160, 8 2019.

[109] A. Natarajan and E. Laftchiev, "A transfer active learning framework to predict thermal comfort," *International Journal of Prognostics and Health Management*, vol. 10, pp. 1–13, 2019.

[110] M. Itani, D. Ghaddar, N. Ghaddar, and K. Ghali, "Model-based multivariable regression model for thermal comfort in naturally ventilated spaces with personalized ventilation," *JOURNAL OF BUILDING PERFORMANCE SIMULATION*, vol. 2021, no. 1, pp. 78–93, 2020.

[111] M. Wu, H. Li, and H. Qi, "Using electroencephalogram to continuously discriminate feelings of personal thermal comfort between uncomfortably hot and comfortable environments," *Indoor Air*, vol. 30, no. 3, pp. 534–543, 2020.

[112] B. Yang, X. Li, Y. Liu, L. Chen, R. Guo, F. Wang, and K. Yan, "Comparison of models for predicting winter individual thermal comfort based on machine learning algorithms," *Building and Environment*, vol. 215, no. March, p. 108970, 2022.

[113] Q. Y. Li, J. Han, and L. Lu, "A Random Forest Classification Algorithm Based Personal Thermal Sensation Model for Personalized Conditioning System in Office Buildings," *Computer Journal*, vol. 64, no. 3, pp. 500–508, 2021.

[114] Y. Zhou, Y. Su, Z. Xu, X. Wang, J. Wu, and X. Guan, "A hybrid physics-based/data-driven model for personalized dynamic thermal comfort in ordinary office environment," *Energy and Buildings*, vol. 238, p. 110790, 5 2021.

[115] H. A. Aziz, "Comparison between Field Research and Controlled Laboratory Research," *Archives of Clinical and Biomedical Research*, vol. 01, no. 02, pp. 101–104, 2017.

[116] S.-i. Tanabe, M. Haneda, and N. Nishihara, "Workplace productivity and individual thermal satisfaction," *Building and Environment*, vol. 91, pp. 42–50, 9 2015.

[117] A. C. Boerstra, M. t. Kulve, J. Toftum, M. G. Loomans, B. W. Olesen, and J. L. Hensen, "Comfort and performance impact of personal control over thermal environment in summer: Results from a laboratory study," *Building and Environment*, 2015.

[118] J. Xie, H. Li, C. Li, J. Zhang, and M. Luo, "Review on occupant-centric thermal comfort sensing, predicting, and controlling," *Energy and Buildings*, vol. 226, p. 110392, 2020.

[119] D. Li, C. C. Menassa, and V. R. Kamat, "Non-intrusive interpretation of human thermal comfort through analysis of facial infrared thermography," *Energy and Buildings*, vol. 176, pp. 246–261, 10 2018.

[120] J. Patterson and A. Gibson, *Deep Learning: A Practitioner's Approach.* O'Reilly Media, 2017.

[121] J. R. Vázquez-Canteli and Z. Nagy, "Reinforcement learning for demand response: A review of algorithms and modeling techniques," *Applied Energy*, vol. 235, pp. 1072–1089, 2 2019.

[122] M. C. Mozer, "The Neural Network House: An Environment that Adapts to its Inhabitants," tech. rep., 1998.

[123] M. Han, R. May, X. Zhang, X. Wang, S. Pan, D. Yan, Y. Jin, and L. Xu, "A review of reinforcement learning methodologies for controlling occupant comfort in buildings," *Sustainable Cities and Society*, vol. 51, p. 101748, 11 2019.

[124] S. Balakrishnan, A. Teaching, A. A. Aziz, and D. Analytics, "C ARNEGIE M ELLON U NIVERSITY D OCTORAL T HESIS A Bio-sensing and Reinforcement Learning Control System for Personalized Thermal Comfort and Energy Efficiency School of Architecture," 2019.

[125] B. B. Lahiri, S. Bagavathiappan, T. Jayakumar, and J. Philip, "Medical applications of infrared thermography: A review," *Infrared Physics and Technology*, vol. 55, no. 4, pp. 221–235, 2012.

[126] L. Antognoli, P. Marchionni, S. Nobile, V. Carnielli, and L. Scalise, "Assessment of cardio-respiratory rates by non-invasive measurement methods in hospitalized preterm neonates," *MeMeA 2018 - 2018 IEEE International Symposium on Medical Measurements and Applications, Proceedings*, 2018.

[127] M. Chakraborty, S. K. Raman, S. Mukhopadhyay, S. Patsa, N. Anjum, and J. G. Ray, "High precision automated face localization in thermal images: oral cancer dataset as test case," *Medical Imaging 2017: Image Processing*, vol. 10133, no. February 2017, p. 1013326, 2017.

[128] T. Giitsidis, E. G. Karakasis, A. Gasteratos, and G. C. Sirakoulis, "Human and fire detection from high altitude UAV images," *Proceedings - 23rd Euromicro International Conference on Parallel, Distributed, and Network-Based Processing, PDP 2015*, pp. 309–315, 2015.

[129] A. Szajewska, "Development of the Thermal Imaging Camera (TIC) Technology," *Procedia Engineering*, vol. 172, pp. 1067–1072, 1 2017.

[130] Y. Ma, X. Feng, J. Jiao, Z. Peng, S. Qian, H. Xue, and H. Li, "Smart Fire Alarm System with Person Detection and Thermal Camera," *Lecture Notes in Computer Science (including subseries Lecture Notes in Artificial Intelligence and Lecture Notes in Bioinformatics)*, vol. 12143 LNCS, pp. 353–366, 6 2020.

[131] L. Chen, N. Liu, M. Hu, and G. Zhai, "Rgb-Thermal imaging system collaborated with marker tracking for remote breathing rate measurement," *2019 IEEE International Conference on Visual Communications and Image Processing, VCIP 2019*, pp. 12–15, 2019.

[132] B. Miethig, A. Liu, S. Habibi, and M. V. Mohrenschildt, "Leveraging Thermal Imaging for Autonomous Driving," *ITEC 2019 - 2019 IEEE Transportation Electrification Conference and Expo*, 6 2019.

[133] A. Arabzadeh, M. A. Notani, A. Kazemiyan Zadeh, A. Nahvi, A. Sassani, and H. Ceylan, "Electrically conductive asphalt concrete: An alternative for automating the winter maintenance operations of transportation infrastructure," *Composites Part B: Engineering*, vol. 173, p. 106985, 9 2019.

[134] I. G. Dino, A. E. Sari, O. K. Iseri, S. Akin, E. Kalfaoglu, B. Erdogan, S. Kalkan, and A. A. Alatan, "Image-based construction of building energy models using computer vision," *Automation in Construction*, vol. 116, p. 103231, 8 2020.

[135] R. Gupta and A. Kotopouleas, "Magnitude and extent of building fabric thermal performance gap in UK low energy housing," *Applied Energy*, vol. 222, pp. 673–686, 7 2018.

[136] A. G. Entrop and A. Vasenev, "Infrared drones in the construction industry: designing a protocol for building thermography procedures," *Energy Procedia*, vol. 132, pp. 63–68, 10 2017.

[137] D. Lai and Q. Chen, "A two-dimensional model for calculating heat transfer in the human body in a transient and non-uniform thermal environment," *Energy and Buildings*, vol. 118, pp. 114–122, 2016.

[138] C. A. Corneanu, M. O. Simón, J. F. Cohn, and S. E. Guerrero, "Survey on RGB, 3D, Thermal, and Multimodal Approaches for Facial Expression Recognition: History, Trends, and Affect-Related Applications," *IEEE Transactions on Pattern Analysis and Machine Intelligence*, vol. 38, no. 8, pp. 1548–1568, 2016.

[139] M. Bodini, "A review of facial landmark extraction in 2D images and videos using deep learning," *Big Data and Cognitive Computing*, vol. 3, no. 1, pp. 1–14, 2019.

[140] FLIR Company, "A Resource Guide for Using Infrared in the Research and Development Industry,"

[141] M. Kristo and M. Ivasic-Kos, "An overview of thermal face recognition methods," *2018 41st International Convention on Information and Communication Technology, Electronics and Microelectronics, MIPRO 2018 - Proceedings*, pp. 1098–1103, 2018.

[142] Z. Chen and X. Huang, "Pedestrian detection for autonomous vehicle using multi-spectral cameras," *IEEE Transactions on Intelligent Vehicles*, vol. 4, no. 2, pp. 211–219, 2019.

[143] C. Ma, N. T. Trung, H. Uchiyama, H. Nagahara, A. Shimada, and R. I. Taniguchi, "Adapting local features for face detection in thermal image," *Sensors (Switzerland)*, vol. 17, no. 12, pp. 1–31, 2017.

[144] T. Vukovic, R. Petrovic, M. Pavlovic, and S. Stankovic, "Thermal Image Degradation Influence on R-CNN Face Detection Performance," *27th Telecommunications Forum, TELFOR 2019*, 2019.

[145] J. B. Mercer and E. F. J. Ring, "Fever screening and infrared thermal imaging: Concerns and guidelines," *Thermology International*, vol. 19, no. 3, pp. 67–69, 2009.

[146] E. Y. Ng, "Is thermal scanner losing its bite in mass screening of fever due to SARS?," *Medical Physics*, vol. 32, no. 1, pp. 93–97, 2005.

[147] N. Silawan, K. Kusukame, K. J. Kek, and W. S. Kuan, "A Novel Environment-Invariant Core Body Temperature Estimation for High Sensitivity and Specificity Fever Screening," *Proceedings of the Annual International Conference of the IEEE Engineering in Medicine and Biology Society, EMBS*, vol. 2018-July, pp. 1612–1615, 2018.

[148] A. H. Alkali, R. Saatchi, H. Elphick, and D. Burke, "Facial tracking in thermal images for real-time noncontact respiration rate monitoring," *Proceedings - UKSim-AMSS 7th European Modelling Symposium on Computer Modelling and Simulation, EMS 2013*, pp. 265–270, 2013.

[149] Y. Cho, S. J. Julier, N. Marquardt, and N. Bianchi-Berthouze1, "Robust tracking of respiratory rate in high- dynamic range scenes using mobile thermal imaging," 5 2017.

[150] T. Negishi, G. Sun, H. Liu, S. Sato, T. Matsui, and T. Kirimoto, "Stable Contactless Sensing of Vital Signs Using RGB-Thermal Image Fusion System with Facial Tracking for Infection Screening," *Proceedings of the Annual International Conference of the IEEE Engineering in Medicine and Biology Society, EMBS*, vol. 2018-July, pp. 4371–4374, 2018.

[151] L. Chen, N. Liu, M. Hu, and G. Zhai, "Rgb-Thermal imaging system collaborated with marker tracking for remote breathing rate measurement," *2019 IEEE International Conference on Visual Communications and Image Processing, VCIP 2019*, pp. 12–15, 2019.

[152] J. K. Lee and H. W. Jeong, "Wearing facemasks regardless of symptoms is crucial for preventing spread of COVID-19 in hospitals," *Infection control and hospital epidemiology*, pp. 1–4, 2020.

[153] I.-K. Lee, C.-C. Wang, M.-C. Lin, C.-T. Kung, K.-C. Lan, and C.-T. Lee, "Effective strategies to prevent coronavirus disease-2019 (COVID-19) outbreak in hospital," *Journal of Hospital Infection*, vol. 105, pp. 102–103, 5 2020.

[154] A. Barnawi, P. Chhikara, R. Tekchandani, N. Kumar, and B. Alzahrani, "Artificial intelligence-enabled Internet of Things-based system for COVID-19 screening using aerial thermal imaging," *Future Generation Computer Systems*, vol. 124, pp. 119–132, 2021.

[155] G. Recommendations and A. C. Systems, "General Recommendations Operating commercial office buildings under epidemic," 2020.

[156] A. Amirazar, M. Azarbayjani, O.-K. Im, A. Zarrabi, R. Ashrafi, R. Cox, and A. Johnson, "Assessing the circadian potential of an office building in the southeastern US," in *Simulation Series*, vol. 50, 2018.

[157] A. H. Zarrabi, M. Azarbayjani, A. Amirazar, and R. Asharafi, "Comparative Study of Different Design Configurations Based on the Daylight and Visual Comfort Performance of Electrochromic Glass in a side-lit Office building," pp. 811–816, 2018.

[158] S. N. Hosseini and I. SheikhAnsari, "A Daylight Assessment on Visual and Non-visual Effects of Light Shelves: A Human-centered Simulation-based Approach," *Journal of Daylighting*, vol. 9, no. 1, pp. 28–47, 2022.

[159] A. Amirazar, M. Azarbayjani, O.-K. Im, A. Zarrabi, R. Ashrafi, R. Cox, and A. Johnson, "Assessing the circadian potential of an office building in the southeastern US," in *Simulation Series*, vol. 50, 2018.

[160] R. Ashrafi, M. Azarbayjani, R. Cox, B. Futrell, J. Glass, A. Zarrabi, and A. Amirazar, "Assessing the performance of UFAD system in an office building located in various climate zones," *Simulation Series*, vol. 51, no. 8, pp. 147–154, 2019.

[161] S. Mostafavi, R. Cox, B. Futrell, and R. Ashafari, "Calibration of white-box whole-building energy models using a systems-identification approach," *Proceedings: IECON 2018 - 44th Annual Conference of the IEEE Industrial Electronics Society*, pp. 795–800, 12 2018.

[162] Z. Zolfaghari, J. Jones, R. Gibbons, and R. Schubert, "Study of the Effect of Light Emitting Diode (LED) on the Optimum Window-to-Wall Ratio and Whole-Building Energy Consumption in Open Offices," no. January, 2020.

[163] M. Sheikhshahrokhdehkordi, J. Khalesi, and N. Goudarzi, "High-performance building: Sensitivity analysis for simulating different combinations of components of a two-sided windcatcher," *Journal of Building Engineering*, vol. 28, no. November 2019, p. 101079, 2020.

[164] P. Pease, J. Chhabra, and Z. Zolfaghari, "Planning for net zero by 2050, what HVAC system interventions will today's code minimum commercial buildings require?," vol. 2050, 2021.

[165] R. Ashrafi, M. Azarbayjani, and H. Tabkhi, "Machine Learning-Based Automated Thermal Comfort Prediction : Integration of Low-Cost Thermal and Visual Cameras for Higher Accuracy," 2022.

[166] A. Aryal and B. Becerik-Gerber, "Skin Temperature Extraction Using Facial Landmark Detection and Thermal Imaging for Comfort Assessment," pp. 71–80, 2019.

[167] A. Selinger and D. A. Socolinsky, "Appearance-based facial recognition using visible and thermal imagery: a comparative study," *Image Rochester NY*, vol. 4, p. 28, 2006.

[168] H. Méndez, C. S. Martín, J. Kittler, Y. Plasencia, and E. García-Reyes, "Face recognition with LWIR imagery using local binary patterns," *Lecture Notes in Computer Science (including subseries Lecture Notes in Artificial Intelligence and Lecture Notes in Bioinformatics)*, vol. 5558 LNCS, pp. 327–336, 2009.

[169] I. A. Kakadiaris, G. Passalis, T. Theoharis, G. Toderici, I. Konstantinidis, and N. Murtuza, "Multimodal face recognition: Combination of geometry with physiological information," *Proceedings - 2005 IEEE Computer Society Conference on Computer Vision and Pattern Recognition, CVPR 2005*, vol. II, pp. 1022–1029, 2005.

[170] H. Chang, H. Harishwaran, M. Yi, A. Koschan, B. Abidi, and M. Abidi, "An indoor and outdoor, multimodal, multispectral and multi-illuminant database for face recognition," *Proceedings of the IEEE Computer Society Conference on Computer Vision and Pattern Recognition*, vol. 2006, no. c, pp. 0–7, 2006.

[171] J. Serrano-Cuerda, A. Fernández-Caballero, and M. T. López, "Selection of a visible-light vs. thermal infrared sensor in dynamic environments based on confidence measures," *Applied Sciences (Switzerland)*, vol. 4, no. 3, pp. 331–350, 2014.

[172] D. T. Robinson, J. Clay-Warner, C. D. Moore, T. Everett, A. Watts, T. N. Tucker, and C. Thai, *Toward an unobtrusive measure of emotion during interaction: Thermal imaging techniques*, vol. 29. 2012.

[173] I. Pavlidis, J. a. Levine, and P. Baukol, "Ioannis Pavlidis Honeywell Laboratories Minneapolis , MN ioannis . pavlidis @ i), honeywell . com James Levine Mayo Clinic Mayo Clinic," *IEEE Transactions on Biomedical Engineering*, no. 6, pp. 315–318, 2002.

[174] H. Nguyen, K. Kotani, F. Chen, and B. Le, "A thermal facial emotion database and its analysis," *Lecture Notes in Computer Science (including subseries Lecture Notes in Artificial Intelligence and Lecture Notes in Bioinformatics)*, vol. 8333 LNCS, pp. 397–408, 2014.

[175] C. Goulart, C. Valadão, D. Delisle-Rodriguez, D. Funayama, A. Favarato, G. Baldo, V. Binotte, E. Caldeira, and T. Bastos-Filho, "Visual and thermal image processing for facial specific landmark detection to infer emotions in a child-robot interaction," *Sensors (Switzerland)*, vol. 19, no. 13, 2019.

[176] D. Pradeep Kumar, K. Uday Kumar Reddy, B. Sai Mounisha, K. Sneha Latha, P. Sathya Narayana Reddy, and V. Uma Maheshwara Reddy, "Facial Recognition and Classification of Drunk Using Facial Diagrams," *Mukt Shabd Journal*, vol. IX, no. IV, pp. 1–12, 2020.

[177] A. Sancen-Plaza, L. M. Contreras-Medina, A. I. Barranco-Gutiérrez, C. Villaseñor-Mora, J. J. Martínez-Nolasco, and J. A. Padilla-Medina, "Facial Recognition for Drunk People Using Thermal Imaging," *Mathematical Problems in Engineering*, vol. 2020, 2020.

[178] "OTCBVS."

[179] X. Chen, P. J. Flynn, K. W. Bowyer, and N. Dame, "Visible-light and Infrared Face Recognition," *The Proceedings of Workshop on Multimodal User Authentication*, pp. 48–55, 2003.

[180] P. Buddharaju, I. T. Pavlidis, P. Tsiamyrtzis, and M. Bazakos, "Physiology-based face recognition in the thermal infrared spectrum," *IEEE Transactions on Pattern Analysis and Machine Intelligence*, vol. 29, no. 4, pp. 613–626, 2007.

[181] A. Srivastava, X. Liu, B. Thomasson, and C. Hesher, "Spectral probability models for ir images with applications to IR face recognition," no. October 2001, 2001.

[182] S. Wang, Z. Liu, S. Lv, Y. Lv, G. Wu, P. Peng, F. Chen, and X. Wang, "A natural visible and infrared facial expression database for expression recognition and emotion inference," *IEEE Transactions on Multimedia*, vol. 12, no. 7, pp. 682–691, 2010.

[183] S. Hu, N. J. Short, B. S. Riggan, C. Gordon, K. P. Gurton, M. Thielke, P. Gurram, and A. L. Chan, "A Polarimetric Thermal Database for Face Recognition Research," *IEEE Computer Society Conference on Computer Vision and Pattern Recognition Workshops*, pp. 187–194, 2016.

[184] R. Shoja Ghiass, H. Bendada, and X. Maldague, "Université Laval Face Motion and Time-Lapse Video Database (UL-FMTV)," in *Proceedings of the 2018 International Conference on Quantitative InfraRed Thermography*, QIRT Council, 7 2018.

[185] K. Mallat and J. L. Dugelay, "A benchmark database of visible and thermal paired face images across multiple variations," *2018 International Conference of the Biometrics Special Interest Group, BIOSIG 2018*, 2018.

[186] K. Panetta, A. Samani, X. Yuan, Q. Wan, S. Agaian, S. Rajeev, S. Kamath, R. Rajendran, S. P. Rao, A. Kaszowska, and H. A. Taylor, "A Comprehensive Database for Benchmarking Imaging Systems," *IEEE Transactions on Pattern Analysis and Machine Intelligence*, vol. 42, no. 3, pp. 509–520, 2020.

[187] M. Kopaczka, R. Kolk, J. Schock, F. Burkhard, and D. Merhof, "A Thermal Infrared Face Database with Facial Landmarks and Emotion Labels," *IEEE Transactions on Instrumentation and Measurement*, vol. 68, no. 5, pp. 1389–1401, 2019.

[188] U. Cheema and S. Moon, "Sejong face database: A multi-modal disguise face database," *Computer Vision and Image Understanding*, vol. 208-209, no. May, p. 103218, 2021.

[189] T. I. Dhamecha, A. Nigam, R. Singh, and M. Vatsa, "Disguise detection and face recognition in visible and thermal spectrums," *Proceedings - 2013 International Conference on Biometrics, ICB 2013*, 2013.

[190] G. Koukiou, "We are IntechOpen , the world ' s leading publisher of Open Access books Built by scientists , for scientists TOP 1 %," *Intech*, p. 13, 2012.

[191] G. Hermosilla, J. L. Verdugo, G. Farias, E. Vera, F. Pizarro, and M. Machuca, "Face Recognition and Drunk Classification Using Infrared Face Images," *Journal of Sensors*, vol. 2018, 2018.

[192] A. Kuzdeuov, D. Aubakirova, D. Koishigarina, and H. A. Varol, "TFW: Annotated Thermal Faces in the Wild Dataset," no. 2021, pp. 0–11, 2021.

[193] M. Abdrakhmanova, A. Kuzdeuov, S. Jarju, Y. Khassanov, M. Lewis, and H. A. Varol, "SpeakingFaces: A Large-Scale Multimodal Dataset of Voice Commands with Visual and Thermal Video Streams," *Sensors*, vol. 21, p. 3465, 5 2021.

[194] R. Miezianko, "Terravic Research Infrared Database," *IEEE OTCBVS WS Series Bench.*

[195] J. G. Wang and E. Sung, "Facial feature extraction in an infrared image by proxy with a visible face image," *IEEE Transactions on Instrumentation and Measurement*, vol. 56, no. 5, pp. 2057–2066, 2007.

[196] M. Marzec, R. Koprowski, and Z. Wróbel, "Methods of face localization in thermograms," *Biocybernetics and Biomedical Engineering*, vol. 35, no. 2, pp. 138–146, 2015.

[197] V. Le, J. Brandt, Z. Lin, L. Bourdev, and T. S. Huang, "Interactive facial feature localization," *Lecture Notes in Computer Science (including subseries Lecture Notes in Artificial Intelligence and Lecture Notes in Bioinformatics)*, vol. 7574 LNCS, no. PART 3, pp. 679–692, 2012.

[198] FLIR Systems, "FLIR A400/A700 Thermal Cameras with Smart Sensor Configuration | FLIR Systems."

[199] F. Jazizadeh, F. M. Marin, and B. Becerik-Gerber, "A thermal preference scale for personalized comfort profile identification via participatory sensing," *Building and Environment*, vol. 68, pp. 140–149, 10 2013.

[200] F. Jazizadeh, A. Ghahramani, B. Becerik-Gerber, T. Kichkaylo, and M. Orosz, "User-led decentralized thermal comfort driven HVAC operations for improved efficiency in office buildings," *Energy and Buildings*, vol. 70, pp. 398–410, 2 2014.

[201] B. Balaji, H. Teraoka, R. Gupta, and Y. Agarwal, "ZonePAC: Zonal power estimation and control via HVAC metering and occupant feedback," *BuildSys 2013 - Proceedings of the 5th ACM Workshop on Embedded Systems For Energy-Efficient Buildings*, 2013.

[202] J. H. Choi and V. Loftness, "Investigation of human body skin temperatures as a bio-signal to indicate overall thermal sensations," *Building and Environment*, vol. 58, pp. 258–269, 12 2012.

[203] K. He, X. Zhang, S. Ren, and J. Sun, "Deep residual learning for image recognition," *Proceedings of the IEEE Computer Society Conference on Computer Vision and Pattern Recognition*, vol. 2016-Decem, pp. 770–778, 2016.

[204] Davis King, "dlib C++ Library: High Quality Face Recognition with Deep Metric Learning," 2017.

[205] T. Negishi, G. Sun, S. Sato, H. Liu, T. Matsui, S. Abe, H. Nishimura, and T. Kirimoto, "Infection Screening System Using Thermography and CCD Camera with Good Stability and Swiftness for Non-contact Vital-Signs Measurement by Feature Matching and MUSIC Algorithm," *Proceedings of the Annual International Conference of the IEEE Engineering in Medicine and Biology Society, EMBS*, pp. 3183–3186, 2019.

[206] "TeCSAR-UNCC/UNCC-ThermalFace."

[207] V. L. Erickson and A. E. Cerpa, *Thermovote: Participatory Sensing for Efficient Building HVAC Conditioning.*

[208] H. Z. E. A. P. R. C. K. J. F. Y. Z. D. D. S. S. Bauman, F. and X. Zhou., "Advanced Integrated Systems Technology Development: Personal Comfort Systems and Radiant Slab Systems," *eScholarship*, pp. 0–13, 2015.

[209] H. Zhang, E. Arens, D. E. Kim, E. Buchberger, F. Bauman, and C. Huizenga, "Comfort, perceived air quality, and work performance in a low-power task-ambient conditioning system," *Building and Environment*, vol. 45, pp. 29–39, 1 2010.

[210] P. P. Ray, "A survey on Internet of Things architectures," 7 2018.

[211] P. Arjunan, M. Saha, H. Choi, M. Gulati, A. Singh, P. Singh, and M. B. Srivastava, "SensorAct: A Decentralized and Scriptable Middleware for Smart Energy Buildings," 2015.

[212] J.-H. Choi and D. Yeom, "Study of data-driven thermal sensation prediction model as a function of local body skin temperatures in a built environment," *Building and Environment*, vol. 121, pp. 130–147, 8 2017.

[213] F. De Oliveira, S. Moreau, C. Gehin, and A. Dittmar, "Infrared imaging analysis for thermal comfort assessment," in *Annual International Conference of the IEEE Engineering in Medicine and Biology - Proceedings*, pp. 3373–3376, 2007.

[214] E. Rublee, V. Rabaud, K. Konolige, and G. Bradski, "ORB: An efficient alternative to SIFT or SURF," *Proceedings of the IEEE International Conference on Computer Vision*, pp. 2564–2571, 2011.

[215] T. Özseven and M. Düğenci, "Face recognition by distance and slope between facial landmarks," *IDAP 2017 - International Artificial Intelligence and Data Processing Symposium*, pp. 3–6, 2017.

[216] "DS1921Z-F5# Thermochron iButton [-5 to 26°C] - High Resolution | iButtonLink."

[217] R. Ashrafi, M. Azarbayjani, and H. Tabkhi, "Machine Learning-Based Automated Thermal Comfort Prediction: Integration of Low-Cost Thermal and Visual Cameras for Higher Accuracy," 4 2022.